Electrodialysis with bipolar membranes for ammonia recovery in wastewater

An innovative concept for the treatment of ammonia residual streams

Giacomo L. Bandinu

Delft University of Technology

TU Delft Delft University of Technology

Challenge the future

Electrodialysis with bipolar membranes for ammonia recovery in wastewater

An innovative concept for the treatment of ammonia residual streams

by

G.L. Bandinu

in partial fulfillment of the requirements for the degree of

Master of Science
in Civil Engineering

at the Delft University of Technology,
to be defended publicly on Thursday January 10^th, 2019 at 2:30 PM.

Supervisor:	Dr. Ir. H. Spanjers,	TU Delft
Thesis committee:	Prof. Dr. Ir. J. van Lier,	TU Delft
	Dr. Ir. D. Vermaas,	TU Delft
	Ir. N. van Linden,	TU Delft

TU Delft Delft University of Technology

A mia Madre,
Che da undici lunghissimi anni,
giorno dopo giorno,
mi mostra come anche le sfide impossibili
possono essere superate…

G.L. Bandinu
Delft, December 2018

Abstract

Municipal and industrial wastewater contains a significant amount of dissolved nitrogen. This is the results of the organic protein degradation and of the large employment of nitrogen (N), usually in the form of ammonia (NH_3), in the industry. Currently, nitrogen is removed in wastewater treatment plant (WWTP) by means of biological treatments. Globally, the most applied treatment consists in the combination of nitrification and denitrification. This technique is characterized by a high energy-demand (44.3 MJ per $Kg_{NH_4^+}$ removed [1]) which accounts for 70% of the total energy consumption in the WWTP [2]. A less energetically intensive alternative treatment is the Anammox process. However, this also presents significant limitations, especially when dealing with extremely polluted stream and in the flexibility of operation [1].

An alternative to reduce the energy cost of nitrogen removal by valorizing the content of residual streams is explored by the *N2kWh* project. The novel concept underlying the *N2kWh* project aims to use NH_3 from waste streams as a fuel source for a solid oxide fuel cell (SOFC). In this way, the energy cost for biological N-removal processes is cut, and, ideally, energy can be even produced. WWTP digested reject water was recognized as potential N-source for energy recovery as a result of its relatively high total ammonia nitrogen (TAN) concentrations (up to 1.5 $g - N \cdot L^{-1}$). A (selective) concentration step and pH regulation are needed in order to convert the TAN in the reject water, mostly present in form of ammonium bicarbonate (NH_4HCO_3), into NH_3 gas which can be stripped and directly fed in the SOFC. Previous studies proved electrodialysis (ED) to be the most energetically efficient technology for the removal and concentration of ammonium bicarbonate. However, due to the high alkalinity in the obtained concentrate, large amount of chemicals is required for the pH regulation. An interesting opportunity to avoid this chemical addition is the employment of a bipolar membrane electrodialysis (BPMED). Through this unique technology, it is possible to simultaneously achieve the concentration of TAN, as well as the regulation of pH without chemicals.

The main objective of this work was to evaluate the potential of BPMED for the recovery of NH_3 in the boundaries of the *N2kWh* project. The energy performance of BPMED was compared with the alternative use of conventional ED plus sodium hydroxide for pH control. In order to obtain valuable information on the operation, three setups were employed: regular ED, BPMED and BPMED coupled with two membrane vacuum stripping devices (VMS). For this purpose, a synthetic solution obtained by dissolving 6.6 $g \cdot L^{-1}$ NH_4HCO_3 salt in demiwater was used to simulate the digested reject water. Experiments were designed to characterize the BPMED operation and clarify which processes influence the performance.

Experimental laboratory results showed that, in terms of energy consumption for the NH_4^+ removal, the BPMED used more energy compared to the ED. The removal of 90% of the initial NH_4^+ is achieved by using an average of 13.2±0.1 $MJ \cdot kg_{NH_4^+}^{-1}$. This value was 3.3 times higher than that achieved with regular ED. This discrepancy was explained by the extra-elements in the stack and the water dissociation process, responsible for the higher voltage measured during BPMED operation. The energy consumption was proven to be higher also as a consequence of the lower current efficiency for salt transport (73% compared to 95% of conventional ED). This was due to the more severe undesired diffusion processes, mainly gas diffusion and hydroxide leakage from the alkaline stream to the diluate, taking place within the BPMED stack. However, the energy consumption for ammonium removal in BPMED was still more than three times lower than the energy consumed by nitrification denitrification and comparable to what used by anammox.

The implementation of the membrane vacuum stripping modules, in series with the BPMED, only slightly increased the overall current efficiency (up to 3.4 % current efficiency gain). The benefit in current efficiency was less significant for higher concentrations and pH in the alkaline stream. Besides

that, the tested technology tandem (BPMED+VMSs) was capable of stripping NH_3 and, consequently, reduce the gas diffusion over the stack.

The energy consumed for the production of $NaOH$ and for the ED operation to reach a pre-defined pH and TAN concentration was estimated to be equal to 82.55 Wh per L of concentrate. This value was substantially higher than what consumed by BPMED (48.7 Wh) to achieve the same result in the alkaline stream.

To conclude, the studied BPMED system was demonstrated to be superior in terms of energy consumption for the recovery of NH_3 gas when compared to the combination of ED and chemical addition. BPMED showed also crucial advantages for the environment, design and safety of the treatment facility. The energy consumption for the removal of nitrogen with BPMED was proven to be lower than what used in the competitive biological technology. Finally, neither the technology nor the operation methods employed were specifically designed/optimized for this application. This made the use of BPMED for the *N2kWh* purpose even more interesting and promising.

Acknowledgement

This research work would not have been possible without the essential contributions of unique people.

To begin, I would like to thank Ir. Niels van Linden, my daily supervisor, for his extraordinary availability during the thesis. It was a real pleasure to collaborate and learn from you. I am really glad to had the opportunity to meet you, and I sincerely hope to have more of chances to work closely with you in the future. I would also like to thank Dr. Ir. HenRi Spanjers for the precious supervision and positive attitude shown during my thesis and in all the other occasions we collaborated together.

A thanks goes also to the other members of my graduation committee, Prof. Dr. Ir. Jules van Lier and Dr. Ir. David Vermaas for the great hints during the several meeting we had. Thank to Mohammed, Tamara and to the rest of the staff from the Sanitary Engineering department. You made my thesis-life way easier with your help, advises and smiles.

I would like to thank my parents and my brother for constantly inspiring me and believing in me. You have always been the first to blindly support my decisions, even if they often made me moved far from you. Finally, a special thanks to all my friends. The old ones from Florence, that, although they don't see me so often anymore, keep supporting me. And, of course, to the new friends met here in Delft, that were my second family in the last two years of my life.

Contents

List of abbreviations

(aq)	Aqueous phase
(g)	Gas phase
$^{\circ}C$	Degree Celsius
Δt	Time interval
ΔP_{NH_3}	NH_3 partial pressure difference [Pa]
Ω	Ohm
A	Ampere
AEM	Anion exchange membrane
BPM	Bipolar membrane
BPMED	Electrodialysis with bipolar membrane
CE_{NaCl}	Current efficiency for sodium chloride transport
$CE_{NH_4^+}$	Current efficiency for ammonium transport [%
CE_{WD}^{mes}	Measured current efficiency for water dissociation [%
CE_{WD}^{act}	Actual current efficiency for water dissociation [%]
CEM	Cation exchange membrane
CEEM	Cation exchange end membrane
CFV	Cross-flow velocity
CO_2	Carbon dioxide
CO_3^{2-}	Carbonate
CP	Concentration polarization
$E_{NH_4^+}$	Energy consumption for ammonium removal [$MJ \cdot Kg_{NH_4^+}^{-1}$]
ED	Electrodialysis
ED-BPM	Electrodialysis with bipolar membrane
EC	Electrical conductivity [$mS \cdot cm^{-}1$]
eq	Equivalent
ERS	Electrode rinse solution
F	Faraday constant [$s \cdot A \cdot mol^{-1}$]
h	Hour
H^+	Hydrogen proton
HCl	Hydrochloric acid
HCO_3^-	Bicarbonate
H_2O	Water
I	Current [A]
J_NH_3	NH_3 diffusion flux [$g_{NH_4^+} \cdot m^{-2} \cdot min^{-1}$]
K_stream	NH_3 diffusion coefficient for BPMED stream [$s \cdot m^{-1}$]
IEXM	Ion exchange membrane
L	Liter
LCD	Limiting current density
MJ	MegaJoule
mol	mole
min	minutes
n	number of membrane pairs or triplet
N	Nitrogen
$NaCl$	Sodium chloride
$NaNO_3$	Sodium nitrate
NH_3	Ammonia
NH_4^+	Ammonium
NH_4HCO_3	Ammonium bicarbonate
OH^-	Hydroxide

Pa	Pascal
STM	Standard membrane stacks
T	temperature [$^{\circ}C$]
TAN	Total ammonia nitrogen [$g \cdot L^{-1}$]
TIC	Total inorganic carbon [$g \cdot L^{-1}$]
R	Electrical resistance [Ω]
RO	Reverse osmosis
s	Second
SBE	Sequencing batch experiment
SOFC	Solid oxide fuel cell
U	electrical potential [V]
U_0	Theoretical potential for water dissociation
VMS	Vacuum membrane stripping
Wh	Watt-hour
wt%	Weight percent
WWTP	Wastewater treatment plant

1

Introduction

1.1. Background: the unbalance of the nitrogen cycle

Since the start of the 20^{th} century, with the development of the Haber-Bosch process, human activities resulted in a large release of nitrogen into the environment [3]. Nowadays mankind fixes more atmospheric N_2 into ammonia (NH_3) than all terrestrial natural processes combined [4]. This provoked an unbalance in the nitrogen cycle which is related to several health and environmental issues [5]. Specifically, the overpresence of N-compounds in the aquatic ecosystem can lead to eutrophication, and to the consequential loss of biodiversity in water bodies [3]. The urgency to reduce the unbalance of the nitrogen cycle is emphasized also by Steffen *et al.* [5] who introduced the frame of planetary boundaries to define the safe operating space for humanity. As shown in Figure 1.1, within the planetary boundaries, the unbalance of nitrogen cycle exposes humankind to the highest risk, together with the loss of genetic diversity.

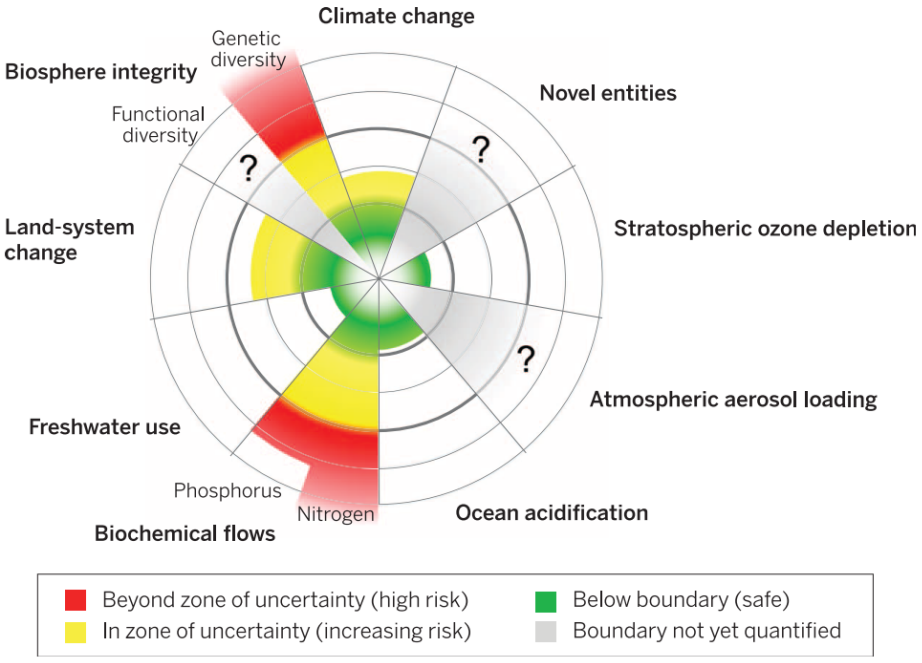

Figure 1.1: Planetary boundaries scheme according to Steffen *et al.* [5]. The green areas represent human activities that are within safe margins, the yellow areas represent human activities that may or may not have exceeded safe margins, the red areas represent human activities that have exceeded safe margins, and the grey areas with question mark represent human activities for which safe margins have not yet been determined. Retrieved from Steffen *et al.* [5, p.736].

Municipal and industrial wastewater usually contain high nitrogen concentrations. N-compounds

have to be removed before discharging the water into the environment.

Currently, this removal is achieved in wastewater treatment plan (WWTP) by means of biological treatment. Globally, the most applied treatment is a combination of nitrification and denitrification. This technology is characterized by a high energy-demand (44.3 MJ per $Kg_{NH_4^+}$ removed [1]) that is mostly related to the aeration process required to promote nitrification. This can account for up to the 70% of the total energy spent in the WWTP [2].

A less energetically intensive alternative to the nitrification-denitrification treatment is the anammox process. This newly developed biological technology is able to remove nitrogen with an energy requirement of 14.9 MJ per $Kg_{NH_4^+}$ [1]. Nevertheless, as nitrification-denitrification, anammox limits to degradate nitrogen-compounds into N_2 gas. This is then released into the atmosphere without acknowledging the valuable compounds (i.e. NH_3) contained in the waste stream. Furthermore, as a result of the particular structure and sensibility of the anammox bacteria, the process presents practical difficulties in the starting up and for the long-term stability of operation [1].

1.2. N2kWh: from pollutant to power

A potential alternative treatment to reduce the energy cost of nitrogen removal by valorizing the content of residual streams is explored by the *N2kWh* project. This project, a collaboration between TU Delft and KU Leuven, aims to use NH_3 from waste streams as a fuel source for a solid oxide fuel cell (SOFC). In this concept, the nitrogen is no longer regarded as a pollutant but as an energy source [6]. The energy cost for biological N-removal processes is cut, and, ideally, energy can be produced.

A SOFC is a device that produces electricity directly from the electrochemical oxidation of a fuel. The main advantages of this class of fuel cells include high efficiency, long-term stability, fuel flexibility, low emissions, and relatively low-cost [7]. Although hydrogen (H_2) is usually the preferred fuel of choice, as high power densities can be obtained, NH_3 is an excellent substitute for H_2 and hydrocarbons for several reasons [7–9]:

- The price of NH_3 is as competitive to hydrocarbons.
- NH_3 can be easily liquefied and the volumetric energy density of liquefied NH_3 is higher than that of liquid H_2, making it ideal for transportation and storage of energy.
- NH_3 is less flammable than other fuels and the leakage of NH_3 can easily be detected by the human nose under 1 ppm.
- Byproducts of cell reactions are merely N_2 and H_2O, no greenhouse gases are emitted.

In order to recover NH_3 to be fed in the SOFC, water containing high nitrogen concentration and low carbon levels has been identified as a particularly suitable candidate. A practical example of water with these properties is rejected water from dewatering of anaerobically digested sludge. This stream, although representing a relatively small volume of the total treated water in WWTP, contributes for 15-20% to the total nitrogen load at WWTPs [10]. Its total ammonia nitrogen (TAN) concentration, up to 1.5 $g \cdot L^{-1}$, originates from the organic nitrogen present in the biomass that has been converted to NH_3 and NH_4^+ during anaerobic digestion of the sludge. The required composition of fuel for the SOFC does not directly match the matrix of this reject water. Moreover, the extraction of this gas is highly influenced by the pH, temperature and NH_4^+ concentration in the fluid. For this reason, pretreatments, a (selective) concentration step, and gas production/extraction step are needed [11]. A conceptual scheme of this treatment chain is shown in Figure 1.2

The ultimate objective of this project is to produce enough energy and heat in the SOFC to, at least, cover the energy consumed for the NH_3 fuel recovery.

1.3. Selective concentration of ammonium-nitrogen

The master thesis research presented in this report is part of the $N2kWh$ project, and it specifically focuses on the step required for the concentration of NH_3 from the residual streams.

Over the last two years, reverse osmosis, electrodialysis and ion exchange were studied in order to select the best method to achieve the highest TAN concentration in the liquid phase before stripping the NH_3 [13]. A 6.6 $g_{NH_4HCO_3} \cdot L^{-1}$ solution (N-concentration comparable to the municipal reject water)

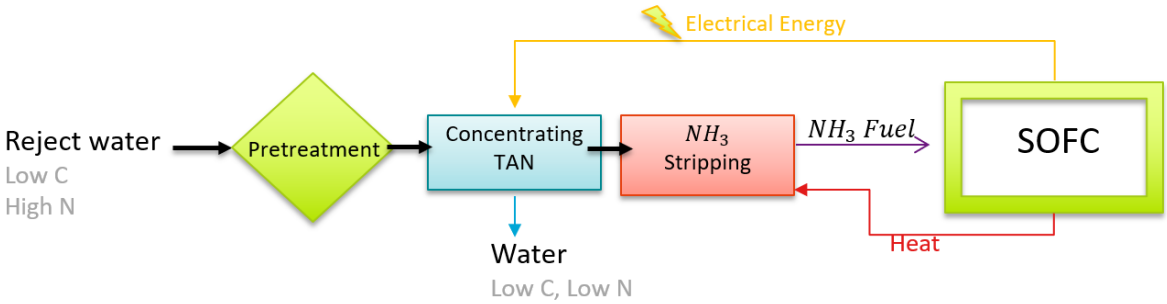

Figure 1.2: Conceptual scheme of the needed treatment for the extraction and recovery of the NH_3 within the *N2kWh* project. Retrieved and adapted from Martens [12, p.4].

was used as feed water for testing and comparing the different concentrating technologies. The results showed that electrodialysis (ED) was the most suitable candidate because able to obtain a high TAN concentration with a relatively low energy consumption [13].

Electrodialysis for TAN concentration

ED is a membrane separation technology where ions are transported through semi-permeable membranes, under the influence of an electrical potential. The net results of this process are two separate streams:

- A diluate stream, which has been depleted from the salts initially dissolved in it.
- A concentrate stream, where all the ions initially present in the diluate stream are collected and concentrated.

ED is mainly used to desalinate brackish water for domestic and industrial use [14]. Recently, emergent ED applications aiming to concentrate nutrients from waste streams are gaining more interest [15, 16]. The scope of most of these applications is the synthesis of a concentrated nitrogen stream that can be used as a valuable alternative to the chemically produced nitrogen fertilizer [17].

Pronk *et al.* [18] utilized laboratory scale ED to concentrate NH_4^+ and phosphate in urine by a factor of 3.2 (reaching a final concentration > 18 $g_{NH_4^+} \cdot L^{-1}$). Mondor *et al.* [17] and Ippersiel *et al.* [19] used electrodialysis to concentrate NH_4^+ to respectively 18.3 $g \cdot L^{-1}$ and 27.45 $g \cdot L^{-1}$ from the liquid fraction of swine manure. In both of these research, the maximum NH_4^+ concentration was limited by the transport of water via osmosis and electro-osmosis [17, 19]. In this case, the migration of ions from dilute to concentrate did no longer lead to an increase of concentration because water was transported proportionally through the membranes [20].

A particularly relevant study for this application was conducted by Ward *et al.* [16], who investigated the nutrients recovery performance of a pilot-scale electrodialysis utilizing domestic anaerobic digester supernatant (initial NH_4^+ concentration 1.07±0.343 $g \cdot L^{-1}$). A concentrated product with a concentration of 7.1 $g_{NH_4^+} \cdot L^{-1}$ was obtained with a power consumption equal to 13.72 $\pm$ 4.2 MJ per Kg of NH_4^+ removed. Although only the 23% of the initial NH_4^+ was removed from the fed water, the energy consumption for NH_4^+ removal was substantially lower than in nitrification-denitrification and competing with what used in anammox.

Finally, within the *N2kWh* project, Deckers [11] performed lab experiments aiming to design the most energetically convenient operation strategy for the removal of NH_4^+ from anaerobic digester reject water. The research was conducted utilizing the same synthetic wastewater (containing 6.6 $g_{NH_4HCO_3} \cdot L^{-1}$) considered for this work. A maximum NH_4^+ concentration of 7.3 $gNH_4^+ \cdot L^{-1}$ was achieved. Besides that, the 90% of the NH_4^+ contained in the feed water was removed with an energy consumption between 2.9-5.1 MJ per kg of NH_4^+. The ED installation was operated with a constant current density of 1.56 $mA \cdot cm^{-2}$. This favored the low energy consumption but, on the other hand, it extended the required membrane surface for the removal process. Even higher concentration was obtained with a staging scheme or lowering the volume ratio between the concentrate and the diluate. However, this involved higher energy consumption for the some amount of N removed [11].

1.4. Problem Definition

Before being fed to the SOFC, the NH_4^+ contained in the ED concentrate has to be converted and stripped as NH_3 gas [12]. The conversion of NH_4^+ to NH_3 is achieved by increasing the pH and the temperature of the solution. Because of the high buffering capacity of the electrodialysis concentrate, a large quantity of alkali (e.g. caustic soda) is needed to reach a pH high enough to allow NH_3 stripping (estimated about 10 by Martens [12]). This large use of chemicals diverges from the trend to reducing the chemicals use in the water treatment sector [21] and introduces additional cost for the overall process.

A valuable alternative to the use of ED and of chemicals for the generation of NH_3 is offered by bipolar membranes electrodialysis (BPMED). Bipolar membranes (BPMs) consist of two oppositely charged ion exchange membranes closely packed together, in such a way that one side of the BP membrane is positively charged, and the opposite is negatively charged. Between these two membranes, a very thin layer of pure water is present (intermediate layer). Applying an electrical potential to the membrane, the water in the intermediate layer (or transition layer) dissociates into H^+ and OH^- [22]. Generally, in the ED stack, bipolar membranes are separated by an anion and a cation exchange membrane. This membrane arrangement results in a three-compartment configuration where two separate streams collect the ions depleted from the diluate. One of these collects all the anions and H^+, and it is addressed as the **acid** stream (low pH). The other accumulates the cations (in this case NH_4^+) and OH^- and is named *base* or alkaline stream (high pH). In this way NH_4^+, once accumulated in the high pH solution, reacts with the produced OH^- forming NH_3 gas. Hence, this technology potentially achieves in one single step the concentration of the NH_4^+ (and thus its removal from the diluate) as well as its conversion to dissolved NH_3 gas.

1.4.1. Electrodialysis with bipolar membrane for TAN recovery

The utilization of BPMED to produce acids and bases from the corresponding salts is economically very attractive and has a multitude of interesting potential applications in the chemical industry as well as in biotechnology and water treatment processes [23]. Nonetheless, only a few studies have been conducted on the potential of BPMED as a technology for recovering NH_3.

Graillon *et al.* [24] have been the first to see BPMED as an attractive way for the recovery NH_3 from a nitrogen-rich effluent. Graillon *et al.* [24] concluded that the application of this concept is limited because of NH_3 gas diffusion across the stack. Because of this limitation, the maximum concentration achieved was 0.7 M of NH_3 in the base stream with a 70% of current efficiency.

To tackle this problem, Ali *et al.* [25] split ammonium nitrate to nitric acid and NH_3 by a coupled process including BPMED and in-situ NH_3 stripping. This, and the application of a high current density ($50 mA \cdot cm^{-2}$), permitted to achieve better results in terms of NH_3 production efficiency and final concentration in the base. Again, the main processes influencing the efficiency were acid concentration and NH_3 concentrations which led to H^+ leakage and gas diffusion, respectively.

Similar conclusions were drawn by Pronk *et al.* [26] who treated urine combining BPMED with an additional mass transfer unit (bubble columns and gas-filled hydrophobic membrane) in order to produce a solution containing NH_4^+ and phosphate at a low pH.

Finally, Li *et al.* [27] tested the bipolar membrane electrodialysis for generation of hydrochloric acid and NH_3 from a synthetic ammonium chloride wastewater. The results showed that, at the current density of 48 $mA \cdot cm^{-2}$, the highest concentration of NH_3, with initial concentration of 110 $g \cdot L^{-1}$ NH_4Cl, was 45.85 $g \cdot L^{-1}$. The higher initial concentration of NH_4Cl was favourable to reduce unit energy consumption and increase current efficiency of the BPMED.

1.4.2. Knowledge gap

None of the above mentioned studies provided an exhaustive quantification of the energy required for the removal of NH_4^+. All the setups were run with a relatively high constant current density. This limited the removal of salt from the feed water due to the quick approach to the LCD in the diluate. In all the documented studies, the experiments were performed at a relatively high current density and using a feed water with extremely high nitrogen concentrations, not comparable to reject water considered in the *N2kWh* project. These conditions led to high degrees NH_3 gas diffusion through the cell.

According to the authors, as a consequence of this phenomenon, the efficiency of the process dramatically dropped. It remains unclear whether, for the TAN concentration considered in the *N2kWh*

project, the NH_3 gas diffusion will result in a significant decrease in the BPMED performance.

In addition to that, the introduction of bipolar membranes in the ED unit will increase the total resistance of the membrane stack and thereby raise the energy consumed per kg of nitrogen removed when compared to regular ED. Nevertheless, as previously mentioned, BPMEDs can avoid the use of chemicals which would introduce great advantages in term of cost and operational complexity. Hence, it would be interesting to investigate whether the expected higher energy consumption of BPMED in concentrating NH_4^+ can be balanced by avoiding the use of chemicals.

1.5. Research Plan

1.5.1. Research objective

This MSc thesis focuses on assessing the potential of BPMED to concentrate NH_3 in a high pH stream within the scope of the *N2kWh* project. One objective is to compare this solution with the alternative combination of regular ED (for the removal/concentration of nitrogen) and chemicals addition (for the pH regulation). Because of its large use in water treatments [28], sodium hydroxide ($NaOH$) is chosen as the caustic base for the pH regulation. Particular attention is given to the energy consumption for the removal of NH_4^+ as well as to the efficiency of pH change (or water dissociation) and NH_4^+ transport. Moreover, a study of the side-processes in the BPMED and their effects on the its performance is undertaken.

From these objectives the following research question is derived:

"Is electrodialysis with bipolar membranes an energetically valuable alternative to the combination of regular electrodialysis and $NaOH$ for the recovery of NH_3 from the reject water of digested sludges, within the N2kWh project scope?"

This research is conducted by performing experiments on ED and BPMED lab-scale installations, utilizing as baseline feed water a synthetic wastewater composed of demiwater with 6.6 $g \cdot L^{-1}$ of NH_4HCO_3. This ammonium bicarbonate concentration is used because it is comparable with the reject water from digested sludge from a conventional WWTP.

1.5.2. Research approach and sub-research questions

Through a literature study, the overall operation and the side-processes taking place in BPMED operation are described and characterized (chapter 2). This permitted to draw hypotheses on the expected behaviour of the installation for the defined conditions. Based on these, specifically designed experiments (described in chapter 3) on three different setups are performed. The results of these experiments are then discussed (chapter 4) and the main conclusions are drawn in order to answer the sub-research questions (chapter 5). Finally, in accordance with the study findings, recommendations on additional studies and potential improvements in the design of the installation are provided in chapter 6.

Based on literature findings and on the above-defined main research question, five sub-research questions are formulated. These create a structured investigation framework that enables an in-depth study of the different aspects related to answering the main research question.

1. Which are the factors and the secondary processes that influence the pH regulation efficiency in the BPMED system?
2. For which processes and to what extent energy is required in the BPMED operations?
3. How and to what extent gas diffusion affect the performance of BPMED?
4. Is it possible to limit gas diffusion by stripping dissolved gases from the concentrates of the BPMED system?
5. Which configuration, chemicals coupled with ED or BPMED, is more energetically favorable for the recovery of NH_3 in the considered stream?

The above-listed sub-research questions are ordered according to a logical sequence. In other words, the answer to the second question is influenced by the outputs of the previous sub-research question, and so on.

2

Theoretical background

2.1. Electrodialysis

Electrodialysis is a membrane separation technique where ion exchange membranes (IEXs) in combination with an electrical potential are used to remove ionic species from an aqueous solution. Differently, from ion exchange columns, no ions on the membrane surface are exchanged with ions in solutions. These membranes consist of highly swollen polymeric structures carrying positive or negative charges [23]. Depending on the surface charge, the membranes are preferentially permeable for only certain ions. This property is referred to as permselectivity [14]. Based on the permselectivity, it is possible to identify different types of membranes. For instance, anion exchange membrane (AEM) and cation exchange membrane (CEM) ideally allow respectively only negatively or positively charged ions to pass the membrane.

In conventional ED, AEM and CEM are arranged in an alternating pattern between an anode and a cathode and separated by flow-spacers to form individual cells. During operation, an electrical potential is established between the membrane stack-ends by means of two electrodes. This potential provokes the ions to move through the membranes. The cations migrate towards the cathode and the anions towards the anode. Thanks to the particular sequence of the membranes, ions are transferred from one solution to the other, leading to concentration of one stream and the dilution of the other. A schematic overview of this process is shown in Figure 2.1. The stream depleted from the ions is named **diluate** whereas the stream that is enriched is usually referred to as **concentrate**.

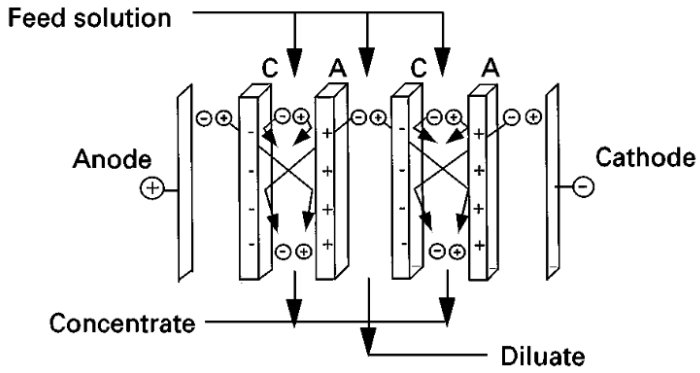

Figure 2.1: Schematic diagram illustrating the principle of ED. In the chamber next to the electrodes the ERS is internally recirculated. Image retrieved from Strathmann [14, p.1708].

At both electrodes, an electrode rinse solution (ERS), generally characterized by a relative high electrical conductivity (EC), allows the transfer of current from the electrodes to the stack. This solution is separated from the rest of the stack by two CEMs addressed as cation exchange end membranes (CEEMs). A scheme of the main elements of an ED cell and stack is depicted in Figure 2.2

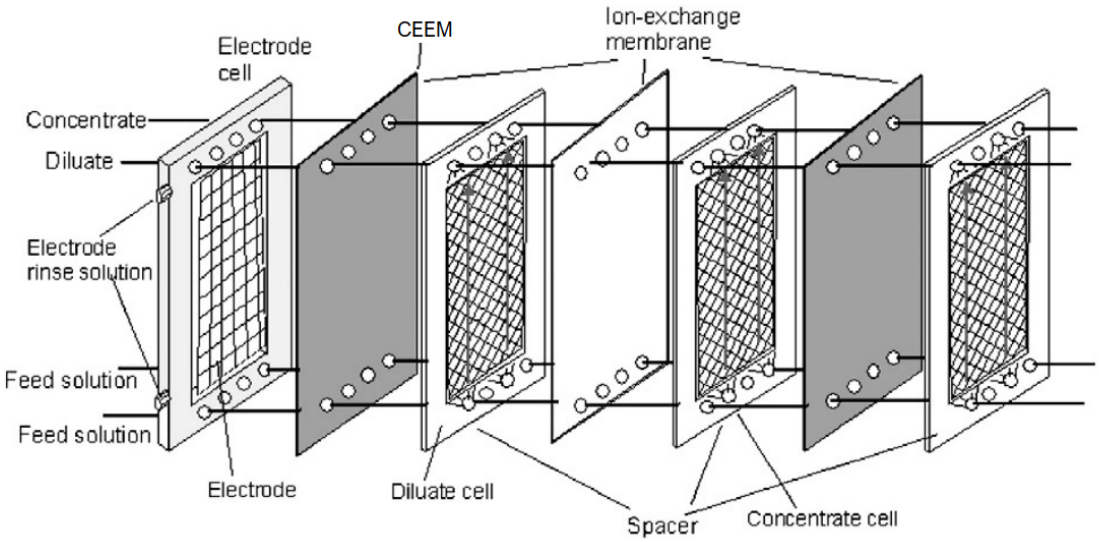

Figure 2.2: Scheme illustrating the main elements arrangement and the stack design in conventional ED. Retrieved and adapted from Strathmann [23, p.270]

2.1.1. Current-voltage curve and electrical resistance

During ED operation an electrical potential (or voltage) is established between the two electrodes. In any conductor, the electrical current I (expressed in Ampere $[A]$) is proportional to the electrical potential driving force (U) according to Ohm's law, which relationship is given by:

$$U[V] = R \cdot I \tag{2.1}$$

R is the electrical resistance. Its value is a function of the specific resistance of the material, the distance between the electron source (the electrodes in this case), and the cross-section area of the material through which the electrical current passes.

From this definition, it is clear that every element, and stream that composes the ED installation, has a certain Ohmic electrical resistance. The total resistance of the stack can be seen as the sum of the resistances of the different ED-unit components. This is shown in Equation 2.2

$$R_{tot}^{ED} = R_{elec} + n \cdot R_{dil} + n \cdot R_{conc} + (n-1) \cdot R_{CEM} + n \cdot R_{AEM} + 2 \cdot R_{CEEM} + 2nR_{sp} \tag{2.2}$$

Where, R_{elec} is the resistance of the electrodes and electrode rinse solution, R_{dil} is the resistance of the diluate, R_{conc} is the resistance of the concentrate. R_{CEM} is the resistance of CEM, R_{AEMs} is the resitance for an AEM and R_{CEEM} is the resistance of the CEEM. n is the number of cell pair, whereas R_{sp} is the ohmic term that accounts for the flow spacer resistances and for the additional resistance brought by side-phenomena occurring in stack (e.g. concentration polarization).

The resistance of the streams in the ED can be calculated as in Equation 2.3.

$$R_s[\Omega] = \frac{1}{EC_s} \cdot \frac{W_s}{A_m} \tag{2.3}$$

Where, EC_s is the electroconductivity of the stream expressed in $[S \cdot m^{-1}]$, W_s is the width of the chamber, that can be assumed equal to the thickness spacer, and A_m is the membranes surface.

Both the current and the voltage (and thereby the stack resistance) are related to the energy consumed in the ED cell. The energy consumed (E) is a function of the applied power (P) and time (Δt), as shown in Equation 2.4

$$E[Wh] = P \cdot \Delta t \tag{2.4}$$

Since the power is the product between current and voltage, Equation 2.4 can be reformulated as follow:

$$E[Wh] = U \cdot I^2 \cdot \Delta t \tag{2.5}$$

Equation 2.5 emphasizes the crucial effect of applied current on energy consumption. The applied current I is directly related to the active surface of the used electrodes (S_{elec}). This makes more complicated to compare different ED installations. For this reason, the concept of electrical current density (i), defined as in Equation 2.6, is generally prefered in literature.

$$i[A \cdot m^{-2}] = \frac{I}{S_{elec}} \tag{2.6}$$

2.1.2. Concentration polarization and limiting current density

In conventional ED, concentration polarization (CP) occurs as a result of the different rate of ion transport between the bulk solution and the membrane. When the ion transport rate is lower in the solution than through the membrane, the ions concentration in the diluate drops at the surface of the IEX facing the diluate solution. This results in a concentration gradient between the membrane surface and the well-mixed bulk. This concentration gradient increases diffusive ion transports toward the membrane interfaces in the diluate. A steady-state situation is obtained when the diffusive transport supplies enough ions to balance those removed from the interface through the transport rate in the membrane [23].

The rate of ions transported across the membranes depends on the i applied to the cell. For this reason, the development of CP in ED is strictly related to the current applied and, of course, to the ions concentration in the streams (often expressed as electrical conductivity). In ED operation, it is possible to define a limiting current density (LCD), which is reached when the ion concentration at the membrane surface approaches 0 as a result of the ion depletion. When the LCD is reached a further increase of the voltage does not produce an increase in the current. This situation is shown in Figure 2.3.

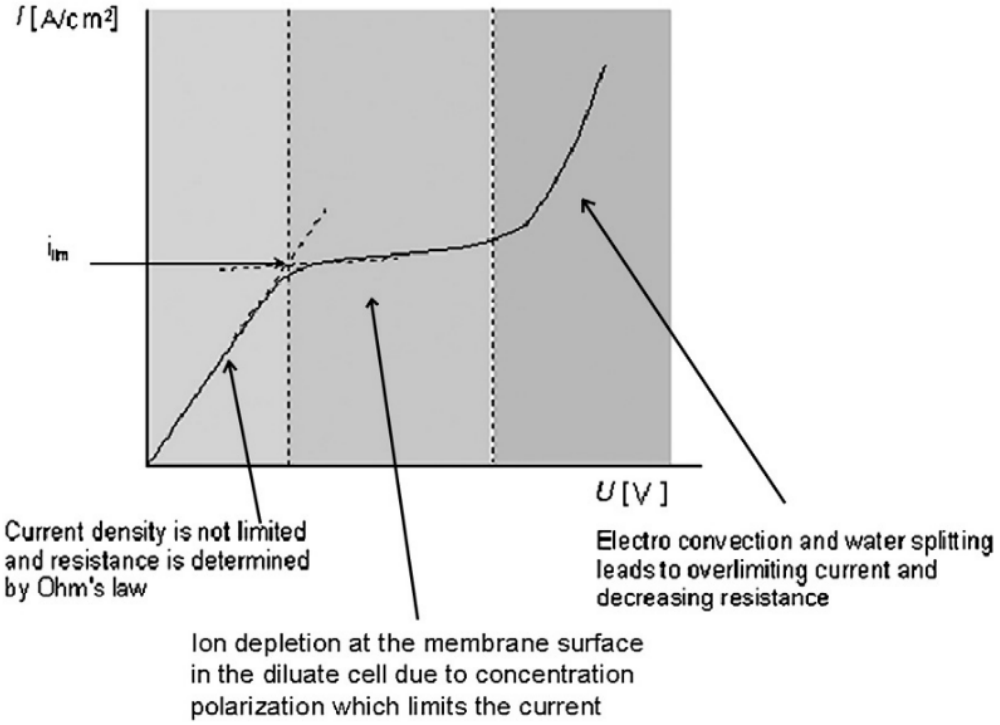

Figure 2.3: Example of current-potential curve in ED operated at constant flow velocities and diluate concentrations. The y-axes represents the applied current density i $[mA \cdot cm^{-2}]$ and the x-axes is the potential U [V]. After the LCD a further increase of the voltage does not results in a rise of the current density. Retrieved from Strathmann [14, p.272].

The LCD is a function of the solution flow velocity, spacer configuration, solution conductivity,

membrane properties, hydrodynamic conditions and other minor design parameters [11, 29]. Thus, it is complicated to theoretically calculate the LCD. In practice, the LCD is determined empirically. The LCD experimental determination has led to a widely accepted equation [29], where it is expressed as a function of the flow velocity and solution concentration:

$$i_{lim} = a u^b C_s^d \tag{2.7}$$

C_s^d is the concentration of electrolyte in the diluate chamber, u is the linear flow velocity in the cells parallel to the membrane surface, a and b are coefficients that are determined by measuring the limiting current density at various linear flow velocities [29].

2.2. Electrodialyisis with bipolar membranes

Conventional ED, when combined with particular membranes (named bipolar membrane), enables to produce acid and base from the corresponding salt [23]. This solvent splitting technique is named electrodialysis with bipolar membranes (BPMED or EDBPM) and it is widely recognized as an energy-efficient means for converting salts to their corresponding acids and bases [22]. This section elaborates on the characteristic of this particular membrane and on its arrangement within the ED cell.

2.2.1. The bipolar membrane

A bipolar membrane is a composed membrane consisting of a cation-selective membrane (with negative fixed charges layer) and an anion-selective layer (with positive fixed charges) [30]. In between these membranes an interface layer, generally referred to as transition layer, is present. This particular configuration allows the membrane to carry out the dissociation of water in presence of an electrical field [31]. When a direct current is applied toward the cathode, electrical conduction is achieved by the transport of H^+ and OH^- ions, which are obtained from the dissociation of water [22, 32].

A schematic representation of BPM components and of the water dissociation process is shown in Figure 2.4

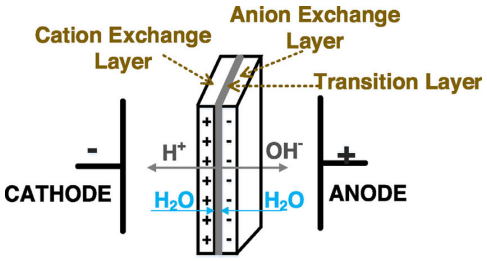

Figure 2.4: Structure of bipolar membrane and its operation. Scheme retrieved from Haddad *et al.* [33, p.70].

Under an applied electrical current, electrolyte concentration in the transition layer decreases and the electrical potential over the BPM increases. When the so-called water dissociation potential is reached, the electric field at the contact of the two bipolar membrane layers is strong enough to separate the OH^- ions and the H^+ [34].

According to Mani [32], in order to obtain a high energy-efficient operation, the membrane should have:

- a good water permeability to provide water from the external solutions to the transition layer
- a very thin transition layer between anion and cation regions to allow efficient transport of H^+ and OH^-. [32]

In literature often the limiting current density of a BPM refers to the i that is needed to make the flux of water leaving the transition layer as dissociated ions higher than the flux of water entering into the same layer. This is independent of the diluate flow-rate because it is a result of the internal CP within the membrane transition layer itself [34, 35]. To avoid confusion, in this document, this limiting current density will be indicated as i_{lim}^{BPM}. According to Pourcelly [35] i applied in this study is several order of magnitude lower than i_{lim}^{BPM} for commercial BPMED. Hence, i_{lim}^{BPM} will not be a concern in this study.

2.2.2. Streams configuration and operation

By changing the order and the type of membranes in the stack different stream configurations can be obtained. Generally, it is possible to distinguish between two main types of membrane arrangements [30]: two-compartments configuration and three-compartment configuration.

The two-compartment configuration consists of a BPMs operating in conjunction with only CEMs or AEMs. According to which membrane is used, they are categorized in two-compartment cation cell or anion cell , respectively.

The two-compartment arrangement has a simple structure and a lower resistance thanks to the lower number of streams and membranes [22, 27, 32]. However, as a result of the membrane arrangement, the two-compartment configuration allows the generated H^+ to recombine with the generated OH^- [36]. Thanks to its membrane sequence, shown for a general salt M^+X^- in Figure 2.5, the three-compartment stack is theoretically free from this problem. Furthermore, in literature is stated that BPMED with this membrane arrangement, can achieve higher concentration for the acid and/or base production [32, 36]. In the three-compartment BPMED, as shown in Figure 2.5, the salt MX is fed to the chamber between the cation and AEMs. When an electrical current is passed across the stack, the cations (M^+) and anions (X^-) move across the monopolar membranes to the acid and base stream to balance the applied charge [23]. Differently from the regular ED, in the BPMED two different concentrates are formed.

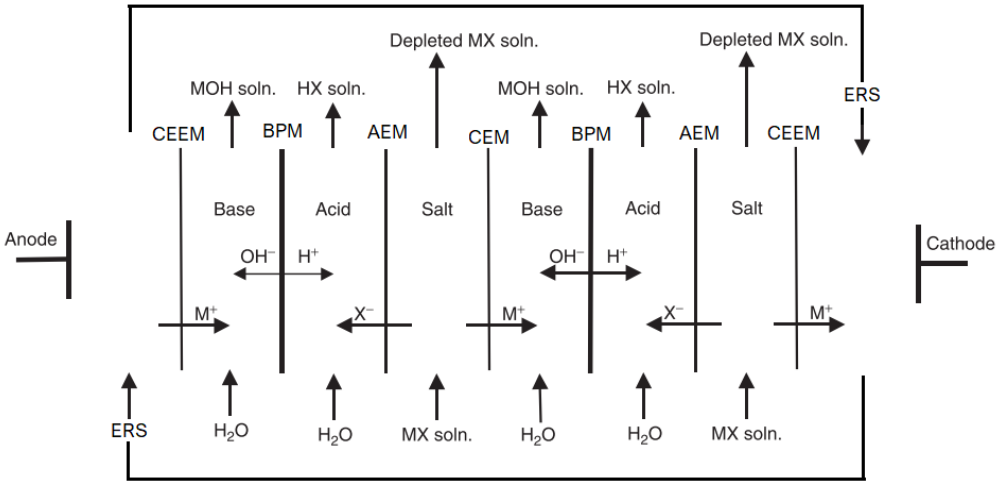

Figure 2.5: BPMED three-compartment essential membrane scheme. The ERS is internally recirculated through the cathode anode chambers. Image retrieved and adapted from Tanaka [22, p.407].

For making possible the recovery of NH_3, it is important to achieve a high concentration of NH_4^+ in a high pH stream. For this reason, the three-compartment membrane configuration (Figure 2.5) was preferred for this application.

2.3. Key performance parameters

In order to monitor the performance of the BPMED for NH_3 recovery, and to compare it to other studies and competing technologies, three fundamental performance parameters are selected. These are:

- Current efficiency for salt transport
- Current efficiency for water dissociation
- Energy consumption for NH_4^+ removal

These parameters are described in the following sections.

2.3.1. Current efficiency

When ions migrate through a membrane from one solution to another, the average current efficiency, during an interval Δt, is the ratio of the equivalent number of the ions removed from the feed solution during Δt and the total amount of charge passed through the membrane.

The concept of current efficiency is used in order to describe the performance of the membranes for a specific process during diverse operating conditions. In the following two subsections the current efficiency for NH_4^+ transport and for water dissociation are described. Moreover, the factors that influence their value are analyzed.

Current efficiency for salt transport

When current is applied to an ED stack the passage of current throughout a membrane is obtained by the transport of ions across the membrane. The ratio between the amount of charge transported as NH_4^+ across the membrane and the total charge applied is referred to as the current efficiency for NH_4^+ transport or removal ($CE_{NH_4^+}$).

$$CE_{NH_4^+}[\%] = \frac{F \cdot z \cdot (M_{\Delta t}^{NH_4^+} - M_o^{NH_4^+})}{\Delta t \cdot n \cdot I} \cdot 100 \tag{2.8}$$

Where $M_{\Delta t}^{NH_4^+}$ is the number of transported moles of NH_4^+ after the period Δt; $M_o^{NH_4^+}$ is the initial number of NH_4^+ moles in the solution; F is the Faradays constant $[s \cdot A \cdot mol^{-1}]$; z is the charge of the target ion (for NH_4^+, z=1); n is the number of membrane pairs (or triplets) considered; and I is the current applied to the stack. In other words, $CE_{NH_4^+}$ determines the percentage of current that is used specifically for the transport of NH_4^+. The current efficiency for NH_4^+ transport is negatively influenced by:

- the presence of other cations in the fed water.
- the ion (and gas) diffusion from the concentrates to the diluate as consequence of the no-perfect permselectivity of the CEMs.

In this case, the current efficiency is expressed for NH_4^+ transport. Nonetheless, the presented concept can be easily extended to every ion in the treated solution.

Current efficiency for water dissociation

Differently to what observed in regular ion exchange membranes (IEXMs), in an ideal BPM, the applied current is mostly transported by ions resulting from the dissociation of water [37]. It is possible to define a current efficiency for the water dissociation in BPM (Equation 2.9).

$$CE_{WD}^{act}[\%] = \frac{F \cdot (H_{\Delta t}^+)}{\Delta t \cdot n \cdot I} \cdot 100 \tag{2.9}$$

Where, $H_{\Delta t}^+$ is the number of H^+ actually produced in Δt. This percentage represents the fraction of the applied current that is actually carried by the ions generated in the BPMs.

In practice, CE_{WD}^{act} is generally lower than 100%. This is due to the undesired transport of co-ions through the BPMs because of the incomplete permselectivities of the ion-exchange layers of the bipolar membrane. This parasitic process has been proved to be more severe with the increase of acid and base concentration [23].

Figure 2.6 shows a scheme of the co-ions leakage through the bipolar membrane as result of the incomplete permselectivity of the BPM.

In the "undesired" case that the current is transported by NH_4^+ and HCO_3^-, the H^+ and OH^- are not produced in the transition layer. Co-ions diffusion also impacts the contamination of the products (acid and base) which consequently also increases with the acid and base concentrations [23].

Not all the H^+ and OH^- produced in the bipolar membrane influence the pH in the acid and the base stream. Part of them is neutralized by other processes occurring in the membrane stack (*i.e.* gas diffusion and H^+ or OH^- leakages). It is then significant, to introduce a parameter that can express only the part of the current that is actually contributing to pH changes in the cell streams. This document will refer to this parameters as *"measured current efficiency for water dissociation"* (CE_{WD}^{meas}). For a time period Δt, CE_{WD}^{meas} can be calculated as in Equation 2.10 [24, 38].

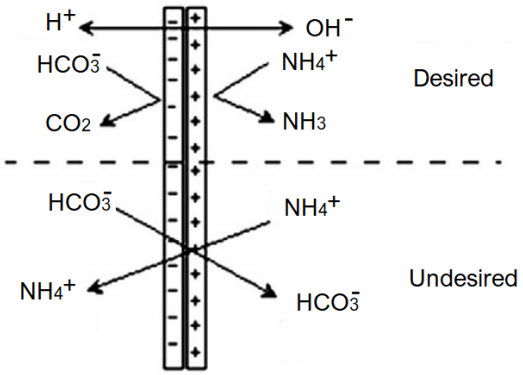

Figure 2.6: Mechanism of contamination of acid and base by salt due to the low permselectivity of the bipolarmembrane for salt ions at high concentration. Retrieved and modified from Strathmann [23, p.279].

$$CE_{WD}^{meas}[\%] = \frac{F \cdot z \cdot (M_{\Delta t}^{H+} - M_{o}^{H+})}{\Delta t \cdot n \cdot I} \cdot 100 \tag{2.10}$$

Where, M_o^{H+} is the initial number of H^+ moles and $M_{\Delta t}^{H+}$ is the number of moles after Δt, n is the number of membrane triplets and I is the applied current.

In all the studies mentioned in chapter 1, subsection 1.4.1, it is argued that the use of a controlled high i brings important benefit to acid-base generation performance in BPMED. Indeed, it accelerates the transmembrane migration of ions and the dissociation of H_2O in BPMs minimizing the effect of the side diffusion processes on the operation efficiency.

2.3.2. Energy consumption for ammonium removal

Within the *N2kWh* project the energy use for the removal of N is a fundamental parameter. In this research, this parameter is expressed as energy consumed per kg of NH_4^+ removed $[MJ \cdot Kg_{NH_4^+}^{-1}]$.

This parameter is calculated as in Equation 2.11:

$$E_{NH_4^+} = \frac{\sum_{n=1}^{i} \Delta P_i \cdot \Delta t_i \cdot 3.6}{\Delta M_{NH_4^+}} \tag{2.11}$$

Where P_i is the electrical power applied to the ED in an interval Δt_i, $\Delta M_{NH_4^+}$ is the variation in NH_4^+ mass in the diluate (or feed) stream. The term 3.6 is a coefficient included in Equation 2.11 to convert the energy consumption from $kWh \cdot Kg_{NH_4^+}^{-1}$ to $MJ \cdot Kg_{NH_4^+}^{-1}$.

In this document, the energy consumption for operation only takes into account the power spent in the ED process. Energy for pumping and for other supporting devices is not considered in the calculation.

2.4. Processes in electrodialysis with bipolar membrane

BPMED is a complex system where several processes occur, influencing each other and playing a role in the overall performance of the device. This section gives an introduction to these processes and their influences on BPMED performance.

2.4.1. Ion electro-migration

To remove salt from a solution in IEX separation processes, ions need to be transported from a solution (diluate or feed water) through a membrane into another solution (concentrate).

The transport rate of the ions is determined by kinetics as well as thermodynamic parameters. The kinetic parameters are related to the mobility and diffusivity of the ions in the membrane matrix and in the electrolyte solution. The thermodynamic parameters are expressed by the voltage (U), which is the driving force necessary to overcome the resistance offered by the membrane and the electrolyte.

An important boundary condition in ED process is given by the electroneutrality requirement which postulates that there is no excess in negative or positive charge in ED chambers. As a result of that, although cations and anions can be considered as independent elements in an electrolyte solution, their fluxes are related in such a way that there is no accumulation of charges on a macroscopic scale.

2.4.2. Water dissociation

One of most remarkable properties of pure water is that it dissociates to form hydrogen ions (H_3O^+, or in the non-hydrated form H^+) and hydroxide (OH^-) ions. This reaction is shown in Equation 2.12.

$$2H_2O \rightleftharpoons H_3O^+ + OH^- \tag{2.12}$$

When an electrical potential field is applied to the water, the water-dissociation reaction is expected to arise. The reaction rate increases along with the rise in the electrical potential gradient (U) [39].

Water dissociation in bipolar membrane

When an electrical current I is applied to the BPM, initially, the ions concentration in the transition layer of the BPM declines as a result of the migration of ions toward the pole with opposite charge. During this phase, water dissociation does not occur until i reaches the value of the LCD in the transition layer [22, 32].

Once the LCD is exceeded in the transition layer ($i > LCD$), the transport of electrical charge across the BPM cannot occur anymore via salt ions. In this situation, water dissociates and the current transport is accomplished by H^+ and OH^- ions [30]. Due to the dissociation equilibrium, H^+ and OH^- removal will continuously be replenished by water entering into the transition layer. The net result of this process is that an alkaline solution is formed on the cathode side of the membrane and an acid solution is created in on the anode side of the BPM.

The Gibbs free energy change that occurs from the internal part of the BPM to the outside during the water dissociation process is given by Equation 2.13:

$$-\Delta G = nFU_r = RTln[(a_H^i + a_{OH}^i)/(a_H^0 + a_{OH}^0)] \tag{2.13}$$

Where a is the activity of the H^+ and OH^- ions, the superscripts i and o refer to the interface and the outer of the membrane respectively, U_r is the reversible electromotive force $[V]$, R is the ideal gas constant, n, in this case, represents the number of $eq \cdot mol^{-1}$ of reactant and T is the temperature in Kelvin. Therefore, the potential necessary for water dissociation is a function of the pH gradient between the transition layer and the acid and basic streams. This relationship is shown in Figure 2.7

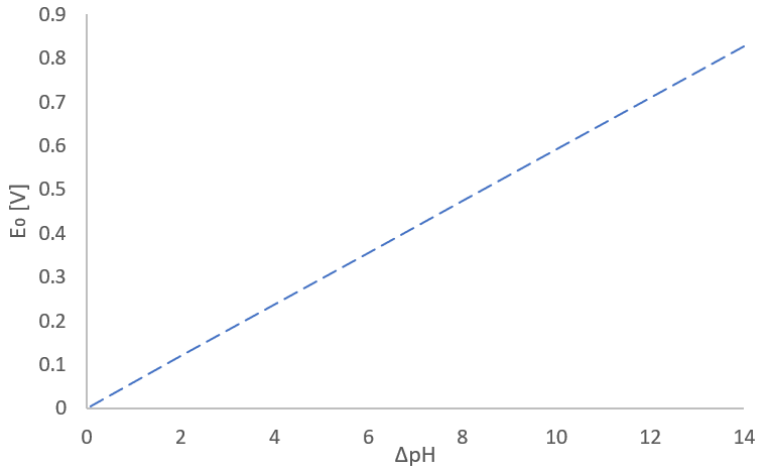

Figure 2.7: Theoretical potential U_0 for different pH gradient between acid and base stream.

For generating 1 M product solution, and assuming a concentration of approximately $10^{(-7)}M$ of H^+ or OH^- and a temperature of 25 °C in the BPM's interface, Equation 2.13 reduces to Equation 2.14:

$$\Delta G = -FE = -RTln(a_H^i + a_{OH}^i) \qquad or \qquad E = \frac{-RT}{F} lnK_w \tag{2.14}$$

In this ideal condition, to overcome this chemical potential an electrical potential of $U_0 = U_r$ has to be applied across the membrane. Through the values of Gibbs free energy for dissociation of water, the theoretical potential for generating acid and base for an ideal (i.e. perfectly permselective) BPM can be calculated equal to 0.828 V [32].

The above calculated U_0 is a theoretical value. In practice, the potential U_r necessary for water dissociation (considering the same pH difference) will be slightly higher, since the H^+ and OH^- ions have to be transported through the cation and the anion side of the BPM, respectively [40].

2.4.3. Osmosis and electro-osmosis

The IEXMs used in ED are specifically designed to reject non-charged molecules, like water. However, several studies and full-scale application showed that during ED process, via osmosis phenomena, water is transported across the membranes [11, 29, 41]. Water transport was proved to limit the applicability of the ED as a method of concentrating electrolyte solutions [11, 19, 20, 41].

The main mechanisms for water transport during ED are osmosis and electro-osmosis [29]. Osmosis is caused by the electrolyte concentration difference between the diluate and concentrate chambers (in case of BPMED between the diluate and base/acid). Galama *et al.* [20] calculated the amount of water transported by osmosis (in mol) with the Equation 2.15:

$$\Delta M_w = D_w \frac{A(C_c - C_d)}{\delta} \cdot \Delta t \tag{2.15}$$

Where D_w is the osmotic water transfer coefficient $[m^2 \cdot s^{-1}]$, A is the membrane area $[m^2]$, C_c and C_d are the concentrations of concentrate and dilute $[mol \cdot m^{-3}]$, respectively, δ is the membrane thickness $[m]$ and Δt is the considered time interval $[s]$.

Electro-osmosis accounts for the water bound to ions transported via ionic migration. It takes place whenever ions are passing through the membrane and it has a minimum flux corresponding to the water in the primary hydration sphere of the ions [20]. As a consequence, the amount of water transported via electro-osmosis is proportional to the amount of transported ions and it is different for each salt, as hydration numbers of salts are different [11, 29]

Water molecules in the first hydration are tetrahedrally coordinated to the NH_4^+ ion [42]. In other words, for each mole of NH_4^+ passing the membrane, four moles of H_2O are also transported. For bicarbonate, seven moles of water pass the membrane for each mole of HCO_3^- [43]. This means that for each mole of transported NH_4HCO_3, eleven moles of water are transported.

2.4.4. Ion diffusion in ion exchange membranes

Diffusion is the movement of particles from an area of high concentration to an area of lower concentration [44]. Due to the non-ideal selectivity of IEXMs, when a concentration gradient is established between two adjacent chambers, ions tend to diffuse through IEXMs[45]. In BPM, this process generally results, not only in a loss of current efficiency for the H^+ and OH^- ion generation but also to a lower degree of purity of the produced acid and base [20, 45]. In regular IEXMs, ions generally diffuse from the concentrate to the diluate reducing the current efficiency of salt transport. Indeed, the ions that diffused back to the diluate need to be transported again, and this requires extra-current. In this report, this process is addressed to as **ion back-diffusion**, or more simply, back-diffusion.

Similarly to what observed for osmosis, there are two factors playing a role in ion diffusion:

- The ion concentration gradient across the membranes
- The available diffusion time

At a low i, the ion back-diffusion will be relevant compared to the migration of ions in the opposite direction, because of the long runtime. This is a consequence of the competition between diffusion phenomena, depending on residence time, and migration, depending on i [25]. For this reason operating at a higher i (but below the LCD) leads to an increase of the current efficiency for ion migration [20]. The ion back-diffusion rate varies for different ions and employed membranes [46].

2.4.5. Co-ions leakages across the bipolar membranes

The leakage of ions through the BPM is usually addressed to as **co-ions leakage**. This process is related to the imperfect permselectivity of the BPMs and it is responsible for the non-ideal behaviour of the membranes. The main consequences of co-ions leakage are the reduction of CE_{WD}^{act} and the limiting of the acid and base concentration [34, 37, 39]. The permselectivity of the ion-exchange layers decreases with increasing acid and base concentration. Hence the co-ions diffusion rate increases with the acid and base concentrations [14]. Strathmann [23] showed with an empirical example the increase of salt concentration (which are considered impurities in the acid and base streams), in this case Na_2SO_4, as a function of the acid and base molarity(Figure 2.8).

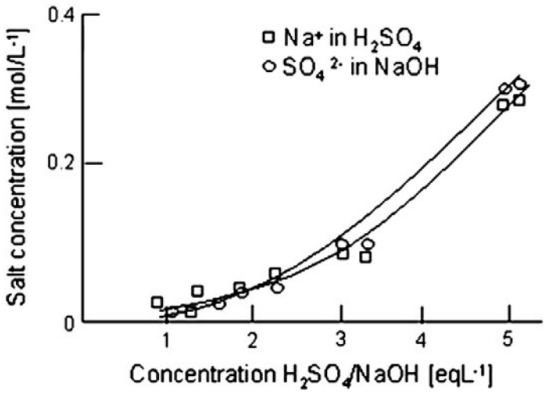

Figure 2.8: Graph illustrating the experimentally determined salt concentration as a function of the acid and base concentration during the acid and base recovery from a Na_2SO_4 solution.Image retrieved from Strathmann [23, p.279].

When co-ions pass across the BPM, they carry current. Hence, water doesn't need to be dissociated in the BPM's transition layer. For this reason, this mechanism limits the H^+ and OH^- electro-generation and thereby the CE_{WD}^{act} [47]. This fact has been proven by Moussaoui *et al.* [38] who correlated the reduction of CE_{WD}^{act} with the concentration of acid and base (in this case for a $NaCl$ solution) for different current densities (Figure 2.9)

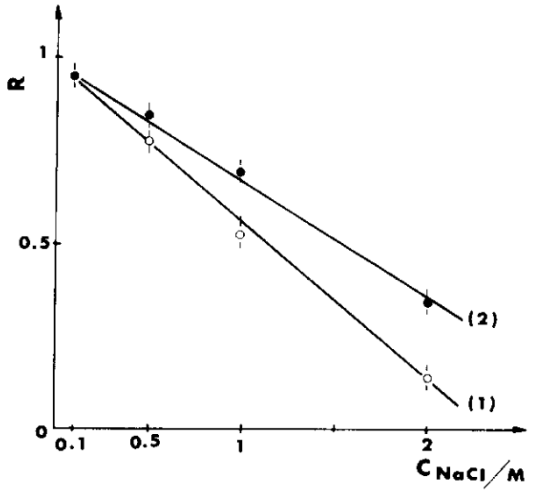

Figure 2.9: Water dissociation current efficiency as a function of the acid and base concentration for 2 different current densities during the acid and base recovery from a $NaCl$ solution. Line (1) is drawn applying a current of 50 $mA \cdot cm^{-2}$, Line (2) 100 $mA \cdot cm^{-2}$. Image retrieved from Moussaoui *et al.* [38, p.286].

Figure 2.10 shows that for each $NaCl$ concentration, the Na^+ flux throughout the BPM rises as the i increases. The increase is not linear with i but it flattens. Therefore, by increasing the i the effect of co-ions leakage on the CE_{WD}^{act} is expected to drop. This is also shown in Figure 2.9.

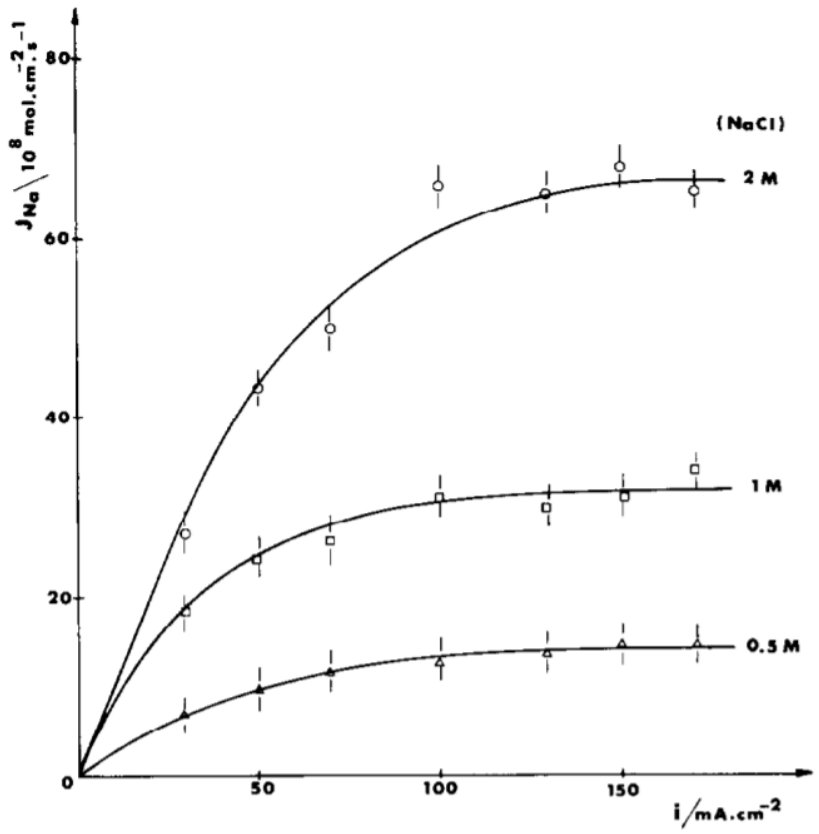

Figure 2.10: Unidirectional flux of sodium ions through the bipolar membrane versus current density for different $NaCl$ concentration. Image retrieved from Moussaoui *et al.* [38, p.288].

A similar study, conducted by Sun *et al.* [48], estimated that the water dissociation current efficiency of a 1M solution ranges between 73% and 98.3% when the i varies between 0.5 $mA \cdot cm^{-2}$ and 25 $mA \cdot cm^{-2}$. This result was obtained for a multi-salt solution. Vermaas *et al.* [49] showed that the co-ion permeation through BPMs is different for different ions but similar in terms of magnitude. Thus, the findings of Sun *et al.* [48] can be reasonably extended to the ions involved in this work.

2.4.6. Gas diffusion across ion exchange membranes

The diffusion flux of gases (J) in liquid media (**gas diffusion**) is described by the first Fick's law (Equation 2.16) [50]:

$$J = -D\nabla\varphi \tag{2.16}$$

Where, J $[mol \cdot m^{-2} \cdot s{-}1]$ is the amount of substance moving per unit of an area during a time interval, D $[m^2 \cdot s^{-1}]$ is the gas diffusion coefficient and φ is the concentration (usually expressed in $mol \cdot m^{-3}$). D depends on the temperature, viscosity of the fluid and the size of the particles. This means that each gas has its own diffusion capacity in water at a constant temperature.

Assuming a perfect mixing in each chamber of the stack, the concentration gradient $\nabla\varphi$ is the difference in concentration between two adjacent solutions. In the ED, the membrane active surface represents the diffusion interface. Due to the configuration of the membrane stack the gas diffusion flux develops along only one dimension. Equation 2.16 can be then simplified as follow:

$$J = -D\frac{d\varphi}{dx} \tag{2.17}$$

Since in ED, membranes active surface represents the diffusion interface, the diffusion coefficient D is also dependent on the properties of the membrane. An overall mass transfer coefficient (K_{mbr})

(unit $s \cdot m^{-1}$), which includes the resistance of the membrane to gas diffusion, can be introduced and Equation 2.17 be rewritten as follow:

$$J = -K_{mbr}\Delta P \tag{2.18}$$

Where ΔP is the difference in saturation vapour pressure (in Pa) for a certain gas between two adjacent chambers of a membrane stack.

2.4.7. Proton and hydroxide leakage across ion exchange membranes

Besides the co-ions leakage across the BPMs described in subsection 2.3.1, the CE_{WM}^{meas} (Equation 2.10) is limited by the non-ideal permselectivity of the IEXMs, which separate the concentrate streams from the diluate. Permeation of H^+ through the AEMs, and of OH^- through CEMs for extreme pH is recognized to limit the CE_{WM}^{meas} [51, 52]. A scheme of this process is depicted in Figure 2.11

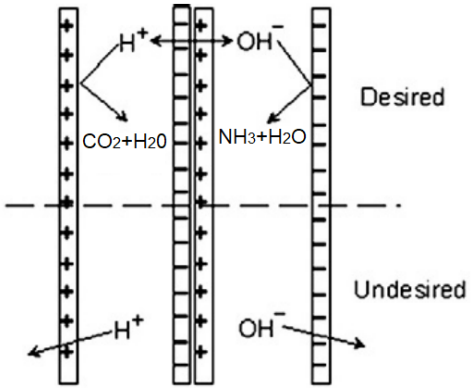

Figure 2.11: Mechanism of H^+ and OH^- leakage through the IEXs. Retrieved and modified from Strathmann [23, p.279].

The transport rates of ions in a solution or across a membrane are proportional to their permeabilities in the solution and in the membrane [14]. The permeability is the product of the ion concentration and mobility. The mobility of different ions in aqueous solution does not differ very much from each other. Exceptions are H^+ and OH^-. Their mobility is an order of magnitude higher than other ions. Although the introduction of so-called acid and base membranes resulted in a substantial improvement [53], at high acid and base concentration (low and high pH respectively), the retention of AEMs for H^+ ions and that of CEMs for OH^- ions is usually poor [23]. This is because their transfer across IEXMs occurs via two mechanisms:

- the regular ion diffusion
- the Grotthus mechanism, when the H^+ and OH^- are transported through the wet IEXMs by migrating from one water molecule to another (so-called tunnel mechanism)

The net result is that H^+ and OH^-, generated in the bipolar membrane, leak to the diluate neutralizing each other and reducing the measured water dissociation current efficiency [25]. Generally this phenomenon is referred to as **proton and hydroxide leakage** and its mechanism is shown in Figure 2.12.

When a H^+ or a OH^- pass the IEXs membrane from the concentrate to the diluate, it transports charge throughout the stream. In other words, for every H^+ or OH^- leaking into the diluate one less salt anion is transported in the concentrate, reducing the current efficiency for salt transport [52]. Moreover, once the H^+ or OH^- ended in the diluate, if they does not recombine, they will compete with the salt cation to be transported into the base stream. This will further reduce the current efficiency for the salt transport.

Besides concentration and membrane permeselectivity, H^+ and OH^- leakage is influenced by the temperature of the solution. It is expected to be higher for higher temperature [54].

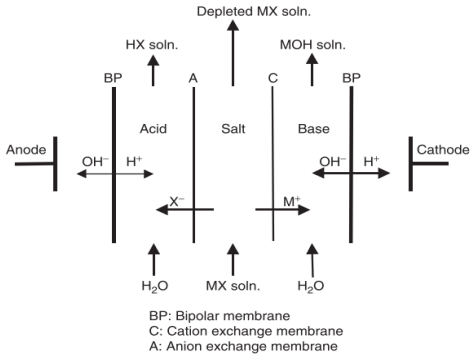

(a) When current is applied across the membrane triplets the bipolar membrane generate ions. At the same time, the salt present in the diluate migrate into the concentrate. The migration of salt ions is balance by the production of H^+ and OH^-.

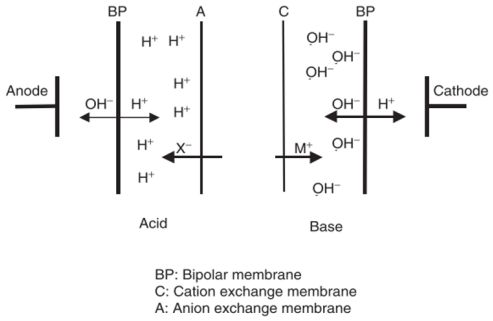

(b) Over the run, the H^+ and OH^- accumulate in the acid and base stream. A concentration potential establishes between the concentrate and the base.

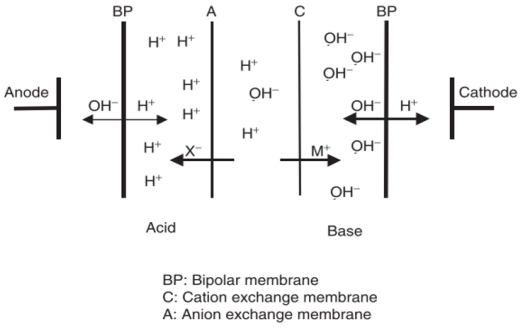

(c) Thanks to their high mobility and to the Grotthus mechanism, the H^+ and OH^- start leaking into the concentrate. This provokes a drop in the current efficiency for salt transport since charges are transported by the ions that migrate back to the diluate.

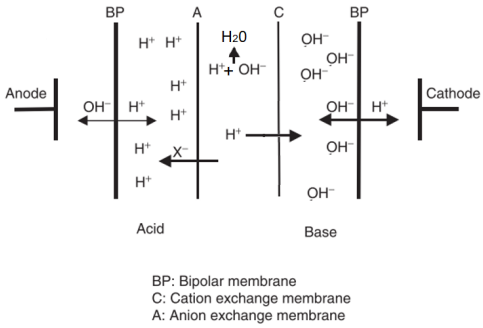

(d) In the diluate, the H^+ and OH^- generated by the BPMs can combine again reducing the water dissociation current efficiency. Alternatively, because of the electrical potential in the cell, they can transport current migrating from the diluate to the concentrates. This will further reduce the current efficiency for salt transport since the H^+ and OH^- directly compete with the salt ions.

Figure 2.12: H^+ and OH^- leakages and their effect on current efficiency reduction.

2.4.8. Processes overview

A schematic overview of the desired and undesired processes taking place in BPMED operation is presented in Figure 2.13.

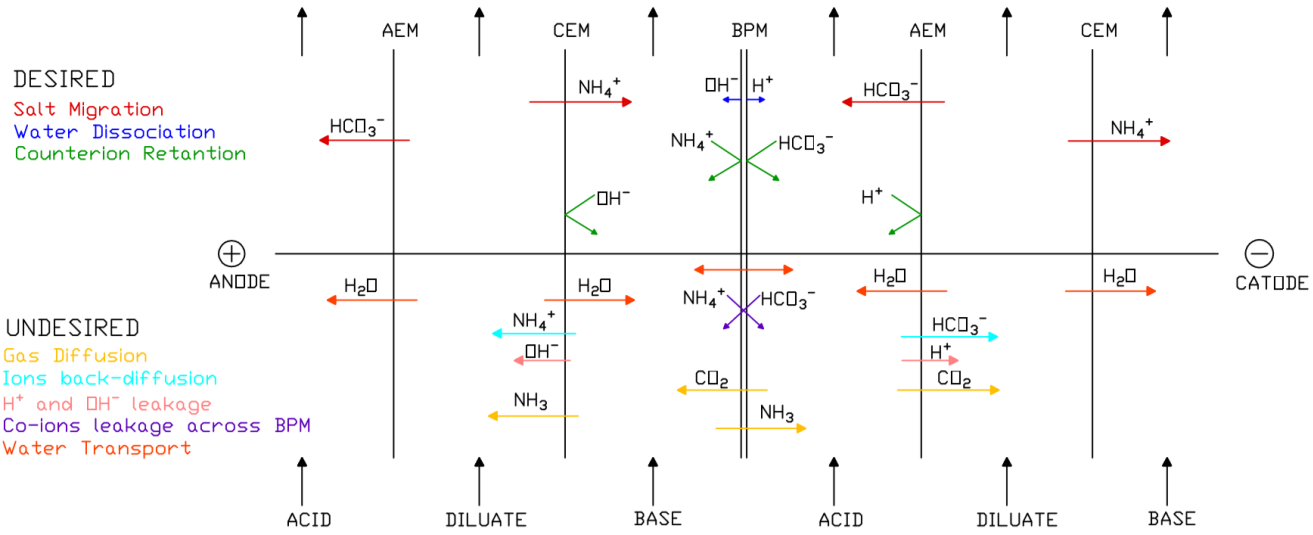

Figure 2.13: Schematic overview of the desired and undesired processes taking places in BPMED operation.

2.5. pH and pH regulation with sodium hydroxide

pH expresses the acidity of an aqueous solution. It is defined as the negative of the logarithm of the concentration of hydrogen ions [55].

The equation to determine the pH of an aqueous solution is shown in Equation 2.19

$$pH = -log[H^+] \tag{2.19}$$

It is also possible to express the ratio of water self-ionization in terms of OH^- concentration. In this case, we generally refer to the pOH, which is complementary to pH and can be calculated as shown in Equation 2.20

$$pH = -log[OH^-] \tag{2.20}$$

The relationship between pH and pOH is reported in Equation 2.21

$$pK_w[T = 25 \circ C] = pH + pOH = 14 \tag{2.21}$$

Where pK_w denotes the cologarithm of the self-ionization coefficient of water (K_w). pk_w is not constant but it depends on the solution temperature. Indeed, as mentioned before, the water self-ionization (Equation 2.12) is endothermic. In other words, for higher solution temperature the auto-dissociation of water is favoured, and more hydrogen ions and OH^- ions are formed. The effect of that is to increase the value of K_w as temperature rises. This means that for a higher temperature the pH will drop without an increase in the actual acidity of the solution. The value of pk_w expressed in Equation 2.21 is, thus, also dependent from the temperature of the aqueous solution. This relationship is shown in Figure 2.14:

The temperature effect on pK_w was considered when the OH^- concentrate was computed from the pH data.

pH regulation with sodium hydroxide

$NaOH$ is produced commercially in two forms: as 50 wt % water solution (the most common) and in the solid state (caustic soda) [28]. $NaOH$ production is mainly achieved via the electrolysis of sodium

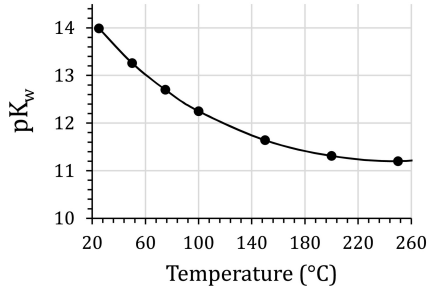

Figure 2.14: Ionization constant of water as a function of temperature Barclay *et al.* [56, p.55]

chloride solution (Chlor-alkali process) with mercury, diaphragms, or membrane cells [57]. The last method is the most used thanks to its lower energy consumption and environmental impact [28, 58]. More explanation on this process are provided in Appendix, section C.2.

Hong *et al.* [57] performed a life cycle analysis (LCA) of the 50 wt % water solution $NaOH$ produced by the chlor-alakali membrane process in China, which is the largest producer and consumer worldwide according to the Chemical Market Associates Inc. Hong *et al.* [57] estimated that about 2180 Wh are consumed for the production of one ton of $NaOH$ solution. This electricity consumption for production is consistent with the energy-use in European plant [28, 57]. The $NaOH$ molecular weight is equal to 39.997 $g \cdot mol^{-1}$. This means that one ton of $NaOH$ 50 wt% solution contains approximately 12000 moles of OH^-. Based on this, and on the concentration of NH_4HCO_3 in the ED concentrate, the amount of $NaOH$ solution needed to increase the pH until a certain value can be calculated. This can, then, be related to the energy consumption for the production of the salt and, compared to what obtained by means of the BPMED. Some assumptions needed to be formulated for the calculation of $NaOH$ required for NH_4^+ conversion. These are presented below:

- Only NH_4HCO_3 is present in the solution and thereby HCO_3^- and CO_3^{2-} are the only buffers in the solution.
- The same numbers of moles of HCO_3^- and NH_4^+ are present in the ED concentrate solution.
- Temperature in the solution is constant and equal to 25°C
- The dilution effect due to the use of the $NaOH$ solution is neglected.

With these assumptions, for a certain concentration of NH_4HCO_3, the necessary $NaOH$ water solution to achieve the desired pH in the concentrate can be calculated.

3

Materials and methods

This chapter describes the used setup and the single modules composing them. The parameters monitored and the equipment employed for the acquisition and analysis of the data are also reported here. Finally, a detailed explanation of the performed experiments is carried out.

3.1. Material

Three separate technologies were employed for the experiments. These were electrodialysis, electrodialysis bipolar and vacuum membrane stripping. In this section, the specifications for each of these units are listed and the most relevant information on their components are provided. Additionally, the installation's features and design are described.

3.1.1. Regular Electrodialysis module

For the regular ED setup a PCCell 64002 unit, supplied by PCA, was used as casing for the ED stack. Embedded in the ED cell, an anode made of Pt/Ir-coated Titanium, and a cathode made of V4A Steel, transmitted current to the to stack enclosed between them. The two electrodes were specifically designed to permit the reversion of the electric field poles. The current was transferred from the electrodes to the stack by the means of an electrode rinse solution. For the ED experiments, standard membrane stacks (STM), also supplied by PCA, were used. Each STM ED stack consisted of the following elements:

- 9 CEMs
- 10 AEMs
- 2 Cation exchange end membranes
- 20 Flow-spacer
- 2 Electrode spacers

These components were organized in ten cell pairs over the ED stack. Each pair consisted of a CEM, an AEM and two flow-spacer alternated with the membranes. At the extremes of the stack, two CEEMs , and their associated spacers, separated the rest of the stack from the electrodes. The total effective membrane area of the ten cell pairs was equal to 0.128 m^2. The spacers had a thickness of $5{\cdot}10^{(-4)}$ m. All membranes in the stack had a total squared surface of 0.11·0.11 m with an active area of 0.08·0.08 m. More membrane's properties are provided in Appendix, section D.3, Table D.1.

3.1.2. Electrodialysis with bipolar membranes module

The cell embedding the ED-BPM stack was a PCCell unit 64004. The main difference with the casing used for the regular ED was that the last one only allowed three streams to enter the ED stack, whereas the PCCell 64004 had two additional stream connections. This difference was fundamental since four streams were involved in the three compartments ED-BPM operation. For the spacers, the

specifications were the same provided for the ED case (subsection 3.1.1). The electrodes in the BPMED had a different design, they did not permit the reversal of the electric field poles.

Differently from the one used in ED, the BPMED stack was organized in 10 membrane triplet, therefore, it contained extra-elements. A list of the components of the BPMED stack is provided below:

- 9 CEMs
- 10 AEMs
- 10 Bipolar membranes
- 2 Cation exchange end membranes
- 30 Flow-spacers
- 2 Electrode spacers

Each triplet consisted of a CEM, an AEM with a BPM in between. The membranes were separated from each others by flow-spacers. Also in this case, the membranes had a total squared surface of 0.11·0.11 m with an active area of 0.08·0.08 m. More membrane's properties are provided in Table D.1 in section D.3 in Appendix.

3.1.3. Vacuum Membrane stripping module

The vacuum membrane module used was a Sterlitech CF042 acrylic crossflow cell with a 42 cm^2 active membrane area. This unit and its components are shown in Figure 3.1. Sterlitech flat-sheet PTFE membranes with polypropylene backing and 0.1 m pore size were placed in the membrane module. This was confined by two Sterlitech CF042 polypropylene diamond-shaped 47 mm spacers. The spacer placed in the feed side cavity of the module had the function to increase feed flow turbulence, whereas, the one installed in the permeate side cavity prevented the membrane to adhere on the membrane casing.

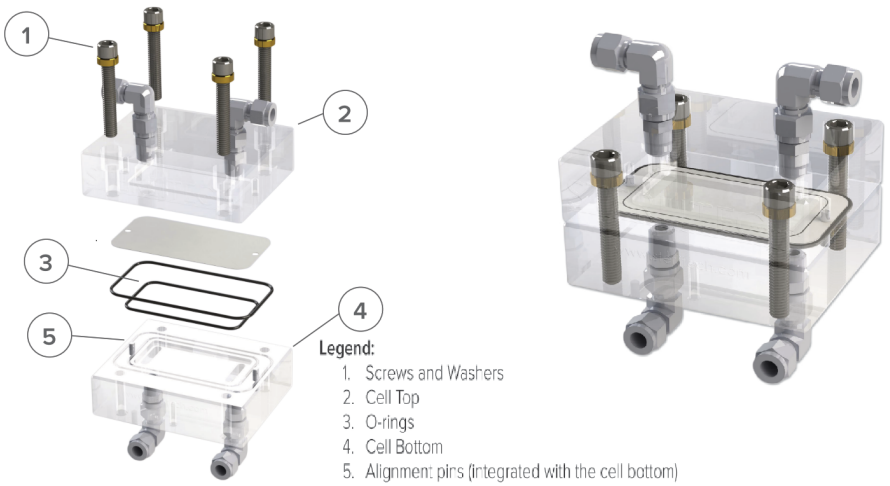

Figure 3.1: CF042A-FO Cell: body assembly and components. Image retrieved from STERLITECH [59, p.2].

3.1.4. Experimental setup schemes

In all the different setups, a mixing table and magnetic stirrers were used to constantly mix the solutions inside glass batches. This was done to ensure the uniformity of the solution. From the batches, a Watson Marlow 520S pump and 4 associated 323 pump-heads, pumped the solutions into Watson Malow Marprene tubes (with an internal diameter of 6.4 mm) to the electrodialysis cell. During all the experiments performed in this thesis, the cross-flow velocity in each tube was equal to 0.116 $cm \cdot s^{-1}$. By considering the geometry of the chambers and the spacer encumbrance, the actual cross-flow velocity in the acid, diluate and base chambers was estimated equal to 2 $cm \cdot s^{-1}$. A TENMA 72-2535

supplied current and voltage to the ED unit. This generator operated with a current range of 0.0–3.0 A and an electrical potential range of 0.0–30.0 V.

In the paragraph below a scheme for each of the setup configuration is presented.

Regular electrodialysis

In the ED setup, three solutions were recirculated in the ED stack. Every solution was stored in a separate batch. Mass-transfer processes could occur only within the ED-cell. Three pump-heads supplied an equal and constant pressure to recirculate every solutions through the installation. The ED-cell electrodes were directly connected to the power supply unit by means of copper cables.

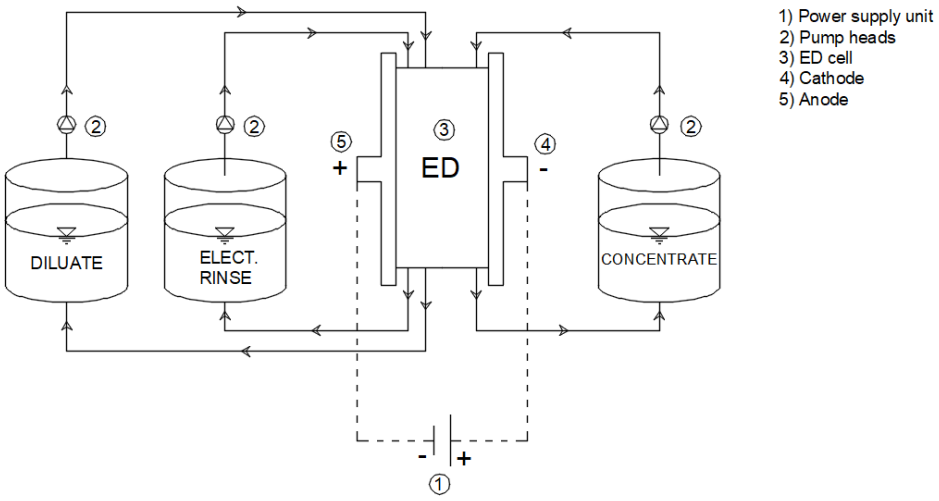

Figure 3.2: Scheme of the regular ED installation setup.

Electrodialysis with bipolar membranes

The BPMED setup was basically identical to the one used for the ED. The only difference consisted of an extra-solution that was recirculated through the installation. As already mentioned, in the BPMED operation two separate concentrate streams (acid and base) were involved.

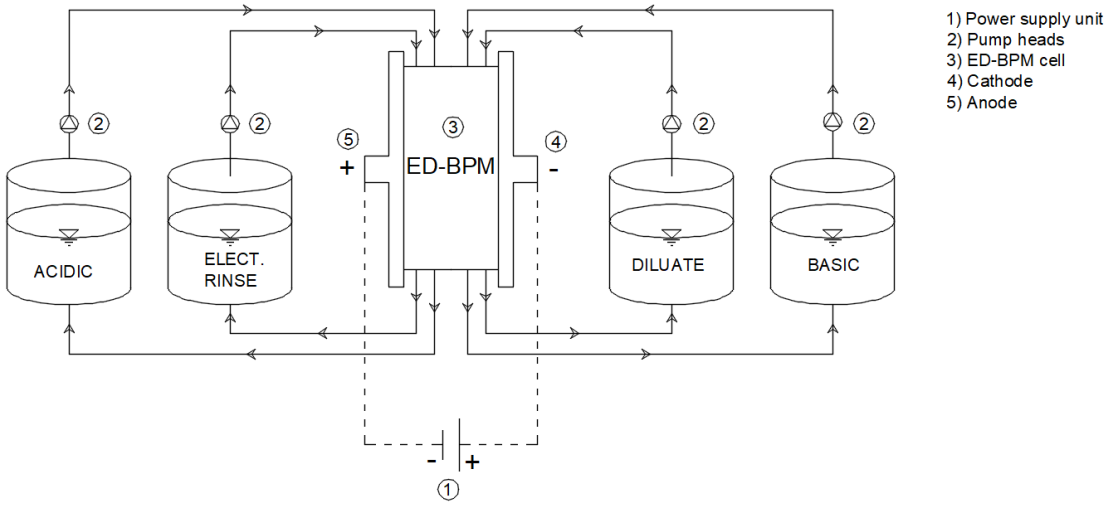

Figure 3.3: Scheme of the BPMED installation setup.

Vacuum membrane stripping in series with BPMED

In this installation, two VMS units were installed in series to the concentrates, coming out from the BPMED-cell. One side of the stripping membranes faced the BPMED concentrate streams. This flowed along the membrane with a cross-flow velocity of $6 cm \cdot s^{-1}$. On the other side, a constant vacuum pressure of $15000 Pa$ was applied by two KNF N816.3KT.45.18 vacuum pumps. This permitted to remove dissolved gas from water flowing across the opposite membrane surface. The gas permeated from the acid stream was passed through a liquid trap containing a high pH $NaOH$ solution. Symmetrically, the result of the base stripping was trapped in a HCl acid solution.

The initial composition of the solution in the trap connected to the acid stream was 738.3 mL of demiwater blended with 4 mL $NaOH$ (0.1M). The trap connected to the base contained a 745.2 mL of demiwater mixed with 2 mL of HCl (1M) acid solution.

Once the stripped gas was passed across the trap, it was released in atmosphere by the vacuum pump.

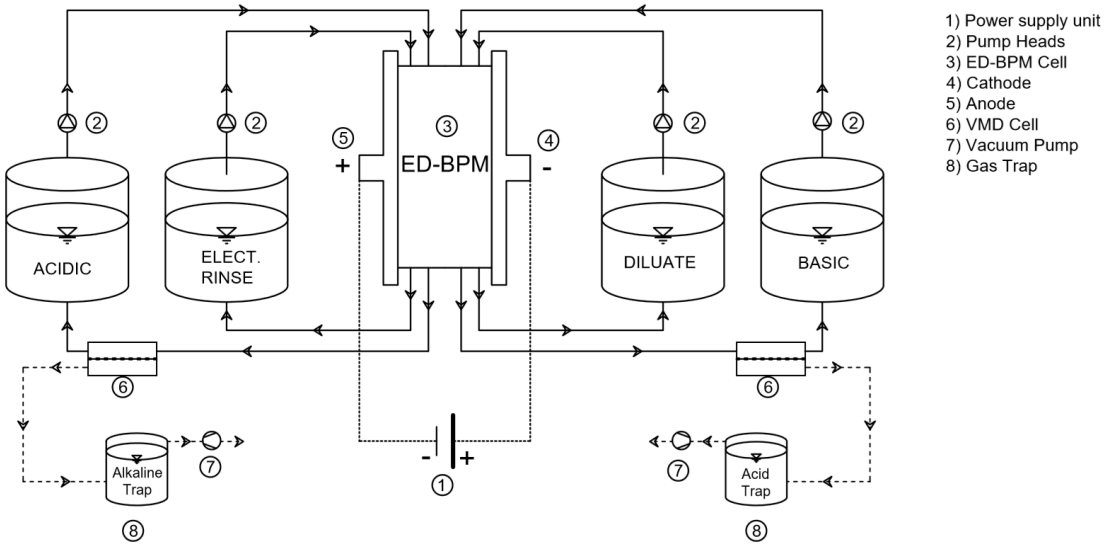

Figure 3.4: Scheme of the BPMED installation combined with the VMS units and gas traps.

3.1.5. Analytic material and equipment

The measured parameters and equipment employed for acquiring data and in the laboratory analysis are reported below.

- *Electrical conductivity (EC), pH and temperature*: EC, pH and temperature were measured simultaneously on a WTW digital precision meter Multi 3630 IDS connected to calibrated WTW TetraCON 925 EC sensors and calibrated WTW IDS SenTix 940 pH sensors. Measurement data was automatically registered in a Microsoft Excel document on an attached laptop or stored in the multimeters. The recording interval varied for each experiment.

- *Mass of solutions*: The masses of the solutions were measured using a Kern PCB 6000-1 digital precision balance. For every experiment, the mass was measured at the start and at the end of every run. This was done to monitor the water transfer through the different chamber of the membrane. The deviation in solutions volume was used to correct the salt mass balance.

- *TAN Solution concentrations*: solution TAN concentrations were measured using MACHEREY-NAGEL NANOCOLOR Ammonium 200 and Ammonium 2000 tube tests. Samples were injected into the test tubes using a Thermo Scientific 100–1000 µL Finnpipette F1 pipette and analyzed with a spectrophotometer NANOCOLOR VIS II. The TAN concentration was then reported in g of NH_4^+ per L.

- *Total inorganic carbon (TIC) concentrations*: TIC in the solution was measured with TOC-VCPH/TOC-VCPN Total Organic Carbon Analyzer supplied by Shimadzu Corporation. More information on this device and on its working principles are reported in Shimadzu Corp. [60].

- *pH validation*: a 702 SM Titrino by Metrohm was used to validate the pH data acquired by the pH probes via an automatic titration.

3.2. Experimental Methods

In the following paragraphs, a description of the performed experiments is presented. All the experiments were carried out in batch mode. The ERS, diluate, acid and base streams were continuously recirculated through the installation. For every experiment, the temperature, pH, conductivity of each stream were continuously monitored. Moreover, data on the applied current density, voltage and running time were also acquired continuously. Finally, the weight of each solution was determined at the beginning and at the end of each run. In all experiments, the ERS consisted of a solution with a concentration of 1 M $NaNO_3$. This was done to be consistent with the previously performed research with the regular ED setup by Deckers [11] and Hordijk [13].

In the experiments run for this thesis, the cross-flow velocity in the concentrate and diluate was kept equal to $2cm \cdot s^{-1}$. This was based on the results presented by Deckers [11] who determined an optimal velocity for the same ED setup used in this thesis. For a constant velocity, a linear relationship exists between the LCD and the lowest-conductivity solution in the cell [11]. This relationship, shown in Figure 3.5, was used to directly relate the LCD with the conductivity of the diluate which, in this application, was the limiting stream. The same velocity was also applied for the experiments with BPMED, assuming that the results from Deckers [11] were extendable to the BPM stack.

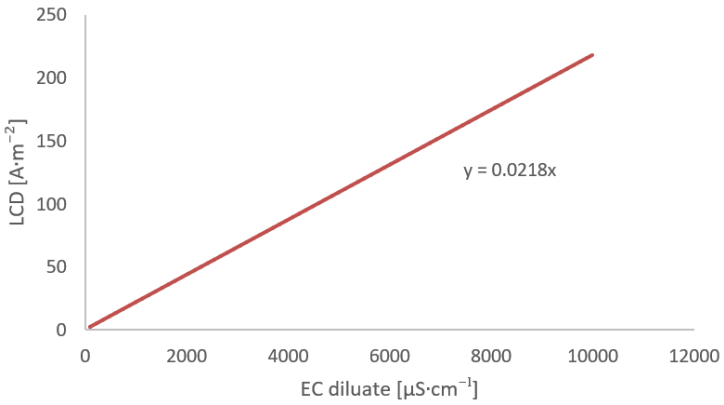

Figure 3.5: Empirical relationship between limiting current density (LCD) and conductivity of the limiting stream (EC diluate) [11].

From now on, in this report, the ERS will be addressed as passive stream whereas the diluate, acid and base (or the diluate and concentrate in case of the ED) will be identified as ”active streams”.

3.2.1. Sequencing batch experiment

A sequencing batch experiment (SBE) was performed for both ED and BPMED installations. At the beginning of this experiment, all the 3 active streams had a volume of 1 L and an initial conductivity of approximately 7.8 $mS \cdot cm^{-1}$. The experiments were always operated using water with an average temperature of about 24 ° C. The initial conductivity value was achieved dissolving 4.15 $g_{NaCl} \cdot L^{-1}$ or 6.6 $g_{NH_4HCO_3} \cdot L^{-1}$ in demineralized water. By applying current to the device, the ions present in the diluate migrated toward the concentrate streams. This caused a drop in the conductivity of the diluate. Once the conductivity reached a value of 1000 $\mu S \cdot cm^{-1}$, which in standard conditions (neutral pH and 25 °C) corresponded to approximately 90% of salt removal, the current supplying and the solution recirculation were stopped. After that, the depleted diluate was replaced with a new solutions with a conductivity of 7.8 $mS \cdot cm^{-1}$, this concluded one run of the SBE. Before replacing the diluate, the installation was drained and the solutions were weight and sampled. Then, the experiment was

restarted and a new run was undertaken. This procedure was repeated 10 times (1 experiment = 10 runs or batches). The concentrate streams were never replaced in this experiment and thereby their concentration was expected to be higher at the beginning of every new run.

The current applied to the cell (I) was not constant during the run but it was continuously set equal to the 63% of the LCD for the diluate ($\frac{i}{LCD}$ rate equal to 0.63). This means that over every run, as a result of the reduction of the diluate EC, the i applied to the cell gradually drop. The choice of 63% of the LCD followed from a theoretical optimization between the energy consumption and the membrane surface required [61]. Further explanation on this concept are provided in section A.1.

An example of the trend in applied i during a run of the SBE is shown in Figure 3.6.

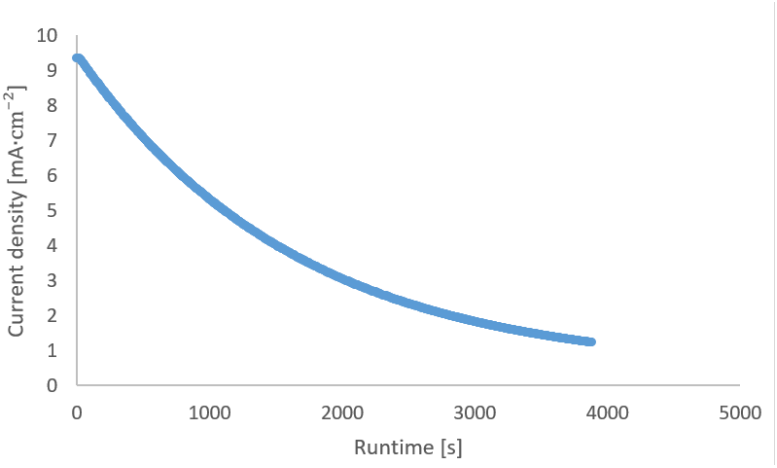

Figure 3.6: Current density trend in the first batch of the SBE with BPMED. The i reduces during the run on account of the decrease of the dilute conductivity.

Sequencing batch experiment with BPMED in series with VMS

The SBE was performed also with the setup obtained coupling two VMS devices with the BPMED (scheme in Figure 3.4). Once passed through the BPMED cell, the acid and the base were directly forced into the membrane stripping devices before being mixed again in batches. This permitted to strip NH_3 and CO_2 from the two streams when the condition (in terms of pH and concentration) were more favourable.

Four different experiments were performed with this installation:

- First batch of the SBE with only the acid stream connected in series to a VMS.
- First batch of the SBE with only the alkaline stream connected in series to a VMS.
- First batch of the SBE with both acid stream and alkaline stream connected in series to two VMSs.
- First 5^{th} batches of the SBE with both acid stream and alkaline stream connected in series to two VMSs.

The first three experiments (run in triplicate) were performed to better characterize the impact on the operation parameters of the single stripping unit. The last experiment was undertaken to assess the impact of the stripping devices for higher pH and TAN in the base streams, when gas diffusion is expected to be more severe.

3.2.2. Fixed current test

This test, performed only with BPMED, aimed to determine the rate of H^+ and OH^- production for different constant voltages (and current densities). The synthetic wastewater normally used contain NH_4HCO_3. This, when dissolved in water, dissociates into NH_4^+ and $HCO3^-$. Bicarbonate is well known for its buffering capacity, that makes hard to relate the change in pH with the actual production of H^+ and OH^- by the bipolar membrane. Moreover, when the pH change toward extreme values, NH_4^+

and $HCO3^-$ shift to their uncharged gas forms NH_3 and CO_2, respectively. These dissolved gases can easily diffuse over the stack (or being stripped in the atmosphere) influencing the pH and the charge balance in the solutions [62]. For this reason, to perform this experiment an alternative salt had to be chosen. Sodium chloride ($NaCl$) was identified as a suitable salt because dissolved in water it forms a non-buffered solution [63]. On top of that, the large number of studies conducted with IEXMs for the treatment of $NaCl$ and its non-reactive properties, made this solution very convenient to use in this specific application.

The H^+ and OH^- production rates were determined based on the change of pH in the streams. Since the used solutions were not buffered, the production of H^+ and OH^- in the transition layer of the BPMs, could be determined monitoring continuously the pH of the 4 streams in the system. This test was performed applying 4 different voltages (6-12-18-23 V), which corresponded to 4 different current densities because the conductivity conditions were analogues in every test. A small deflection in the applied current for a fixed voltage was detected at the end of the run due to the reduction of conductivity in the diluate. However, the deviation in current in the interval used to extrapolate the results was negligible.

Similar experiments were performed by Simons [37] and Moussaoui *et al.* [38]. Nonetheless, in both of these studies EDBPM were operated at relatively high current density and salt concentration compared to the condition explored in the *N2kWh* project. Therefore, the results were not expected to be reliable for this application.

3.2.3. Resistance test

The "resistance test" was performed in order to estimate the voltage and the electrical resistance related to a certain membrane stack or to a singular stack component. In this experiment, the active streams were blended in a single batch in order to maintain constant the conductivity of the solution. The conductivity of this solution was equal to 7.8 $mS \cdot cm^{-1}$ (6.6 $g_{NH_4HCO_3} \cdot L^{-1}$ in demineralized water at 24°C). In this condition, different current density inputs were given to the cell. For each current density the corresponding voltage was recorded and a current-voltage curve was drawn. This permitted to calculate the ohmic resistance (R).

The resistance test was also performed without a membrane between the two electrodes, which were then only separated by the associated flow spacers. This experiment is referred to as *Blank test* and it was performed to assess the resistance associated with the electrodes. By introducing a membrane between the two electrode spacers, the resistance of the single membrane could be experimentally assessed.

3.2.4. Diffusion test

This test was carried out to assess the magnitude of gas diffusion in BPMED. The solutions were recirculated through the cell without applying any current for 8 hours. It was assumed that gases diffuse throughout the membranes independently of the current, as already verified by Ali *et al.* [25]. Therefore, the mass transfer across the stack chambers could only occur due to diffusion. The acid and the diluate initially consisted of a solution with 4.15 $g_{NaCl} \cdot L^{-1}$, whereas, in the base stream, ammonium hydroxide was added to a base solution of 3.8 $g_{NaCl} \cdot L^{-1}$. The resulting blend was an alkaline solution (pH=11.6) with a concentration of 12.5 $g_{NH_4^+} \cdot L^{-1}$ and a conductivity of 7.8 $mS \cdot cm^{-1}$. According to the ammonium equilibrium explained in section A.2 in Appendix, for this conditions, almost all the TAN contained in the base was in NH_3 gas form. This minimized the TAN transport via ions diffusion. During the experiment, samples of the 4 streams were taken and their concentration of TAN was tested. In order to prevent the volatilization of the NH_3 from the base, the system was almost completely sealed.

The diffusion test was performed also to assess the gas diffusion rate of the CO_2 produced in the acid stream to the base and the diluate. In this case, the base and the diluate initially consisted of with 4.15 $g_{NaCl} \cdot L^{-1}$ dissolved in demi water. The acid was made by dissolving 2.87 g of $NaHCO_3$ in 1 L of demiwater. After that, 32.7 ml of a solution 1 M HCl was added to lower the pH to 4 and convert the bicarbonate into CO_2. Finally, 2.66 g of $NaCl$ were added to equalize the conductivity with the other two active streams. In the CO_2 diffusion test the solutions were recirculated in the installation for 6 h in total.

4

Results and Discussion

4.1. Electrodialysis with ammonium bicarbonate

In order to compare the $E_{NH_4^+}$ of the BPMED to the energy used by regular ED, the SBE was firstly run with the regular ED. The results of this experiment are presented in this section.

4.1.1. Energy consumption for ammonium removal in regular electrodialysis

90% of the NH_4^+ originally contained in the diluate was removed in all the 10 runs. This was achieved with an average $E_{NH_4^+}$ of 4.27±0.27 $MJ \cdot kg_{NH_4^+}^{-1}$ for each batch, which was lower than the energy ideally produced in the SOFC for the same quantity of N. Moreover, the $E_{NH_4^+}$ used in this lab test was almost eight times lower than the energy used in nitrification denitrifiation, and about two times lower than anammox.

The energy consumption in the 10 batches of the SBE is shown in Figure 4.1.

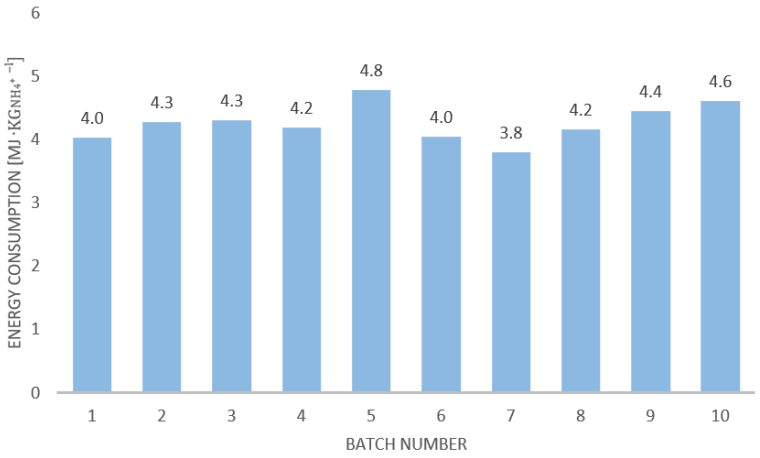

Figure 4.1: Energy consumption, in $MJ \cdot Kg_{NH_4^+}^{-1}$, for the ten runs of SBE run with regular ED.

After the 10 batches, the NH_4^+ concentration in the concentrate was equal to 9.98 $gNH_4^+ \cdot L^{-1}$. This was obtained with a total energy consumption of 16.8 Wh (with an average of 1.68±0.12 Wh per batch-run). The TAN concentration obtained after every batch is shown in Figure 4.2.

Differently from what obtained by Deckers [11], who operated with a constant and lower average i, the trend in concentration did not show a maximum but it kept increasing almost linearly. This suggests that, with the employed operation method, even higher concentration could be accomplished for a similar NH_4^+-removal energy cost.

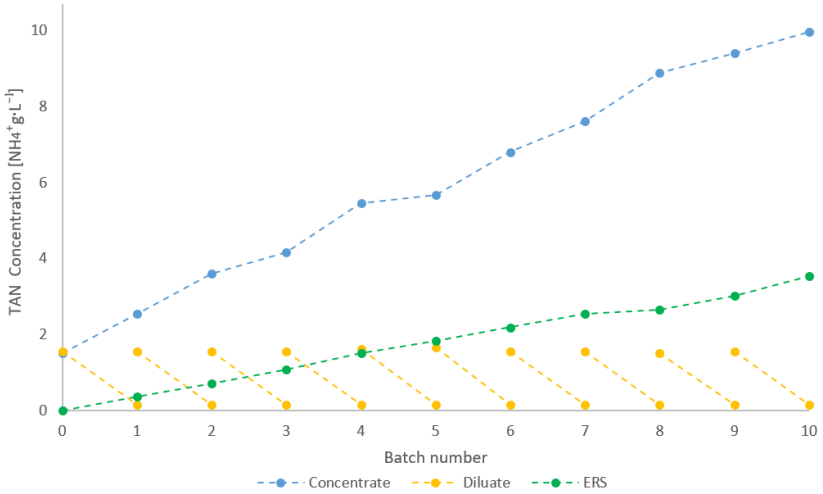

Figure 4.2: TAN concentration in the concentrate, diluate and ERS for the SBE with ED. The TAN concentration in the concentrate stream increases almost linearly along the 10 runs.

As already observed in literature [11, 16, 41], also in this application, the ions back-diffusion caused a decrease in the $CE_{NH_4^+}$ over the experiment. This is shown in Figure 4.3, where the $CE_{NH_4^+}$ for the 10 consecutive runs in the SBE are compared.

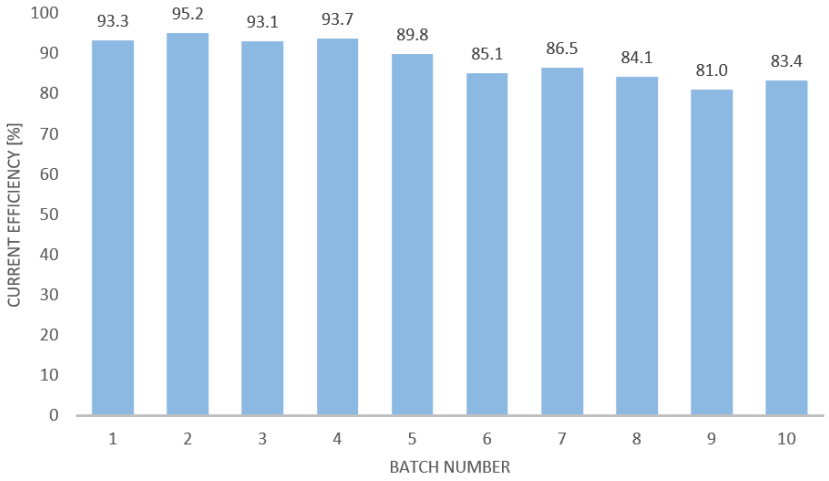

Figure 4.3: Current efficiency for NH_4^+ removal ($CE_{NH_4^+}$) in the 10 runs of the SBE with ED. With the increase of the concentrate concentration the efficiency drops.

The ion back-diffusion from the concentrate toward the diluate increases with the concentration gradient between the two active streams [45]. This explains why the $CE_{NH_4^+}$ dropped batch by batch. As the ion accumulation increased in the concentrate, the chemical potential between diluate and concentrate rose. However, Figure 4.1 shows that the value of the energy consumption didn't increase substancially. The impact of the decrease in $CE_{NH_4^+}$ on the energy consumption was leveled by the decrease of the stack electrical resistant (R_{tot}^{ED}) thanks to the increasing EC in the concentrate over the runs. Indeed, the lower is the potential drop over the cell the lower is the energy consumption (as shown by Equation 2.5).

In a previous study on the quantification of ions back-diffusion in the regular ED stack, the influence of back-diffusion on $CE_{NH_4^+}$ was calculated. The results of this study allowed to relate the salt transported via back-diffusion to the difference in EC between concentrate and diluate (ΔEC) [61]. The ΔEC is continuously measured over the SBE runs. Then, the total mass of salt transported by ion back-diffusion could be calculated and an estimation of the back-diffusion impact on $CE_{NH_4^+}$ was

drawn. Back-diffusion could not totally explain the values of $CE_{NH_4^+}$. Indeed, two other processes were recognized to be responsible for the non-optimal performance of the installation:

- Ionic short-circuits, which is mainly dependent from the system design [64].
- NH_4^+ leakage to the electrode rinse solution, which is caused by the membrane arrangement in the stack that allows the exchange of cations between the electrode rinse solution and the concentrate.

The sum of these accounted for less than 10% loss in CE_{NH4+} [65]. Since the mitigation of these effects directly involves the change of the stack design, the reduction of those are not tackled in this thesis.

4.1.2. Voltage and electrical resistance composition in regular ED stack

The resistance test, explained in chapter 3, section 3.2, allowed to draw the voltage-current curve for the studied ED-stack (Figure 4.4). This showed that, for the range of current in which ED was operated, the total potential drop over the ED cell could be distributed into two components: an initial threshold, and an ohmic-behaving part (voltage increase linearly with the applied i). Thus, the potential of the entire stack can be expressed as in Equation 4.1

$$U_{tot}^{ED} = U_{cell} + I \cdot R_{tot}^{ED} \tag{4.1}$$

R_{tot}^{ED} is the sum of all the ohmic resistances of the single elements of the stack and it is graphically represented by the slope of the green curve in Figure 4.4. The total resistance could be split over the different stack components according to Equation 2.2 shown in chapter 2, subsection 2.1.1.

The ohmic resistances of the AEM, CEEM and CEM were individually determined experimentally. The electrical resistance for all the membranes of the ED stack used in this work are reported in Table 4.1

Membrane type	Resistance per single element $[\Omega \cdot m^{-2}]$
CEM	37.5
AEM	25
CEEM	25

Table 4.1: Experimentally determined membrane resistances in the regular ED stack.

The resistance of the diluate and concentrate chambers were determined based on the conductivity of the solutions and on the geometry of the chambers, reasonably assumed equal to the thickness of the flow-spacers. The contributions to the total resistance of the stack of the electrodes, ERS and associated spacers were determined by performing a blank test (as described in section 3.2) and they were equal to 0.66 Ω in total.

Finally, based on Equation 2.2, R_{sp} could be easily calculated as the difference between R_{tot}^{ED} and the previously calculated contributions(Equation 4.2).

$$10 \cdot R_{sp} = R_{tot}^{ED} - R_{elec} - 10 \cdot R_{conc} - 10 \cdot R_{dil} - 9 \cdot R_{CEM} - 10 \cdot R_{AEM} - 2 \cdot R_{CEEM} \tag{4.2}$$

R_{sp} was assessed equal to 0.23 Ω per membrane pair. The linear correlation between R_sp and the number of cell pairs in the stack (n) was verified repeating the experiment and the above-explained calculation for different stack size. Also the salt transport rate was monitored to assess the effect of n on the amount of salt transport over time. The Current-Voltage curves for different stack sizes are shown in Figure 4.4

From Figure 4.4, it can be observed that all the three curves seem to converge in a single point (indicated with a red circle on the y-axes) when $i \to 0$. By assuming a linear behavior of the Current-Voltage curves between 1.5 and 0 $mA \cdot cm^{-2}$, this voltage value was estimated equal to 2.03$\pm$0.12 V. In Equation 4.1 this term is indicated with U_{cell} and it was assumed as constant for the cell.

This is a simplification. Indeed U_{cell} is actually the results of two separate contributions listed below:

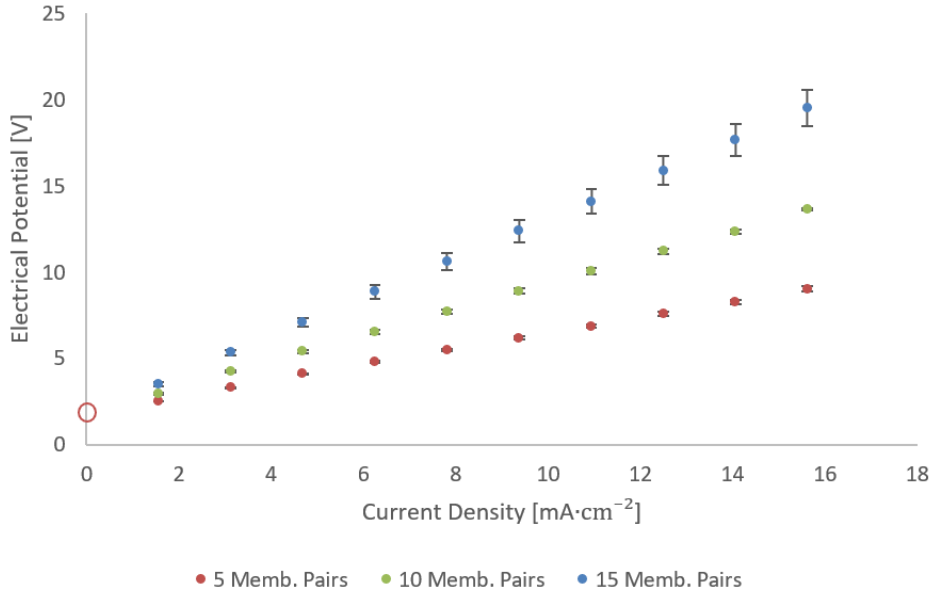

Figure 4.4: Current-Voltage curve for regular ED stack with 5, 10 and 15 membrane pairs.

- Reversal equilibrium potential: this is the voltage necessary for the water electrolysis reaction (theoretically 1.23 V) occurring at the electrodes. It is often called the Nernst potential, as it can be calculated from the Nernst equation [66].
- Tafel Overpotential: this is a logarithmic function of the applied i and depends on the operation condition and on the electrodes material [67].

The determination of the actual behavior of the shown curve for very low i level falls beyond the scope of this research. Therefore, for this application, a simplification was introduced and U_{cell} was considered constant in the considered range of i.

The presented voltage drop analysis allowed to draw an overview of contributions to the total voltage drop over the ED cell (U_{tot}^{ED}). This is shown in Figure 4.5

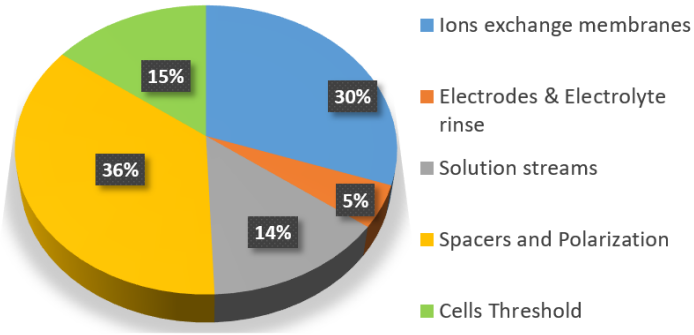

Figure 4.5: ED stack potential drop contributions for different elements. The following are considered: i equal 15.625 $mA \cdot cm^{-2}$ $EC_d = EC_c = 7.8mS \cdot cm^{-1}$

4.2. Electrodialysis with bipolar membranes with sodium chloride

As explained in section 2.5, pH is representative of the activity of H^+ in a certain solution. By measuring pH changes in the streams, the production of H^+ and OH^- by the BPMED could be estimated. Based on the activity of H^+ and on the current input, the current efficiency for the water dissociation (CE_{WD}^{meas})

was calculated as shown in chapter 2, subsection 2.3.1. This allowed to draw conclusions on how efficiently the current supplied was used for the pH control in the base and in the acid stream.

Two types of experiments were carried out with $NaCl$. In the first group of experiments, the BPMED's energy consumption and H^+ and OH^- generation were measured in triplicate at different fixed voltages (6V, 12V, 18V and 23V). By the means of these experiments, the relationship between applied current density (or voltage) and the H^+ and OH^- production rate in the BPMs could be interpolated. In the second group of experiments the first run of SBE was performed with the BPMED. The concentration of salt in the diluate was calculated based on the conductivity. An empirical function, which relates the mass of $NaCl$ dissolved in the water with the EC in the solution, was employed and it is shown in Appendix, section B.1. This experiment permitted to observe the behavior of pH and current efficiency (for salt transport and water dissociation) in absence of gas diffusion and buffering capacity. To better compare the performance of the ED and BPMED, the second experiment was also performed with regular ED.

4.2.1. Water dissociation rate

As expected from the theory, when a constant current was applied to the cell, ions were produced constantly over time in the BPMs. An example of this is shown in Figure D.1 in Appendix. The accumulation of H^+ and OH^- in the solutions over time is well approximated by a linear functions.

At the end of the fixed current experiments, the H^+ (or OH^-) runtime curves slightly flattened diverging from the observed linear trend. In other words, a reduction in the H^+ (or OH^-) accumulation over time was observed. This behavior could not be explainded by the reduction in the water dissociation rate, which was expected to stay constant with the current, Indeed, it was most probably caused by H^+ and OH^- leakage through the AEMs and CEMs. Due to the H^+ and OH^- leakage, a part of the ions produced did not result in pH change. This means that the slope of the curve shown in Figure D.1 should be steeper. This discrepancy can be included in the curve considering the current efficiency for water dissociation.

Besides the leakage of H^+ and OH^-, the current efficiency for water dissociation was also lowered by the co-ions transport across the BPMs. However, as explained in section 2.4, this mechanism is expected to be small compared to the CE_{WD}^{meas} reduction owning to the H^+ and OH^- diffusion through the IEXMs [23, 48].

For the four tested constant voltages, a linear trend in the H^+ and OH^- accumulation over time was observed. The slopes of the obtained curves are representative of the water dissociation rate, this increased linearly with the applied i. Figure 4.6 shows how, for the current interval considered in this application, the trend could be well approximated ($R^2 = 0.926$) with a straight line that intersects the origin. This allowed to link the ions generation to the applied i and, consequentially, to the voltage.

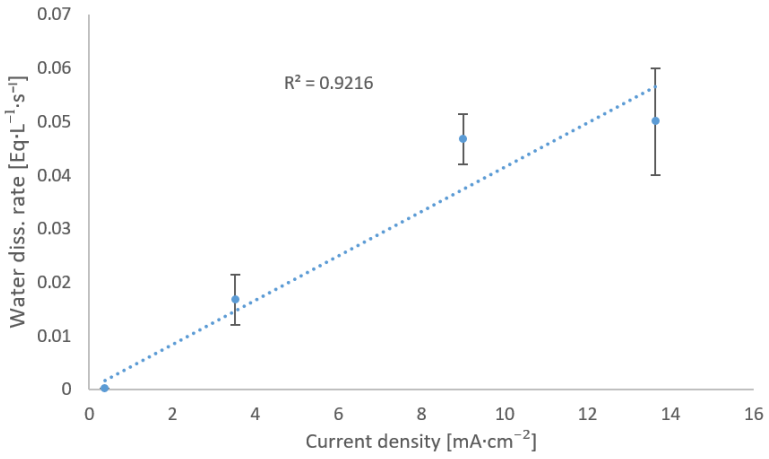

Figure 4.6: Water dissociation rate for different i in BPMED.

4.2.2. Current efficiency for water dissociation

The first batch of the SBE was performed in triplet using $NaCl$ as salt in the active streams.

The slope of the curve that represents the H^+ accumulated in the solutions (shown in Figure D.2 in Appendix) decreased over the runtime. In subsection 4.2.1, it was demostrated that the ions production in the BPMs increased almost linearly with the applied i. As shown in Figure 3.6 in section 3.2, i decreased during the experiment as a result of the salt depletion in the diluate stream. For this reason, a reduction in the ions electro-generation was expected over the run. However, by plotting the measured water dissociation current efficiency (Figure 4.7), it was clear that the reduction in CE_{WD}^{meas} also influenced the flattening of the H^+ and OH^- accumulation trend.

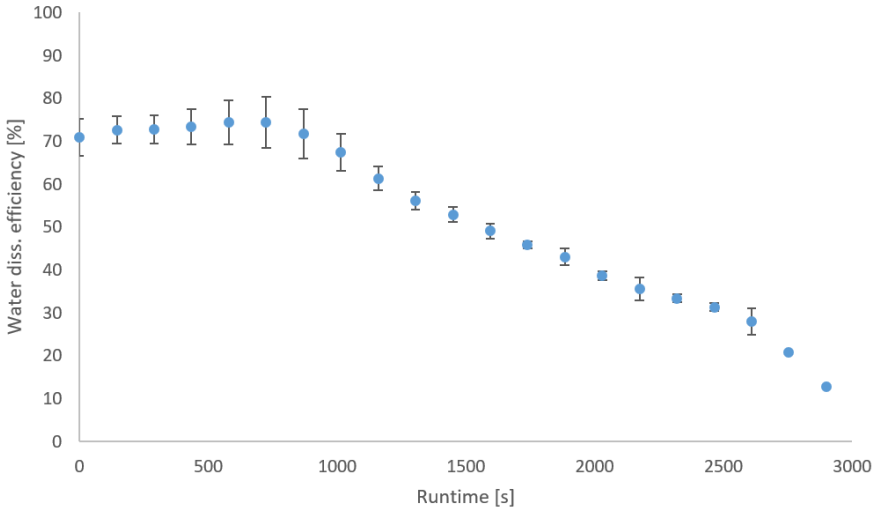

Figure 4.7: Measured water dissociation current efficiency CE_{WM}^{meas} for the 1^{st} batch of the SBE with $NaCl$. Only the first 50 minutes of the run are shown in this graph.

Without any buffering involved in the process, the decrease of CE_{WD}^{meas} has to be associated to three diffusion processes occurring in the BPMED operation:

- Gas diffusion
- H^+ and OH^- leakage through the IEXMs
- Co-ions leakage across BPMs

The composition of the solutions in this experiment excluded the gas diffusion to play a role. Therefore, the drop in water dissociation rate was most probably related to the undesired diffusion of ions through the membranes (co-ions, H^+ and OH^- leakages). In other words, the non-perfect permselectivity of the membranes for ion diffusion was the limiting factor for electrical ion-generation [32].

$NaCl$ has a molar weight of 58.44 $g \cdot mol^{-1}$. Initially, the acid and base have a concentration of 4.15 $g_{NaCl} \cdot L^{-1}$ that is 0,07M. By assuming that all the 90% of the electrolyte originally present in the diluate move to the concentrate stream (this means 90% of salt removal), the concentration gradient between the concentrate compartment and the BPM's transition layer ranges between 0,07M and 0,13M in the experiment. Sun *et al.* [48] showed that the effect of co-ions leakage on the water dissociation current efficiency increases with the reduction of the applied current. This can partially justify the reduction of CE_{WD}^{meas} within the experiment. However, based on the value reported by Sun *et al.* [48], the expected maximum reduction (for the considered concentration gradient and i) should be approximately 25%, whereas, in the last part of the experiment, no-increase in H^+ and OH^- concentration was detected anymore. As a consequence of that, the reduction in CE_{WD}^{meas} has to be explained also with another process that occurs in the stack: H^+ and OH^- leakage through the IEXMs.

Differently to the co-ions leakage in BPMs, this process provokes a reduction also in the current efficiency for salt transport. The trend of the salt transport current efficiency over the experiment is shown in Figure 4.8.

It was possible to identify two groups of ions that could diffuse: H^+/OH^- and salt ions. Both of them were more concentrated in the acid and base, hence, they tended to diffuse into the diluate stream reducing the current efficiency of the process. Experiments on ion back-diffusion in IEXMs have

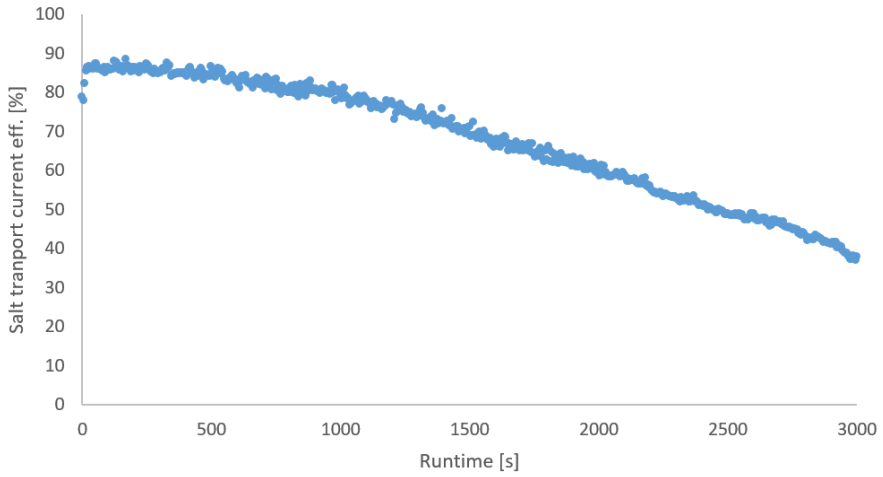

Figure 4.8: Current efficiency for salt transport in the first batch of the SBE run with $NaCl$ with BPMED. The current efficiency is based on the depletion of the EC in the diluate stream. The average current efficiency over the run is 68.23%.

been carried out by the *N2KWh* research team [61]. These aimed to express the back-diffusion as a function of the gradient in concentration between the concentrates and the diluate. The results of these experiments, shown in Appendix (section D.2), suggested that the relatively low concentration difference during the first batch caused a drop in the salt transport current efficiency lower than 1.5 % in the first run of the SBE.

Consequentially, ion back-diffusion, in this case, played a minor role in the reduction of the current efficiency for BPMED.

To further support this conclusion the first batch of the SBE with $NaCl$ was run (not in triplet) with regular ED. In this last experiment the efficiency was only affected by the back-diffusion since H^+ and OH^- are not generated. In this way, it was possible to partially quantify the role of Na^+ and Cl^- in reducing the current efficiency. The current efficiency of the first batch for the ED was significantly higher 89.7 % against the 68.2 % obtained for the BPMED. The role of the ions leakage was made even more evident via a comparison of the current efficiency evolution over the run(Figure 4.9)

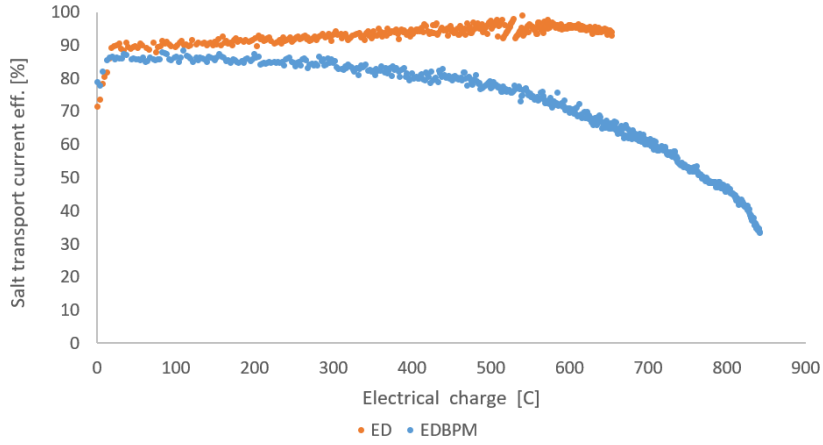

Figure 4.9: Comparison of the salt transport current efficiency between ED and BPMED for the 1st batch of the SBE with $NaCl$. The current efficiency is plot for the first 500 C used during the experiments.

Initially, the two efficiency trends were comparable. During the run, with the rise of the pH in the concentrate streams, H^+ and OH^- leakages start taking place and the curves in Figure 4.9 diverged. It is, thus, evident that the H^+ and OH^- leakage across the IEXMs severely influenced the BPMED performance in terms of water dissociation, as well as salt transport. This, obtained with $NaCl$, can be extended to NH_4HCO_3 for which, however, less extreme pH are expected because of the buffering capacity of the solution.

To summarize, three different diffusion phenomena were identified to reduce CE_{WD}^{meas} and the current efficiency for salt transport:

- The co-ions leakage through the BPMs impacted CE_{WD}^{act} reducing the actual H^+ and OH^- electro-generation rate.
- The ion back-diffusion through the IEXMs reduced the current efficiency for salt transport.
- OH^- and H^+ leakages, which occurred mainly for extreme pH difference between the concentrates and the diluate, affect both CE_{WD}^{meas} and the current efficiency for salt transport.

It is important to note that the severity of all the above-listed processes were strongly influenced by the applied i. Indeed the higher is the i, the higher is the current efficiency. This is due to the competition between diffusion phenomena, depending on residence time, and ion electrical migration, depending on i. Diffusion phenomena, which are undesirable, is less important when i increases [25]. For this reason the two curves in Figure 4.9 are initially comparable. With the depletion of the diluate stream, the applied i was lowered. This amplified the effect of the diffusion phenomena which were more severe in BPMED than in the regular ED. For this reason, in the second half of the run, the BPMED installation worked at very low current and consequently at very low salt transport and water dissociation current efficiency. This extended the runtime, which ended to be almost double for BPMED than for ED. To conclude, the more severe diffusion processes and the relatively low current applied in the second half of the run were responsible for the poorer performance of the BPMED.

4.3. Electrodialysis bipolar with ammonium bicarbonate

In this section, the results of the SBE for NH_4HCO_3 are presented. The process efficiency for N-removal and the voltage drop over the BPMED stack are investigated.

4.3.1. Sequencing batch experiment with BPMED with ammonium bicarbonate

In terms of $E_{NH_4^+}$ the BPMED used more energy compared to the ED. The removal of the 90% of the initial NH_4^+ in the diluate was achieved using a total of 48.7Wh for the ten batches (with an average of 4.87$\pm$0.33 Wh per batch). The NH_4^+ was removed over the ten batches with an average energy requirement of 13.2$\pm$0.1 $MJ \cdot kg_{NH_4^+}^{-1}$. This value was 3.3 times higher than that achieved with regular ED. The higher $E_{NH_4^+}$ was related to two factors:

- The higher voltage in the BPMED stack, on account of the presence of extra elements and because of the occurrence of water dissociation process.
- The lower $CE_{NH_4^+}$.

The energy consumption for the ten batches of the SBE with BPMED are shown in Figure 4.10. The values for $E_{NH_4^+}$ also in this case did not vary substancially over the runs. In this case the energy consumption was three times lower than the energy consumed by nitrification denitrification and comparable to what used by anammox. However, it has to be noted that this installation not only removed nitrogen, but it also produced an NH_3 stream, which can be stripped and ideally fed to the SOFC. This could potentially produce 9.6 $MJ \cdot Kg_{NH_4^+}^{-1}$ reducing the overall energy need of the treatment[65].

Figure 4.11 shows the TAN concentration in the acid, base and ERS during this experiment.

Based on Figure 4.11 conclusions on the different behaviors of ED and BPMED in the SBE can be drawn.

- The TAN concentration achieved in the alkaline stream after ten batches was lower than that achieved in the concentrate of regular ED.
- As expected, also for this stack TAN accumulated in the electrode rinse solution but with a slightly lower concentration. This was probably related to the lower concentration in the concentrate streams.

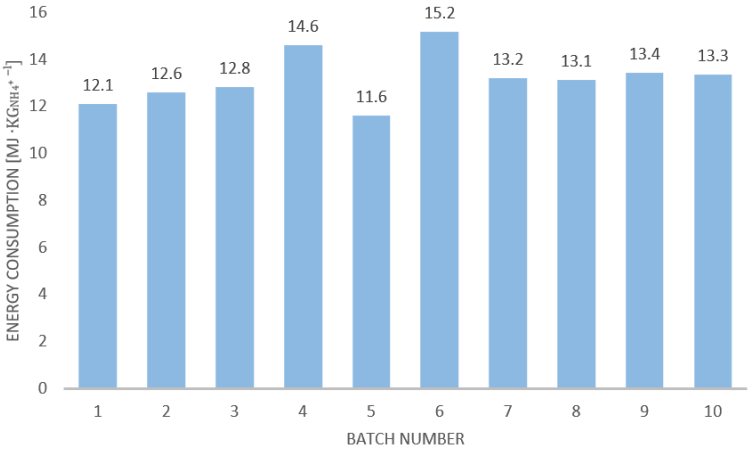

Figure 4.10: Energy consumption, in $MJ \cdot Kg_{NH_4^+}^{-1}$, for the ten runs of SBE with BPMED with NH_4HCO_3.

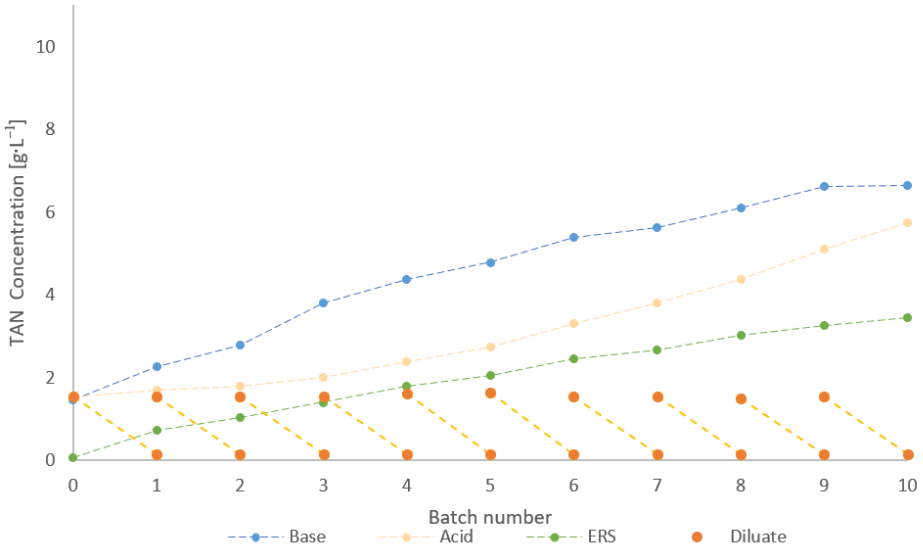

Figure 4.11: TAN concentration in the base, acid and electrode rinse during the SBE with BPMED with NH_4HCO_3.

- Differently from what observed in ED, where the TAN concentration in the concentrate streams increased almost linearly, for BPMED, the concentration trend of the base streams flattened more rapidly.
- The concentration in the acid, on the other hand, rose more rapidly batch by batch.
- The average voltage in the first batch of BPMED run with NH_4HCO_3 was 15% of the voltage measured when the installation treated $NaCl$

The trends of the concentrates can be related to the occurrence of NH_3 diffusion, which was expected to be more severe for the latest batches being TAN concentration and pH in the base higher. Also, the co-ions leakage through the BPM could play a role. However, based on literature data, this was not expected to be so severe to individually explain the observed increase of acid TAN concentration.

It is also interesting to examine the pH trend for the acid and base streams (Figure 4.12). Figure 4.12a shows the pH of the concentrates whereas Figure 4.12b shows the OH^- accumulation in the base.

As depicted in Figure 4.12, the pH of the acid concentrate initially dropped, then stabilized and increased afterwards. This increase can be attributed to gas diffusion from the concentrate streams. As a result of the extreme pH in the acid and in the base chambers, NH_4^+ and HCO_3^- convert to their

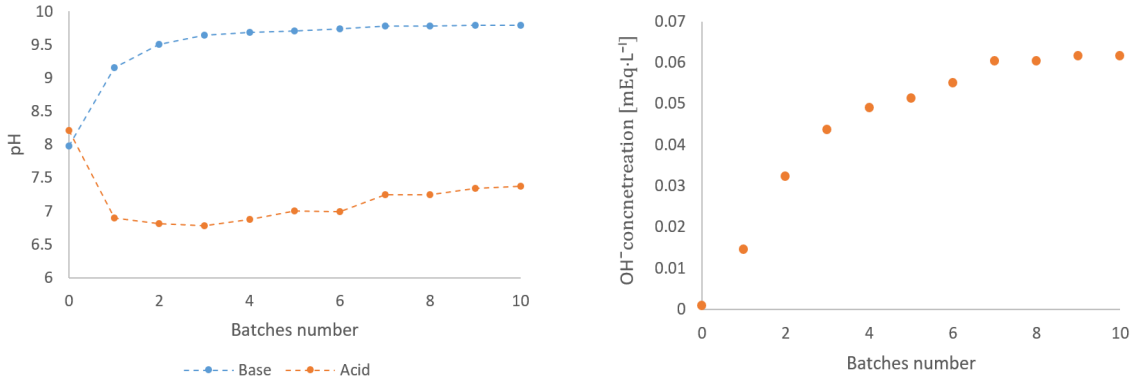

(a) (b)

Figure 4.12: (a): pH in the acid and alkaline stream during the SBE run with NH_4HCO_3. (b): OH^- concentration in the alkaline stream during the SBE run with NH_4HCO_3. The concentration of OH^- is expressed in $mEq \cdot L^{-1}$.

non-ionized forms (NH_3 and CO_2, respectively). The formed NH_3 gas could diffuse from the base into the acid resulting in H^+ uptake in the acid. At the same time, the low pH in acid promoted the uptake of H^+ with the conversion of HCO_3^- into CO_2 gas. The last could diffuse toward the diluate or in the base where the pH was far above the *pK* of the $CO_2 - HCO_2$ equilibrium [26]. This led to the re-ionization of CO_2 gas and to the uptake of OH^- in the alkaline stream.

$CE_{NH_4^+}$ over the ten batches is shown in Figure 4.13. The $CE_{NH_4^+}$ losses could be partially explained by the diffusion of NH_3. Indeed, NH_3 gas, which was formed in the base after NH_4^+ was transported in the alkaline stream, diffused back to the diluate. There, because of the lower pH, it was re-converted to its ionized form (NH_4^+). This needed to be transported one more time into the base. As a result of that, extra-energy was used. The negative effect of this process on $CE_{NH_4^+}$ is expected to be particularly severe at the end of the run, when the i is lower and the NH_3 partial pressure difference among the chambers is higher.

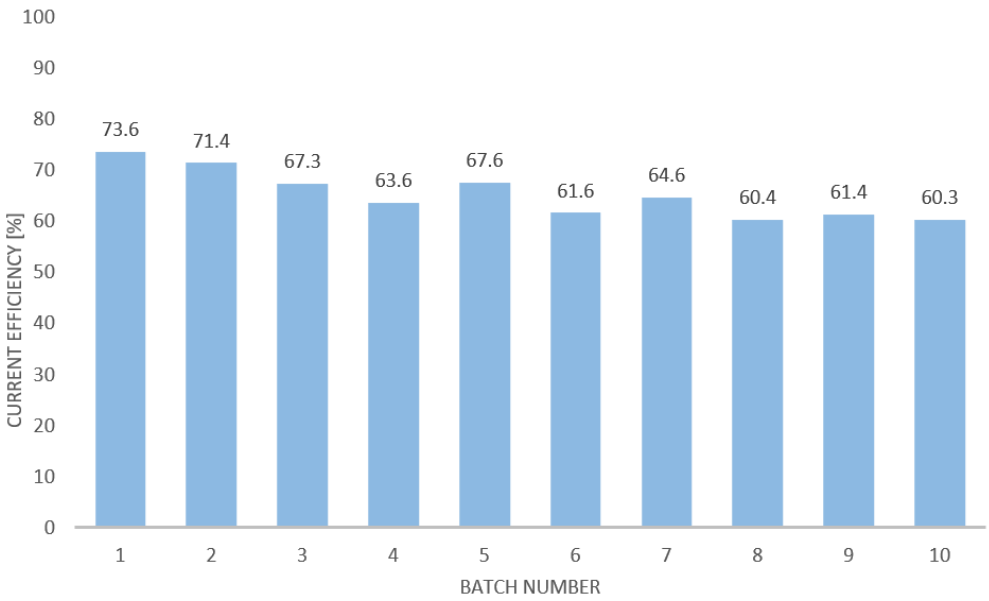

Figure 4.13: Current efficiency for NH_4^+ removal in the ten runs of the SBE with BPMED with NH_4HCO_3.

Moreover, during operation, a chemical gradient in salt ions is created between the concentrate streams and the diluate. This, as also observed in the regular ED (section 4.1), led to back-diffusion of salt ions. However, in this case, thanks to the lower concentration and to the conversion of the ions into uncharged gases, this process was responsible only for 1% loss in the $CE_{NH_4^+}$.

Besides the salt ions and gas diffusion, the H^+ leakage through the AEMs and the OH^- ion leakage through the CEMs were proven to also have an influence on the $CE_{NH_4^+}$. These parasitic ion transports, besides contributing to the loss of current efficiency of water dissociation, limits the upper concentration of H^+ and OH^- in the acid and base solution [24]. An explanation of this mechanism was given in subsection 2.4.7 in chapter 2. This process has alredy been proven to be severe in subsection 4.2.2 and, with gas diffusion, is thought to mostly contribute to the low $CE_{NH_4^+}$.

An additional interesting observation can be done by comparing the current efficiency of the first batch in the SBE (run with NH_4HCO_3 solution) and the current efficiency for the same test performed with $NaCl$. The buffering capacity of NH_4HCO_3 was expected to reduce the pH increase in the concentrate streams and thereby to limit the OH^- and H^+ leakage. For this reason, despite the gas diffusion, the current efficiency in the first batch with NH_4HCO_3 was higher (73% against 68%). This can be also observed in Figure 4.14

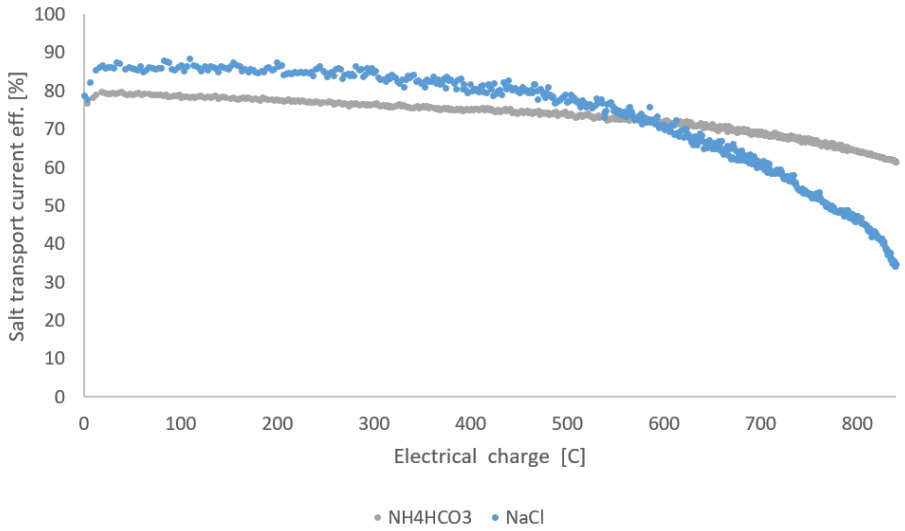

Figure 4.14: Comparison of the salt transport current efficiency trend for BPMED run with $NaCl$ and NH_4HCO_3. The current efficiency trend was calculated based on the depletion of the diluate.

Initially, the current efficiency for the $NaCl$ was higher, probably on account of the absence of CO_2 and NH_3 diffusion. Along the experiment, with the more extreme pHs and the lower i applied, the current efficiency of $NaCl$ transport dropped steeply. With NH_4HCO_3, $CE_{NH_4^+}$ decreased less sharply. The lower activity of the OH^- and H^+, resulting from the combination of CO_2 spontaneous stripping and bicarbonate buffering, helped to control the H^+ and OH^- leakage across the IEXMs leading to a higher current efficiency for the overall process. From this observation, it can be concluded that OH^- and H^+ leakages played a principal role in the salt transport current efficiency reduction for the first batch, particularly for $NaCl$.

To summarize, three different processes affected $CE_{NH_4^+}$ in BPMED:

- The salt ions leakage through the IEXMs (or back-diffusion), which, however, have been proven to be marginal (especially in the first batch).
- The gas diffusion from the base toward the diluate, which directly reduced the current efficiency for salt transport.
- The H^+ and OH^- leakage, which occurred at extreme pH difference between the concentrates and the diluate and affected both CE_{WD}^{meas} and $CE_{NH_4^+}$.

The last two seemed to be more relevant. Further considerations on the effect of these diffusion processes are done later in the report via the quantification of NH_3 diffusion across the stack.

4.3.2. Voltage and electrical resistance in BPMED

Based on the resistance test undertaken on the BPMED cell, the results are shown in Figure 4.15, the total voltage across the BPMED stack was modeled as in Equation 4.3:

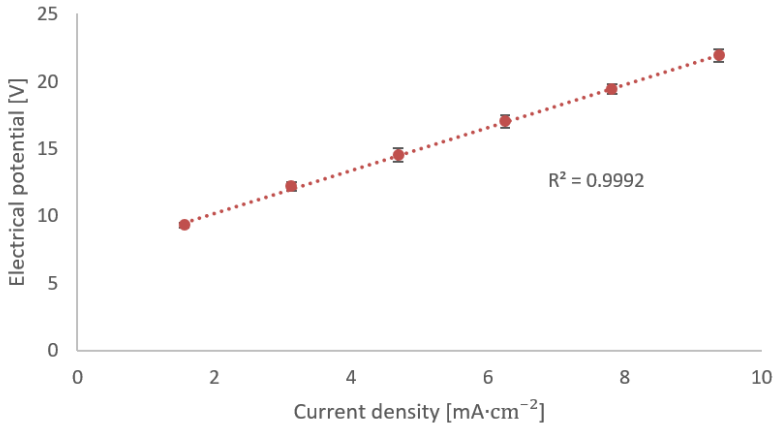

Figure 4.15: BPMED current-voltage curve for initial standard condition :$EC_d = EC_a = EC_b = 7,8mS \cdot cm^{-1}$

$$U_{tot}^{EBPM} = U_{cell} + U_{over} + i \cdot R_{tot}^{BPMED} + n \cdot V_{BPM} \tag{4.3}$$

R_{tot}^{BPMED} is the ohmic resistance of the BPMED cell and it is composed by electrical resistances of the different elements that compose the cell as shown by Equation 4.4

$$R_{tot}^{BPMED} = R_{elec} + n \cdot R_{dil} + n \cdot R_{acid} + n \cdot R_{base} + (n-1) \cdot R_{CEM} + n \cdot R_{AEM} + 2 \cdot R_{CEEM} + n \cdot R_{BPM} + 3n \cdot R_{sp} \tag{4.4}$$

Where, R_{elec} is the combined electrical resistance of the electrodes and the electrode rinse chambers, R_{dil} is the resistance of the diluate stream, R_{acid} is the resistance of the acid, R_{base} is the resistance of the base, R_{CEM}, R_{CEEM} and R_{AEM} are the resistance of the CEM, CEEMs and AEMs, respectively. R_{BPM} is the ohmic resistance of the BPM whereas R_{sp} is the contribution to R_{tot} given by the spacer and ohmic losses.

The resistances of the three streams were calculated based on the conductivity, as done in the regular ED. R_{elec} and the membrane resistances were separately assessed with blank tests, whereas the resistance of the spacers was assumed equal to the one calculated for the regular ED (see subsection 4.1.2). The electrical resistances of the membrane are reported in Appendix, Table D.1, section D.3. From Table D.1, it is evident that the AEMs in the BPMED stack had a higher resistance compared to the one used in ED. Due to the presence of sorbed water in the membrane, regular AEMs are H^+ conductors [68]. In ED operation this is not a concern since, generally, there is not a significant $[H^+]$ gradient between the stream. However, in BPMED, H^+ can easily diffuse to the diluate affecting the process performance, as explained in chapter 2, subsection 2.4.7. This phenomenon was studied by several authors and new AEMs having a reduced H^+ leakage were specially designed [47]. These membranes are designed to absorb less water and, consequentially, are less permeable to H^+. However, for the same reason, their electrical resistance (R_{AEM}) is usually higher.

Regarding the non-ohmic part of Equation 4.5, U_{cell} was found equal to the one calculated for the ED and independent of the number of triplets in the stack. Contrarily, the term U_{over} seemed to linearly increase with the number of BPMs in the cells (n) and with the applied current. This term was further split as in Equation 4.5.

$$U_{over} = n \cdot (U_0 + U_{irr}) \tag{4.5}$$

Where U_0 is the theoretical potential for water dissociation. This is always lower than the measured one. For this reason, a term that accounts for the voltage drop associated with the dissipative processes (U_{irr}) is also included in Equation 4.5 [22].

U_0 is generally referred to as reversible potential in literature and is logarithmically dependent on the pH difference between the two layers of the BPMs. The pH gradient through the BPM, which is higher

than the pH gradient measured in the batch, results from the water dissociation rate in the membrane. This depends on the applied i (Figure 4.6). Therefore, also U_0 can be seen as function of the applied i. Thus, U_0 (and U_{over}) increases logarithmically with the applied current. For this reason, it would be theoretically incorrect to consider U_{over} linear over the current. However, because the i range, in which the BPMED was operated (between 15-160 $A \cdot cm^{-2}$), was relatively small, the current-voltage curve results almost perfectly linear as shown in Figure 4.15. This permitted to reformulate Equation 4.5 as follow:

$$U_{over} = n \cdot (U_0^{Batch} + U_{irr}) + i \cdot n \cdot R_{over}^{BPM} \tag{4.6}$$

Where U_0^{Batch} is the theoretical potential for water dissociation based on the pH measured in the batches, U_{irr} is the voltage drop owning to dissipative processes and R_{over}^{BPM} is an artificial ohmic resistance introduced in the equation to consider the linear increase of the potential with the current. The last value was assessed equal to 0.65 Ω for the used stack.

Based on the Equation 4.4 and on the data obtained in the current-resistance tests, the ohmic resistance at standard initial condition ($EC = 7.8ms \cdot cm^{-1}$ for all diluate, acid and base) and for a i of 15.6 $mA \cdot cm^{-2}$ was estimated 25.2 Ω. This value is more than double the resistance measured for regular ED. The higher resistance was a combination of the extra elements present in the BPMED-stack and of the additional voltage drop required for the water dissociation process.

In conclusion, it could be deduced that only a part of this extra-energy was actually used for the water dissociation (U_0), whereas the rest was dissipated due to the additional electrical resistance (related to extra-elements in the BPMED stack) and to irreversible processes occurring in the bipolar membranes (U_{irr}) [34, 39].

An overview of the contributions to the stack electrical resistance of each element is given in Figure 4.16.

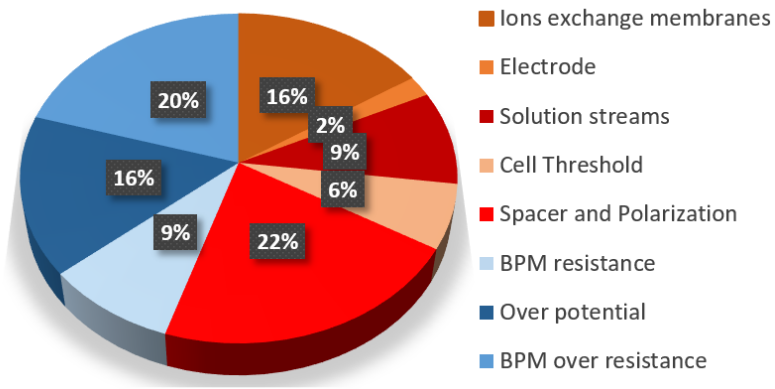

Figure 4.16: BPMED stack potential contributions for different elements at initial standard condition :$EC_d = EC_a = EC_b = 7.8mS \cdot cm^{-1}$ and for a i of $15.6mA \cdot cm^{-2}$. The contributions are split for the two process: water dissociation (bluish shares) and salt transport (red shares).

In Figure 4.16, an attempt is done to discriminate the voltage drops contributions for the two main processes occurring in the BPMED cell, namely, water dissociation (bluish shares) and salt transport (red shares).

It is important to note that the BPMED is a complex system where these two processes are extremely interrelated and occur in a complementary way. Indeed, most of the elements in the stack play a role in both the processes. However, it is still extremely interesting, to explore the potential drop brought by those extra elements. From this analysis, it can be deduced that, for the considered condition, half of the voltage drop could be attributed to elements and processes that were present exclusively in the BPMED stack. In other words, the water dissociation process for a certain current input doubled the potential drop across the cell. This extra required potential definitely impacted the $E_{NH_4^+}$ of the process (as shown in Equation 2.5).

It must be noted that the rise of the potential cannot be directly related to the increase of the $E_{NH_4^+}$ observed in BPMED. Indeed, other parameters, as the current efficiency for salt transport, played a

fundamental role for energy utilization in both, ED and BPMED.

4.4. Gas diffusion in electrodialysis with bipolare membranes

Literature addresses diffusion of NH_3 gas as the limiting phenomena in the application of BPMED for the concentration of NH_3 from NH_4HCO_3 solutions [11, 25]. The empirical results of the SBE run with this salt solution, discussed in section 4.3, showed that the diffusion of NH_3 contributed to the accumulation of NH_4^+ into the acid stream. Gas diffusion from the concentrate stream to the diluate (and the resulting re-ionization of the NH_3) reduced $CE_{NH_4^+}$ and lowered the TAN concentration in the base. For these reasons, a better comprehension of this phenomena and of its magnitude is fundamental to assess the potentiality of BPMED for the recovery of NH_3.

Due to the complexity of the BPMED and the several processes simultaneously occurring during operation, it is difficult to extrapolate and quantify the contribution of gas diffusion to the reduction of the $CE_{NH_4^+}$ from the result of the SBE. For this reason, a specifically customized experiment, described in section 3.2, was performed to calculate the gases diffusion rate. The results of the diffusion tests with NH_3 and CO_2 are presented in the following sub-section.

4.4.1. Ammonia diffusion from the alkaline compartment

Figure 4.17 shows the TAN concentrations evolution over the diffusion experiment. As expected, the concentration of the total NH_3 nitrogen decreased over time as result of gas diffusion. Moreover, during the experiment, the slope of the concentration curve decreased. Indeed, NH_3 gas diffused toward the acid and diluate depleting the TAN concentration in the base while increasing the concentration in the other compartment. This decreased the gas partial pressure difference between the stack's compartments (gas diffusion driving force) slowing the gas diffusion process. This trend is consistent with the theory presented in chapter 2 in subsection 2.4.6.

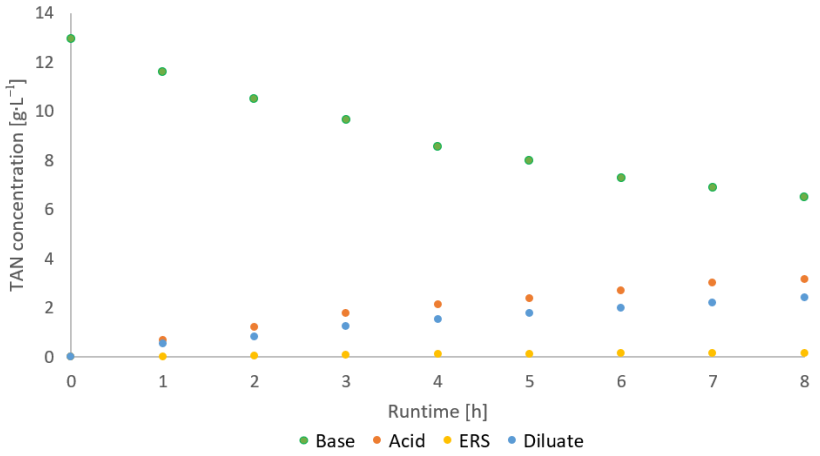

Figure 4.17: TAN concentration in the base, acid, diluate and ERS during the NH_3 diffusion test.

An opposite trend in concentration was observed in the other streams. Also in this case, the slope of the curves decreases along the runtime due to the reduction of the driving force. The concentration in the acid was higher than in the diluate. Therefore, NH_3 diffused preferentially through the BPM. Since the initial driving forces were equal, it can be stated that the K_{BPM} was higher than K_{CEM} in the employed stack. A relatively small amount of NH_3 was transferred into the ERS by gas diffusion. The observed rate of NH_4^+ accumulation in the ERS observed in section 4.3 was thus mainly resulting from the ion diffusion across the CEEM. In full-scale installations, a much larger number of membrane triplets is used (50–100 triplets), which will decrease the relative loss of ions into the electrode rinse solution proportionally [26].

By summing the total mass of TAN salt accumulated in the different compartments, a really small reduction in the mass was measured over the experiment. This suggested that, although the installation was almost sealed, NH_3 volatilization could still occur. However, the losses were relatively small (only 5.6% of the initial mass after 8 hours) and they could be caused by measurement errors.

Diffusion of NH_3 also impacted the pH of the different solutions. The pH decreased over time in the base stream while it increased in the other streams.

An NH_3 diffusion coefficient (K_{strm}) can be defined for each stream compartment. This coefficient expresses the tendency of each chamber to diffuse NH_3 gas. The higher is the K_{strm} the faster is the diffusion of NH_3 from or toward the adjacent compartment. This parameter could be calculated plotting the gas diffusion rate in $g_{NH_4^+} \cdot m^{-2} \cdot min^{-1}$ against the average NH_3 partial pressure difference between the stream and the adjacent chambers. This was done for the three active streams and it is shown in Figure 4.18. The NH_3 partial pressure difference (Δp_{NH_3}) needed to be calculated by considering the pH of each stream because not all the measured TAN was in the gas phase. The calculation of the NH_3 partial pressure based on TAN concentration and pH was performed using PHREEQC. The employed script is reported in Appendix, section C.1.

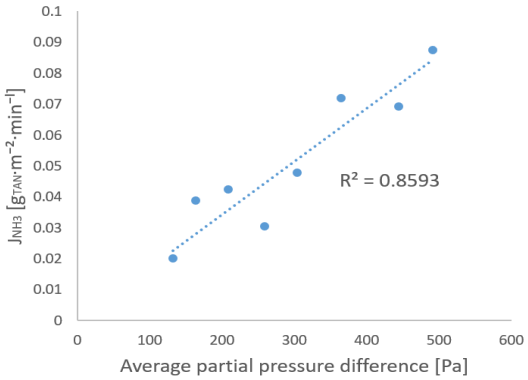

(a) NH_3 diffusion flux in the acid stream (J_A). The slope of the curve represent the NH_3 diffusion coefficient of the acid chamber K_{acid}.

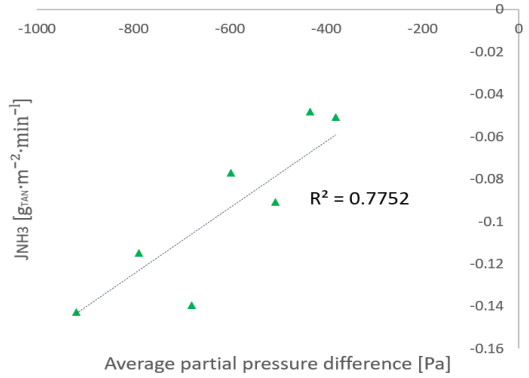

(b) NH_3 diffusion flux in the base stream (J_B). The slope of the curve represent the NH_3 diffusion coefficient of the base chamber K_{base}. In this case, since the driving force (Δp_{NH_3}) is negative also the flux (J_B) is negative.

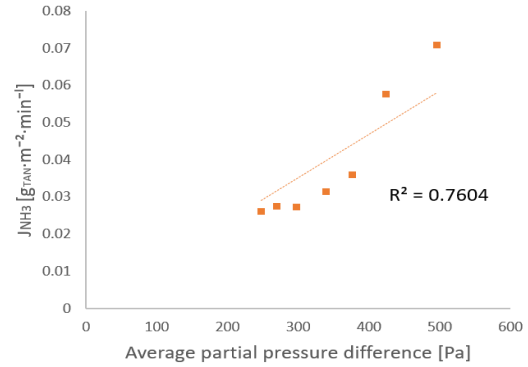

(c) NH_3 diffusion flux in the diluate stream (J_D). The slope of the curve represent the NH_3 diffusion coefficient of the diluate chamber K_{dil}.

Figure 4.18: NH_3 diffusion flux for the three considered BPMED chambers. For the calculation of the partial pressure the effect of the NH_3 diffusion toward the electrode rinse solution have been neglected.

The measured values for J in Figure 4.18 were distributed along a straight line that crosses the origin. For every chamber the slope of the line in Figure 4.18 was the value of the stream NH_3 diffusion coefficient K_{strm} in $[s \cdot m^{-1}]$. As expected, the slope of the curve in Figure 4.18a was steeper than the one in Figure 4.18c. Table 4.2 shows the K_{strm} for the different BPMED chambers.

The value of the K_{strm} is the combination of the two membrane coefficients (K_{mbr}) delimiting the chamber. By the means of only the results of the diffusion test, it was not mathematically possible to calculate the NH_3 diffusion coefficient for the employed membranes (K_{mbr}). Additional experiments involving stack re-arrangement are needed to assess this value. Since the numerical determination of this value for the employed membrane falls outside the scope of this research, a specific experiment

K_{strm}	NH_3 diffusion coefficient $[s \cdot m^{-1}]$
K_{base}	$1.6 \cdot 10^{-9}$
K_{acid}	$1.2 \cdot 10^{-9}$
$K_{diluate}$	$1.7 \cdot 10^{-9}$

Table 4.2: K_{strm} $[s \cdot m^{-1}]$ for NH_3 in the 3 active streams according to the performed diffusion test.

to determine those values was not carried out. However, in the design of a BPM for this specific application, the $K_{mbr}s$ should be considered as a fundamental parameter in the membrane selection. A similar conclusion was also reported by Ali *et al.* [25], who showed that the current efficiency for NH_3 production varies from 84% to 57% for two different CEMs tested. However, it was not very clear whether this gain was only associated to a better blocking of NH_3 gas or to a higher permselectivity with respect to OH^- leakage.

The curve of J_D expresses the severity of NH_3 diffusion from the base and acid toward the diluate. This value was not big enough to completely explain the relatively low $CE_{NH_4^+}$ observed in the experiment with NH_4HCO_3. Assuming that NH_3 diffusion takes place with the NH_3 diffusion flux associated with the maximum partial pressure potential observed during the SBE (last batch run), only 0.21 $g_{NH_4^+} \cdot h^{-1}$ would be transported into diluate. This corresponds to a reduction of about 11.3% in the current efficiency of salt transport. During the SBE, the average current efficiency was between 73 to 60.3 %. Considering a 10% loss due to ionic short-circuits and NH_4^+ leakage into the ERS compartment, NH_3 diffusion was still not severe enough to completely explain the observed $CE_{NH_4^+}$ even in the first batch of the SBE. This finding points out the crucial role of H^+ and OH^- leakage in lowering $CE_{NH_4^+}$.

4.4.2. Carbon dioxide diffusion from the acid compartment

For the CO_2 diffusion test, the acid stream was saturated with CO_2. The CO_2 concentration during the experiment was measured by testing the TIC. Based on the composition of the water used in the test and on the theory about TIC equilibrium (section A.2 in Appendix), the concentration of TIC was assumed equal to the concentration of CO_2.

The evolution of the TIC concentration in the acid over the experiment is shown in Figure 4.19. The CO_2 concentration in the acid confirms what was observed in the base during the NH_3 diffusion test: an initial high CO_2 diffusion rate that gradually flattened over time. However, by plotting the TIC concentration in the other streams, only slight changes in concentration were observed (Figure 4.19).

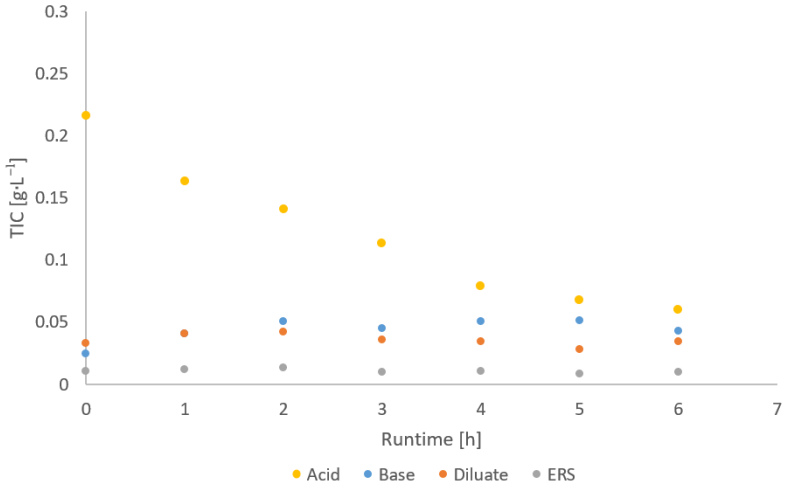

Figure 4.19: TIC concentration in the acid, base, diluate and ERS during the CO_2 diffusion test.

The fate of the CO_2 initially dissolved in the acid is clear when the cumulative concentration in the streams is plotted (Figure 4.20).

The low solubility of CO_2 and the pressure drop over the distribution system promoted the stripping of the CO_2 gas. For this reason, the gas did not accumulate in the other streams but it was stripped

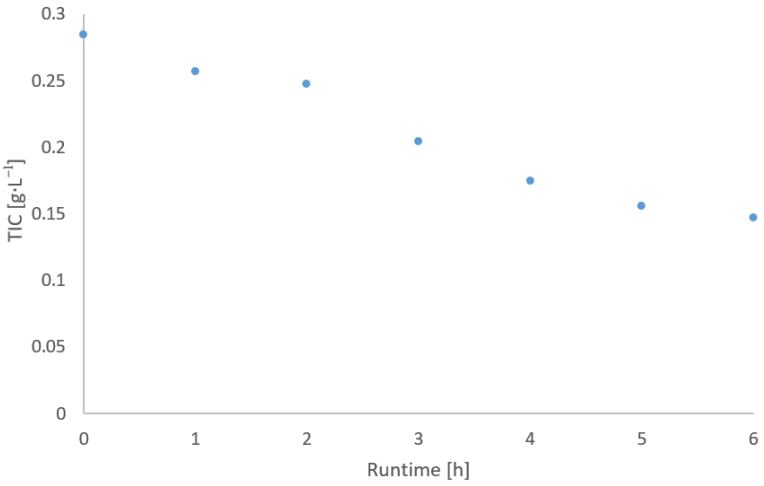

Figure 4.20: TIC total mass in the streams during the CO_2 diffusion test. The reduction in mass could be assigned to the volatilizing of CO_2 from the system.

and released to the atmosphere. This explains why the concentration of TIC in the other stream did not increase substantially.

For this reason, the data acquired during this experiment could not be used to draw conclusions on the diffusion coefficients for CO_2. However, the experiment showed how easily CO_2 was stripped from the streams. Thus, the accumulation of dissolved CO_2 gas in the streams over the SBE experiment is not a concern. This has two main implications for operation:

- The CO_2 diffusion driving force (Δp_{CO_2}) developed principally when the water flows along the stack and ,as a consequence of that , it is mostly influenced by the applied current.
- Due to the low solubility and to the turbulence in the distribution spacer, CO_2 could form gas bubbles within the stack. This and the higher EC of the concentrate streams could partially explain the discrepancy in voltage (about 15%) observed when the BPMED is operated with $NaCl$ and NH_4HCO_3.

4.5. BPMED coupled with vacuum membrane stripping

With the purpose of limiting the diffusion of CO_2 and NH_3 within the stack, two VMSs were installed in series with the concentrate streams of BPMED, as shown in Figure 3.4. This section describes the result of the tests run with this set-up.

4.5.1. Effect of vacuum membrane stripping on current efficiency

The first batch of the SBE was run with BPMED in combination with two VMS devices. The experiment was performed to assess whether the gas diffusion can be significantly reduced by coupling the EBBPM cell with a membrane vacuum stripping device. Initially, the stripping was applied alternately only to the base or only to the acid. After that, both the concentrate streams were connected to a different VMSs.

The resulting current efficiencies for salt transport are shown in Figure 4.21

Although less than expected, the implementation of the gas stripper in the system slightly increased the overall $CE_{NH_4^+}$. This could be observed in both the cases: when the VMS was applied only to one stream, and when it was applied to the two concentrates on the same run. The gain in $CE_{NH_4^+}$ with the base stripping was moderately higher than with the acid. When the two strippers were employed simultaneously a further increase in $CE_{NH_4^+}$ was obtained. Moreover, when the base stream was stripped a lower NH_4^+ concentration was observed in the acid (1.46$\pm$0.05 against 1.57 $\pm$0.05 $g_{NH_4^+} \cdot L^{-1}$). This proved that the tested configuration was actually capable of reducing the gas diffusion over the stack.

A similar evolution of the $CE_{NH_4^+}$ over the experiment was observed for the four configurations as is shown in Figure 4.22.

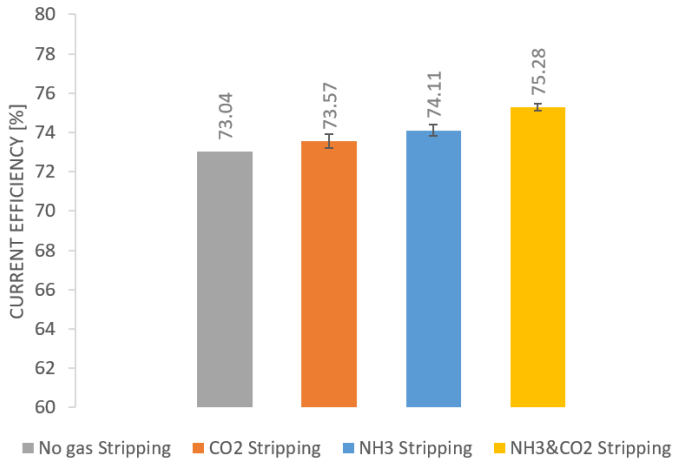

Figure 4.21: Current efficiency for NH_4 transport in the first batch of the SBE. Different combination of BPMED and membrane vacuum stripping are compared.

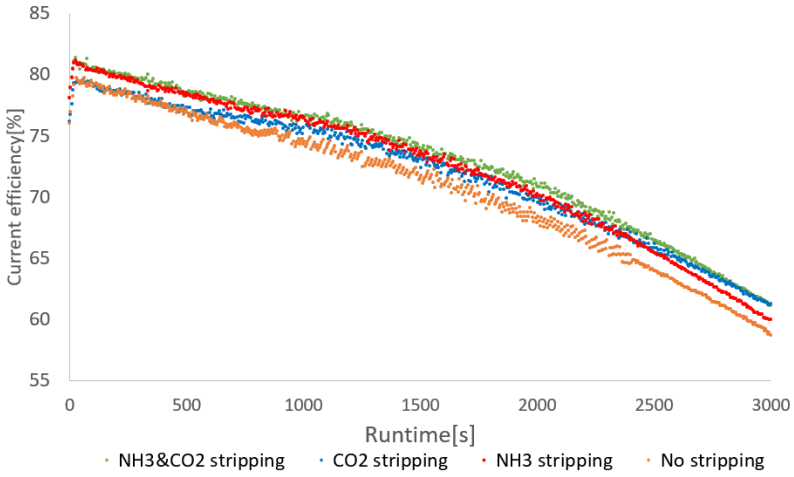

Figure 4.22: Current efficiency for NH_4 transport. Different combinations of BPMED and membrane vacuum stripping are compared. The $CE_{NH_4^+}$ trend is based on the diluate salt depletion.

The curve representing the $CE_{NH_4^+}$ without stripping is the lower for the whole run. On the other hand, as expected, when both the stripping devices were included in the installation the $CE_{NH_4^+}$ was always the highest. Particularly interesting was the behavior of the $CE_{NH_4^+}$ for the two single stream stripping unit configurations. When the stripping device was applied only to the base, the $CE_{NH_4^+}$ was initially higher than when CO_2 was stripped from the acid. This lasted only for the first section of the experiment. Indeed, after about 1700 seconds, the $CE_{NH_4^+}$ obtained with the only stripping of the acid resulted higher than the $CE_{NH_4^+}$ achieved with the only stripping of the base stream. The cause behind this behavior is complex because it was the result of multiple operation factors (i.e. applied current over the run, the solubility of the gases involved and system properties). Further customized experiments are need to justify these trends in $CE_{NH_4^+}$.

4.5.2. Sequencing batch experiment with BPMED coupled with VMS

In order to evaluate the effect of stripping for higher pH and NH_3 concentration in the base, the first five batches of the SBE were run coupling the BPMED with two VMSs in series to the concentrates streams.

The obtained $CE_{NH_4^+}$ over the five runs are compared in Figure 4.23. The high $CE_{NH_4^+}$ obtained for the first batch was because of the relatively high initial concentration in the first run. This, in general,

promotes the $CE_{NH_4^+}$ [27]. A similar explanation can be given for the high value recorded in the 5^{th} batch when the strippers were not applied.

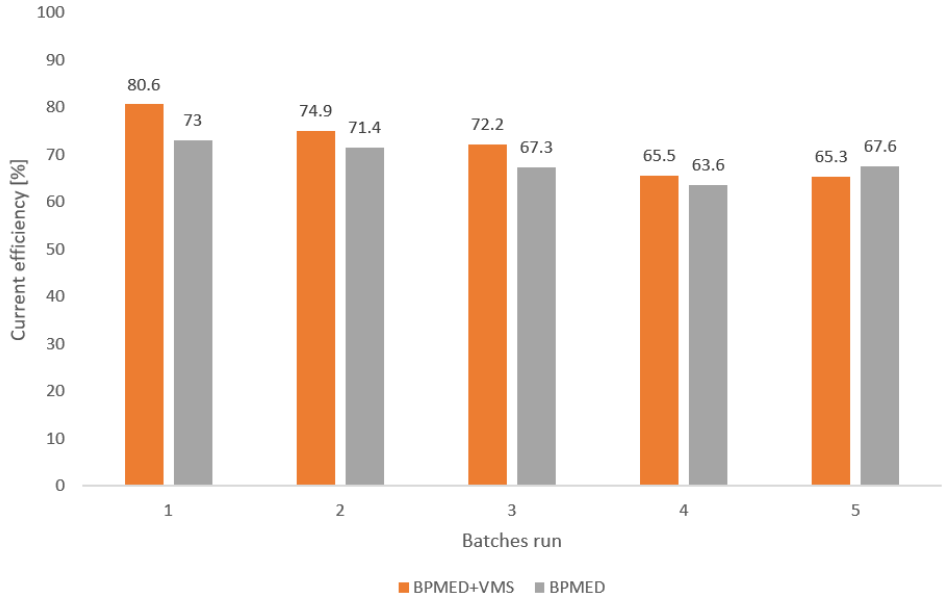

Figure 4.23: Current efficiency for NH_4^+ transport in the first five batches of the SBE. The bar-chart shows the gain in $CE_{NH_4^+}$ with the implementation of the membrane stripping devices.

As expected, the $CE_{NH_4^+}$ benefited from the implementation of the membrane stripping. However, the gains seemed to be less substantial for the latest batches. When the strippers were added to the installation, a slight increase in base pH was observed. This is shown in Figure 4.24.

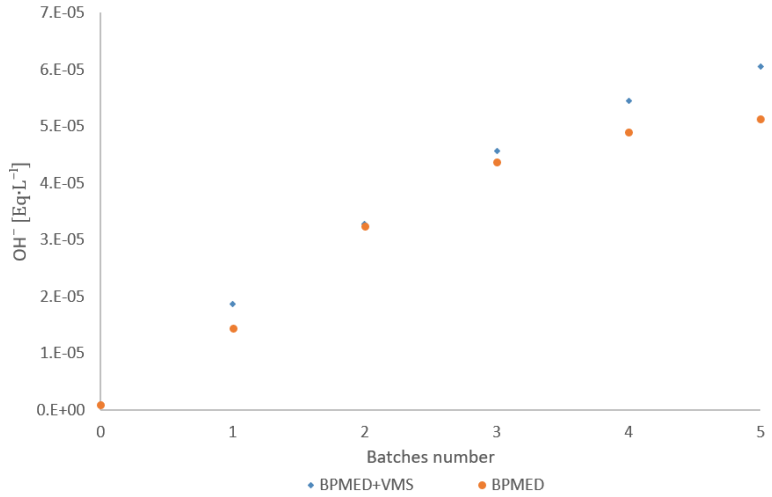

Figure 4.24: OH^- concentration in the alkaline stream during the SBE. The OH^- concentration is based on the measured pH.

The increment of the base pH can be assigned to the combination of CO_2 diffusion reduction across BPMs, and to the initial stripping of CO_2 from the base stream. With the rising of the pH in the base over the experiment, the OH^- leakage increased. This could be observed monitoring the pH of the diluate which presented a steeper increase over the experiment runs, as depicted in Figure 4.25.

In Figure 4.24, it is shown that the rate in the accumulation of OH^- in the alkaline stream decreased over the batches in the SBE. As argued in subsection 4.4.2, the severity of CO_2 diffusion was expected to be almost the same in every batch, because there was almost no accumulation of dissolved CO_2 along the SBE. Therefore, the reduction in OH^- accumulation rate in the base was probably caused by the OH^- leakage toward the diluate. By comparing the rate of OH^- accumulation in the first batch

with the later runs, the amounts of missing OH^- can be roughly estimated. These were in the right order of magnitude to explain the observed increases in diluate pH over the 5 batches, Figure 4.25.

The leakage of OH^- toward the diluate was expected to be higher than what measured by considering the increase of OH^- accumulation in the diluate. However, the buffering capacity of the diluate, due to its HCO_3^- initial concentration and to the CO_2 gas diffusion, probably masked the pH change caused by this leakage.

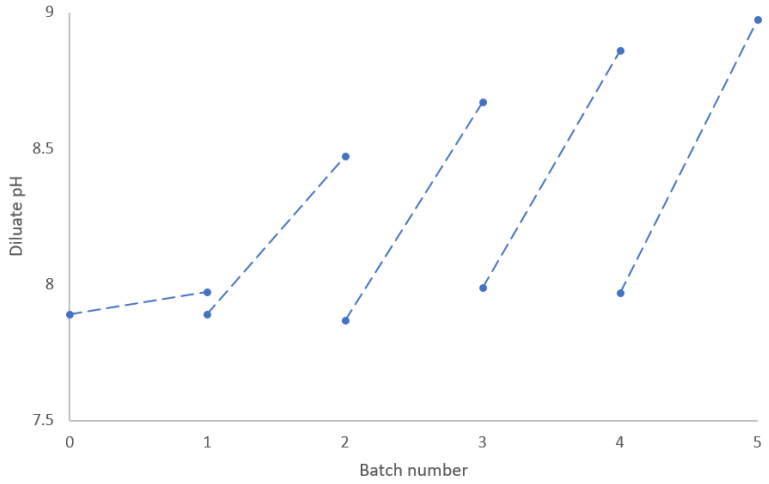

Figure 4.25: Diluate pH evolution in the 5 batches tested with membrane stripping combined with BPMED.

The TAN concentration in the base and acid streams did not seem to be significantly affected by the presence of the strippers. As currently designed and operated, the used installation was only partially able to limit NH_3 diffusion in the BPMED cell. However, the combination of BPMED and VMS was capable of stripping NH_3 also without any optimization of the two technologies. Indeed, at high pH and concentration in the base, the device stripped the dissolved NH_3. This was proven by the rising NH_4^+ concentration in the acid trap connected to the stripping device of the base stream (Figure 4.26).

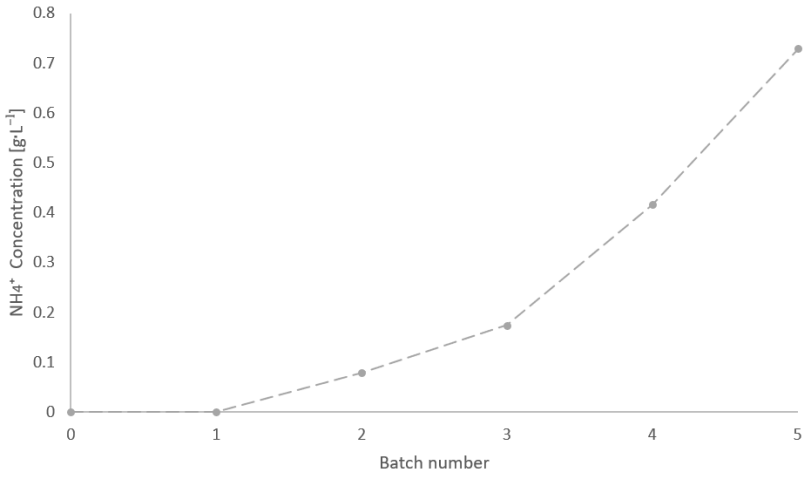

Figure 4.26: TAN concentration in the acid trap connected to the stripping device of the base stream.

With the presented configuration, the stripped NH_3 mass was low and thereby also the gain in $CE_{NH_4^+}$. However, by optimizing this combination of technologies, the performance could be highly improved. This will lead to a more substantial gain in the $CE_{NH_4^+}$ and to a consequential reduction of the energy cost in operation.

Another probable reason why the gas stripper was not so effective in reducing NH_3 diffusion is that VMS reduces the NH_3 concentration of the water that was fed to the BPMED base chamber. However, when the alkaline stream passes along the cell its NH_4^+ concentration and pH suddenly increased. The

NH_4^+ conversion to NH_3 within the cell and gas diffusion occurred before the water could passed by the stripper. This was confirmed by the observation that gas diffusion was experienced also in the first batch, when base concentration and pH were relatively low in the alkaline batch.

To conclude, OH^- leakage and gas diffusion, combined to the low current applied at the end of the SBE's runs, are thought to be the main causes of the $CE_{NH_4^+}$ drop in single batch runs, as well as during the whole experiment. The VMS in series with the BPMED was not able to properly limit NH_3 diffusion. This was because the stripping unit was not optimized and because the gas, formed in the cell, had enough time to diffuses before being stripped in the VMS. Ideally, a direct stripping from the cell could potentially tackle the last issue. However, a technology able to directly strip gas from an ED cell has never been designed.

4.6. Energy use: BPMED compared with ED-Sodium hydroxide

Electrodialysis with the bipolar membrane was able to reach a concentration of 6.635 $g_{NH_4^+} \cdot L^{-1}$ using in total 48.7 Wh. To achieve the same concentration in the concentrate stream, the regular ED spent only 10.2 Wh. The extra energy necessary for operation in BPMED was mostly related to the water dissociation process, as discussed and proven in subsection 4.3.2. This process indeed permitted to obtain a high pH in the base, which promotes the stripping of NH_3 [12]. This high pH can also be achieved with the use of chemicals.

The $NaOH$ needed to reach a pH of 9.8 in a 1-litre solution containing 0.388M of NH_4HCO_3 was calculated. The considered pH and concentration were comparable to the maximum pH and TAN concentration obtained in the SBE with BPMED. This reaction was simulated with the software PHREEQC Interactive. The designed script is shown in Appendix, section C.1. The final pH of the ED concentrate solution was equal to 7.85, based on empirical data.

To raise the pH till 9.8, 0.415 moles of $NaOH$ are consumed. This is equal to 33.19 g of a 50%wt $NaOH$ solution. According to the data for the energy consumed in the production of this solution provided by Hong *et al.* [57], a total of 72.35 Wh per litre of solution treated are required. By considering the energy spent in the ED for concentrating NH_4HCO_3, the required energy reaches 82.55 Wh. This is higher than what consumed by BPMED.

It can be argued that during the production of sodium bicarbonate also chlorine or chlorine-based compounds are produced (i.e. sodium hypochlorite, hydrochloric acid). These compounds have also a value on the market and thereby it could partially compensate the energy cost for the lye production. However, pH control with BPMED offers several other practical advantages over the dosing of caustic soda. The most relevant are listed below:

- BPMED when coupled with VMSs was able to produce CO_2 gas, which also is a valuable resource in industry.
- With BPMED, no extraction of salt and transport of chemicals are involved. These according to Hong *et al.* [57] account for an extra 109.7 $kWh \cdot t_{NaOH}^{-1}$.
- The storing and dosing of caustic soda increase the complexity of the treatment facility and require the installation of storage tanks and dosing devices. This implies a higher footprint of the treatment installation.
- The exposition to caustic soda is dangerous for humans. General precautions and prevention measures have to be taken in processes involving this compound. Moreover, the treatment of empty containers and storage is necessary before the disposal. This involves additional cost.
- A residual liquid stream containing a high concentration of sodium bicarbonate is obtained, which has a market value but it hardly has a direct on-site application.

Besides the previously listed considerations, also a reflection on the environmental issues linked to the production of $NaOH$ solution should be done. In addition to the significant contribution to carbon emissions as a result of the energetically intensive production process, the caustic soda industry also emits numerous compounds into the local environment (i.e. heavy metals and organochlorine compounds) [57]. Many of these compounds (especially those associated with chlorine) are toxic and cannot be completely eliminated by the means of conventional treatments [69].

To conclude, the studied BPMED system was proven to be superior in terms of energy consumption when compared to the combination of ED and chemical addition. On top of that, this concept showed crucial advantages for the environment, plant design and safety issues. Finally, it is relevant to mention that, neither the technology nor the operation method used, were specifically designed/optimized for this application. This makes even more interesting and promising the use of BPMED for the *N2kWh* purpose.

5

Conclusions

The main goal of this work was to evaluate the potential of BPMED for the recovery of NH_3 within the scope of the *N2kWh* project. The energy performance of this technology was compared with the alternative use of regular electrodialysis plus $NaOH$ for pH regulation.

In order to obtain valuable information on the process taking place in operation, three different setups were used: regular ED, BPMED and BPMED coupled with two VMS devices. Three main parameters were defined and employed to monitor and analyze the performance of the setups. These parameters were: current efficiency for NH_4^+ transport ($CE_{NH_4^+}$), current efficiency for water dissociation (CE_{WD}^{meas}), and energy use for NH_3 removal (expressed in $MJ \cdot Kg_{NH_4^+}^{-1}$). Experiments were specifically designed to assess the impact of the various occurring processes on the BPMED performance. The main conclusions drawn from the obtained experimental results are reported in this chapter.

Water dissociation current efficiency

Results on water dissociation current efficiency showed that three processes reduced CE_{WD}^{meas} by influencing the pH trend in the concentrate streams:

- The co-ions leakage through the BPMs impacted the actual electro-generation of ions in the BPMs transition layer, reducing the pH in the concentrate streams.
- The diffusion of NH_3 and CO_2 gases also affected the pH adjustment in the concentrate due to the re-ionization of the diffused gases.
- H^+ and OH^- leakages across IEXMs, which occurred as a consequence of a pH difference between the concentrates and the diluate, was also proven to reduce CE_{WD}^{meas}.

The negative impact on CE_{WD}^{meas} of the above-listed processes were more severe when the applied current density (i) was lower.

Energy consumption and salt transport current efficiency

In terms of energy consumption for the NH_4^+ removal ($E_{NH_4^+}$) the BPMED used more energy compared to the ED. The removal of the 90% of the initial NH_4^+ was achieved using an average of 4.87±0.33 Wh per litre, or, 13.2±0.1 $MJ \cdot kg_{NH_4^+}^{-1}$. This value was 3.3 times higher than that achieved with regular ED. However, the $E_{NH_4^+}$ in BPMED was still about three times lower than the energy consumed by nitrification denitrification and comparable to what used by anammox.On top of that, it has to be noted that this installation not only removed nitrogen, but it also produced an NH_3 stream, which can be stripped and ideally fed to the SOFC. This could potentially produce 9.6 $MJ \cdot Kg_{NH_4^+}^{-1}$ reducing the overall energy need in the treatment [65].

The discrepancy in $E_{NH_4^+}$ between regular ED and BPMED was explained via an analysis of the electrical potential drop over the ED and BPMED cell. This suggested that the extra elements in the stack and the water dissociation process are responsible for the additional voltage measured in BPMED.

Moreover, the $E_{NH_4^+}$ was proven to be higher also due to the lower $CE_{NH_4^+}$ in BPMED (73% against 95% in conventional ED).

Regarding the $CE_{NH_4^+}$, three different processes reduced it in BPMED operation:

- The salt ions leakage through the IEXMs (or back-diffusion), which, however, have been proven to be marginal.
- The gas diffusion from the base toward the diluate, which directly reduces the $CE_{NH_4^+}$ for NH_4^+ transport.
- The OH^- leakage from the base toward the diluate, that seemed played a crucial role in the $CE_{NH_4^+}$ reduction.

All these diffusion phenomena more severely affected the $CE_{NH_4^+}$ when the applied i was lower. This is due to the competition between diffusion phenomena depending on residence time and salt migration depending on i.

Ammonia and carbon dioxide diffusion over the BPMED stack

A study focused on NH_3 and CO_2 diffusion was performed. This showed that NH_3 diffusion was 25% more severe across the BPMs than to CEM. NH_3 diffusion increased the TAN concentration in the acid stream over the experiment and reduced the maximum concentration in the base chamber. The NH_3 diffusion toward the diluate was not severe enough to individually explain the low $CE_{NH_4^+}$. This finding validated the crucial role of OH^- and H^+ leakages for the $CE_{NH_4^+}$ reduction.

Thanks to the low solubility of CO_2, the accumulation of dissolved gas in the stream over the experiment was not a concern in the case of CO_2. This had two main implications for operation:

- The CO_2 diffusion driving force developed principally when the water flowed along the stack. Therefore CO_2 diffusion could be probably directly related to the applied current.
- Due to the low solubility and to the turbulence in the distribution spacer, CO_2 could form gas bubbles within the stack. This and the higher EC in the concentrate streams obtained with $NaCl$ could explain the discrepancy in voltage (15% difference) observed when the EDBPM was operated with $NaCl$ and NH_4HCO_3.

Electrodialysis bipolar coupled with membrane vacuum stripper in series

In order to control gas diffusion and raise the energy efficiency, two membrane vacuum stripping modules (VMS) were placed in series with the concentrate streams from BPMED. The gases stripped by the VMSs were passed through acid and base traps to capture the stripped CO_2 and NH_3. The implementation of the VMS slightly increased the overall $CE_{NH_4^+}$ in both cases: when the VMS step was applied only to one of the two concentrate streams, and when it was applied to both simultaneously. The gain in $CE_{NH_4^+}$ with the base stripping was moderately higher than with the acid (1% increase against 0.5% respectively). When the two strippers were employed simultaneously a further increase in $CE_{NH_4^+}$ was obtained (up to 3.4% $CE_{NH_4^+}$ gain). This increase seemed to be significant only for the first batches of the SBE.

When the base stream was stripped a lower NH_4^+ concentration was observed in the acid (1.46 ± 0.05 $g_{NH_4^+} \cdot L^{-1}$ against 1.57 ± 0.05 $g_{NH_4^+} \cdot L^{-1}$). Besides that, a rise in the TAN concentration of the acid trap connected to the strippind device of the base stream was observed. This proved that the tested concept was capable of stripping NH_3 and, consequently, reducing the gas diffusion over the stack.

Electrodialysis plus chemicals against BPMED

To raise the pH till 9.8 in a 6.6 $g \cdot L^{-1}$ NH_4HCO_3 solution, which were the maximum pH and NH_4^+ concentration achieved in the base during the SBE with BPMED, 0.415 moles of $NaOH$ per litre of treated NH_4HCO_3 solution were necessary. According to literature, the energy consumed for the production of this amount of $NaOH$ is 72.35 Wh. By adding the energy spent in the ED for concentrating NH_4HCO_3, the energy used in the overall process increased to 82.55 Wh. This was higher than what was consumed by BPMED (48.7 Wh) to achieve the same conditions in the base concentrate. Thus, the studied

BPMED installation was shown to be superior in terms of energy consumption when compared to the combination of ED and chemical addition. Additionally, this concept showed crucial advantages for the environment, design and safety of the treatment facility.

Finally, it must be mentioned that, neither the technology nor the operation method employed, were specifically designed/optimized for this application. This made even more interesting and promising the employment of BPMED for the purpose of the *N2kWh* project.

6

Recommendations

The scarce literature present on the use of BPMED for recovery of NH_3, emphasizes the innovative concept investigated in this work. On the other hand, it arises several sparks for further related studies and design improvements. The most relevant are collected in this chapter.

Fouling prevention in BPMED

A major problem affecting the efficiency of almost all membrane separation processes in long-term operation is fouling [35, 70]. In ED, suspended solids that carry positive or negative electrical charges can deposit on the membrane surface. These will increase the resistance of the membrane dramatically [23]. In ED, the problem has been eliminated to a large extent by temporarily reversing the polarity of the electrodes. Unfortunately, due to its particular membrane arrangement, this technique cannot be applied to BPMED. The fouling type and severity results from the membrane system design, operation strategy and from the composition of the feed water. A characterization of the fouling in BPMED operated with the water considered in the *N2kWh* project should be performed. Based on this, suitable pretreatment strategies could be designed in order to guarantee a smooth operation of the BPMED.

Reduction of the energy consumption in regular ED

In subsection 4.1.2, the contributions of the elements composing the ED to the total voltage drop over the cell were analyzed. Based on this, it was immediately clear that the most substantial contribution to the total potential drop over the stack was due to R_{sp}. A more accurate characterization of this term would be a good starting point for the reduction of voltage drops in ED.

Another consideration has to be done on the contribution to the potential drop brought by the two terms: U_{cell} and R_{elec}. These accounted for the 20% of the total potential drop in the considered condition. Differently from the other terms in Equation 4.1, U_{cell} and R_{elec} are independent of the number of membrane pairs in the stack. In an industrial size ED plant, where 100 to 200 cell pairs are arranged between the electrodes [23], their relative contribution to the total voltage drop decreases. Because of that, the total voltage drop will not increase linearly with the stack size. This will potentially lead to a cut in the OPEX, since the NH_4^+ mass transport rate increases with a one-to-one relationship with the stack size. The decrease of the relative contribution of U_{cell} and R_{elec} over the stack size can be seen in Figure 6.1.

Nevertheless, by increasing stack size, a small but tangible reduction in $CE_{NH_4^+}$ transport was observed. This will significantly reduce the energetic gain of the scaling-up. The drop in $CE_{NH_4^+}$ is probably caused by ionic short-circuits [20, 64]. A study of this phenomenon for this particular application should be undertaken to assess whether the benefits brought by a system scaling-up will overcome the observed reduction in $CE_{NH_4^+}$.

For BPMED the voltage drop associated with the electrodes and with the cell account only for a small part of the total voltage. For this reason, the scaling-up of the BPMED installation is not expected to decrease significantly the $E_{NH_4^+}$.

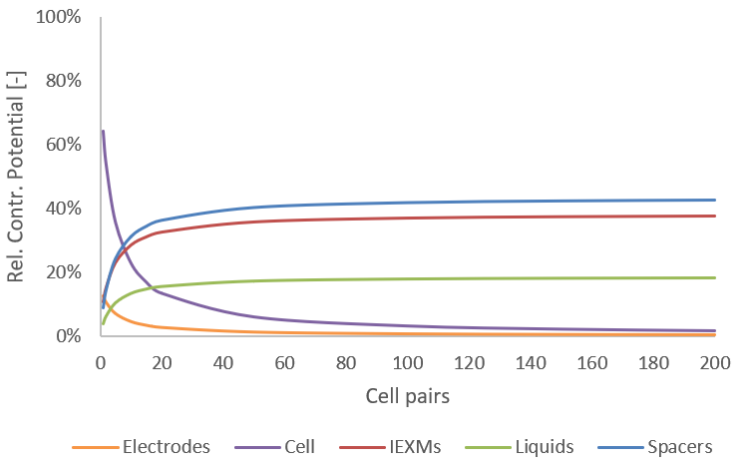

Figure 6.1: Evolution of electrical potential distribution over ED stack size for i equal 15.625 $mA \cdot cm^{-2}$ at initial standard condition :$EC_d = EC_c = 7.8mS \cdot cm^{-1}$. The y-axes addresses the relative contribution (in %) for each elements in in %.

Gas diffusion in BPMED and operation optimization

In this research, the stripping devices were connected to the outputs of the BPMED concentrate and a constant vacuum pressure was applied. No optimization of the vacuum pressure neither of the membrane surfaces was performed. For instance, the cross-flow velocity of the water in the VMS was fixed to 6 $cm \cdot s^{-1}$. According to Mojab *et al.* [71], under this conditions the flow was laminar and, therefore, the stripping process not optimized. Nevertheless, the $CE_{NH_4^+}$ still benefits from the implementation of the membrane stripping. However, the response of the $CE_{NH_4^+}$ for different conditions and stripping setups showed two peculiar trends:

- The gains seem to be less significant for the last batches.
- The increase of $CE_{NH_4^+}$ at the beginning of the runs seems to be attributed mostly to the base stripping. Contrarily, the stripping of CO_2 in the acid seems to mostly benefit the final part of the SBE run.

This behaviour is related to the mechanisms of gas diffusion inside the membrane and their interaction with the membrane stripping unitis. A better understanding of the gas diffusion phenomena within the stack will lead to a clarification of the observed trends. Further investigations on this are suggested for future studies. This will allow the optimization of this technologies combination and to fully exploit the benefits brought by the VMSs.

The applied i has a crucial influence on the performance of the device. It is well-known that the proper increase of i is helpful to improve the performance of BPMED [24–27]. The current distribution over the run used for the SBE was based on a theoretical optimization validated with empirical data for regular ED operation. A customized way of i supplying for BPMED should be developed. For instance, by reducing the NH_4^+ removal-rate or increasing the $\frac{i}{LCD}$ rate properly during the run, the BPMED could be operated at higher average i. Another possibility is to increase the cross-flow velocity in the stack to rise the LCD. These solutions will lead to an improvement in performance and to the potential reduction of $E_{NH_4^+}$.

Improvement of cation exchange membrane properties

The OH^- leakage through the CEM membrane affected the performance of the BPMED in term of maximum ammonia concentration and pH in the base. The implementation of a CEM with a higher perm-selectivity for OH^- (as already done for the AEM with respect of H^+) is expected to significantly improve the BPMED performance.

Besides that, the gas diffusion coefficient for BPMEDs and CEMs were found to be fundamental parameters for limiting gas diffusion. They were directly related to the installation performance in terms of base concentration and current efficiency. For this specific application, besides the electrical

resistance and the permselectivity, also the resistance of the membrane to gas diffusion should be considered during the membrane choice for the stack design.

Alternative methods for the pH regulation of the alkaline stream

The combination of ED and $NaOH$ required almost double of the energy used by BPMED for achieving the same result. However, most of this energy requirement (87%) is related to the production of the $NaOH$ solution. A different way to increase the pH, or an alternative method for the production of $NaOH$, could bring an important reduction of the energy consumed. This would make the ED competitive again with the BPMED for the considered purposes. The combination of ED for ammonium concentration and BPMED for pH regulation is an interesting solution to investigate. Using the concentrate of ED as feed water for the BPMED would permit to operate the BPMED with higher i and thus with higher efficiency. Moreover, in this way, only a small fraction of the reject water would be treated by the BPMED. This could reduce the overall energy consumption.

pH and TAN concentration in the alkaline stream

Martens [12] identified a minimum pH and TAN concentration (pH of 10 and 10 $g \cdot L^{-1}$) in the to-strip solution in order to obtain an NH_3 stream good enough to be fed into the SOFC. During, the experiments performed in this study none of the two requirements were achieved. It is important to note that the experiments were not designed to specifically reach these values, but to characterize the behaviour of the BPMED for the production of an enriched NH_3 stream. Indeed, although a flattening in the base concentration occurred after the 9^{th} batch of the SBE, the trend in concentration was still increasing.

It is, thus, still interesting to investigate whether this installation is able to provide a concentrate that fulfills the requirements defined by Martens [12]. In case it is not, or if the required energy exceeds the one of the combination of ED and chemicals, the previously mentioned recommendations for the optimization of the process should be taken as starting points for optimizing the concept and making this goal achievable.

Bibliography

[1] A. Magrí, F. Béline, and P. Dabert, *Feasibility and interest of the anammox process as treatment alternative for anaerobic digester supernatants in manure processing - An overview,* Journal of Environmental Management **131**, 170 (2013).

[2] Environmental Dynamics International, *Aeration Efficiency Guide,* (2011).

[3] J. N. Galloway, *The global nitrogen cycle: changes and consequences,* Environmental Pollution **102**, 15 (1998).

[4] A. R. Townsend, R. W. Howarth, F. A. Bazzaz, M. S. Booth, C. C. Cleveland, S. K. Collinge, A. P. Dobson, P. R. Epstein, E. A. Holland, D. R. Keeney, M. A. Mallin, C. A. Rogers, P. Wayne, and A. H. Wolfe, *Human health effects of a changing global nitrogen cycle,* Ecol Environ **1**, 240 (2003).

[5] W. Steffen, K. Richardson, J. Rockström, S. E. Cornell, I. Fetzer, E. M. Bennett, R. Biggs, S. R. Carpenter, W. De Vries, C. A. De Wit, C. Folke, D. Gerten, J. Heinke, G. M. Mace, L. M. Persson, V. Ramanathan, B. Reyers, and S. Sörlin, *Planetary boundaries: Guiding human development on a changing planet,* Science **347** (2015), 10.1126/science.1259855, arXiv:461472a [10.1038] .

[6] N. van Linden, *Efficient ammonium recovery by electrodialysis for energy production,* Conference scientific poster (2018).

[7] S. P. Badwal, S. Giddey, C. Munnings, and A. Kulkarni, *Review of progress in high temperature solid oxide fuel cells,* Journal of the Australian Ceramic Society **50**, 23 (2014).

[8] S. A. Hajimolana, M. A. Hussain, W. M. A. W. Daud, and M. H. Chakrabarti, *Dynamic modelling and sensitivity analysis of a tubular SOFC fuelled with NH 3 as a possible replacement for H 2,* Chemical Engineering Research and Design **90**, 1871 (2012).

[9] A. Fuerte, R. X. Valenzuela, M. J. Escudero, and L. Daza, *Ammonia as efficient fuel for SOFC,* Journal of Power Sources **192**, 170 (2009).

[10] C. Fux, M. Boehler, P. Huber, I. Brunner, and H. Siegrist, *Biological treatment of ammonium-rich wastewater by partial nitritation and subsequent anaerobic ammonium oxidation (anammox) in a pilot plant,* Journal of Biotechnology **99**, 295 (2002).

[11] J. Deckers, *Optimizing electrodialysis processes for concentrating ammonium rich streams,* MSc Thesis (2017).

[12] E. L. J. Martens, *Vacuum membrane distillation for the production of ammonia fuel gas for solid oxide fuel cells,* MSc Thesis (2018).

[13] C. Hordijk, *Concentrating Ammonium,* MSc Thesis (2017).

[14] H. Strathmann, *Electrodialysis,* in *Membrane Separations*, edited by Academic Press (Academic Press, University of Twente, 2000) pp. 1707–1717.

[15] T. Xu and H. Chuanhui, *Electrodialysis-Based Separation Technologies: A Critical Review,* Wiley InterScience (2008), 10.1002/aic, arXiv:0201037v1 [arXiv:physics] .

[16] A. J. Ward, K. Arola, E. Thompson Brewster, C. M. Mehta, and D. J. Batstone, *Nutrient recovery from wastewater through pilot scale electrodialysis,* Water Research **135**, 57 (2018).

[17] M. Mondor, L. Masse, D. Ippersiel, F. Lamarche, and D. I. Massé, *Use of electrodialysis and reverse osmosis for the recovery and concentration of ammonia from swine manure,* Bioresource Technology **99**, 7363 (2008).

[18] W. Pronk, M. Biebow, and M. Boller, *Treatment of source-separated urine by a combination of bipolar electrodialysis and a gas transfer membrane,* Water Science and Technology **53**, 139 (2006).

[19] D. Ippersiel, M. Mondor, F. Lamarche, F. Tremblay, J. Dubreuil, and L. Masse, *Nitrogen potential recovery and concentration of ammonia from swine manure using electrodialysis coupled with air stripping,* Journal of Environmental Management **95**, S165 (2012).

[20] A. H. Galama, M. Saakes, H. Bruning, H. H. M. Rijnaarts, and J. W. Post, *Seawater predesalination with electrodialysis,* Desalination **342**, 61 (2014).

[21] J. Mansouri, S. Harrisson, and V. Chen, *Strategies for controlling biofouling in membrane filtration systems: challenges and opportunities,* Journal of Materials Chemistry **20**, 4567 (2010).

[22] Y. Tanaka, *Chapter 3 Bipolar Membrane Electrodialysis,* Membrane Science and Technology **12**, 405 (2007).

[23] H. Strathmann, *Electrodialysis , a mature technology with a multitude of new applications,* DES **264**, 268 (2010).

[24] S. Graillon, F. Persin, G. Pourcelly, and C. Gavach, *Development of electrodialysis with bipolar membrane for the treatment of concentrated nitrate effluents,* Desalination **107**, 159 (1996).

[25] M. A. Ali, M. Rakib, S. Laborie, P. Viers, and G. Durand, *Coupling of bipolar membrane electrodialysis and ammonia stripping for direct treatment of wastewaters containing ammonium nitrate,* Journal of Membrane Science **244**, 89 (2004).

[26] W. Pronk, M. Biebow, and M. Boller, *Electrodialysis for recovering salts from a urine solution containing micropollutants,* Environmental Science and Technology **40**, 2414 (2006).

[27] Y. Li, S. Shi, H. Cao, X. Wu, Z. Zhao, and L. Wang, *Bipolar membrane electrodialysis for generation of hydrochloric acid and ammonia from simulated ammonium chloride wastewater,* Water Research **89**, 201 (2016).

[28] G. Scheneider and S. Gohla, *Sodium Hydroxide,* ULLMANN'S, Encyclopedia of industrial chemistry **33**, 9 (2006).

[29] H. J. Lee, F. Sarfert, H. Strathmann, and S. H. Moon, *Designing of an electrodialysis desalination plant,* Desalination **142**, 267 (2002).

[30] X. Tongwen, *Electrodialysis processes with bipolar membranes (EDBM) in environmental protection — a review,* Resources, Conservation and Recycling **37**, 1 (2002).

[31] A. Bazinet, L. Lamarche, and D. Ippersiel, *Bipolare-membrane electrodialysis: application of electrodialysis in food industry,* Trends in food science & Technology **9**, 107 (1998).

[32] K. N. Mani, *Electrodialysis water splitting technology,* Journal of Membrane Science **58**, 117 (1991).

[33] M. Haddad, L. Bazinet, O. Savadogo, and J. Paris, *A feasibility study of a novel electro-membrane based process to acidify Kraft black liquor and extract lignin,* Process Safety and Environmental Protection **106**, 68 (2017).

[34] F. G. Wilhelm, *Bipolar Membrane Electrodialysis: Membrane development and transport characteristics*, Ph.D. thesis, Twente University (2001).

[35] G. Pourcelly, *Electrodialysis with bipolar membranes: Principles, optimization, and applications,* Russian Journal of Electrochemistry **38**, 919 (2002).

[36] C. Huang and T. Xu, *Electrodialysis with Bipolar Membranes for Sustainable Development,* Environmental science & technology **40**, 5233 (2006).

[37] R. Simons, *Preparation of a high performance bipolar membrane,* Journal of Membrane Science **78**, 13 (1993).

[38] R. E. Moussaoui, G. Pourcelly, M. Maeck, H. D. Hurwitz, and C. Gavach, *Co-ion leakage through bipolar membranes Influence on I-V responses and water-splitting efficiency,* Journal of Membrane Science **90**, 283 (1994).

[39] Y. Tanaka, *Water dissociation in ion-exchange membrane electrodialysis,* Journal of Membrane Science **203**, 227 (2002).

[40] B. Bauer, F. J. Gerner, and H. Strathmann, *Development of bipolar membranes.* Desalination **68**, 279 (1988).

[41] M. Mondor, D. Ippersiel, F. Lamarche, and L. Masse, *Fouling characterization of electrodialysis membranes used for the recovery and concentration of ammonia from swine manure,* Bioresource Technology **100**, 566 (2009).

[42] L. X. Dang, *Solvation of ammonium ion. A molecular dynamics simulation with nonadditive potentials,* Chemical Physics Letters **213**, 541 (1993).

[43] K. Leung, I. M. B. Nielsen, and I. Kurtz, *Ab Initio Molecular Dynamics Study of Carbon Dioxide and Bicarbonate Hydration and the Nucleophilic Attack of Hydroxide on CO 2,* The Journal of Physical Chemistry B **111**, 4453 (2007).

[44] D. M. Himmelblau, *Diffusion of dissolved gases in liquids,* Chemical Reviews **64**, 527 (1964).

[45] M. Turek, *Cost effective electrodialytic seawater desalination,* Desalination **153**, 371 (2003).

[46] T. Rottiers, K. Ghyselbrecht, B. Meesschaert, B. Van der Bruggen, and L. Pinoy, *Influence of the type of anion membrane on solvent flux and back diffusion in electrodialysis of concentrated NaCl solutions,* Chemical Engineering Science **113**, 95 (2014).

[47] J. L. Gineste, G. Pourcelly, Y. Lorrain, F. Persin, and C. Gavach, *Analysis of factors limiting the use of bipolar membranes: A simplified model to determine trends,* Journal of Membrane Science **112**, 199 (1996).

[48] K. Sun, R. Liu, and Y. Chen, *A Stabilized, Intrinsically Safe, 10% Efficient, Solar-Driven Water-Splitting Cell Incorporating Earth Abundant Electrocatalysts with Steady-State pH Gradients and Product Separation Enabled by a Bipolar Membrane,* Advanced energy materials **6** (2016).

[49] D. A. Vermaas, S. Wiegman, T. Nagaki, and W. A. Smith, *Ion transport mechanisms in bipolar membranes for (photo)electrochemical water splitting,* Sustainable Energy and Fuels **2**, 2006 (2018), arXiv:1612.08814 .

[50] I. M. Krieger, *Diffusion coefficients for gases in liquids from the rates of solution of small gas bubbles,* Journal of Physical Chemistry **71**, 1123 (1967).

[51] E. Gain, S. Laborie, P. Viers, M. Rakib, G. Durand, and D. Hartmann, *Ammonium nitrate wastewater treatment by coupled membrane electrolysis and electrodialysis,* Journal of Applied Electrochemistry **32**, 969 (2002).

[52] Y. Lorrain, G. Pourcelly, and C. Gavach, *Influence of cations on the proton leakage through anion-exchange membranes,* Journal of Membrane Science **110**, 181 (1996).

[53] G. Pourcelly, I. Tugas, and C. Gavach, *Electrotransport of Sulfuric-Acid in Special Anion-Exchange Membranes for the Recovery of Acids,* Journal of Membrane Science **97**, 99 (1994).

[54] E. Gain, S. Laborie, P. Viers, M. Rakib, D. Hartmann, and G. Durand, *Ammonium nitrate wastewaters treatment by an electromembrane process,* Desalination **149**, 337 (2002).

[55] R. H. Petrucci and W. S. Harwood, *General Chemistry, Principles and Modern Applications, Seventh Edition Ralph H. Petrucci and William S. Harwood,* Journal of Chemical Education **74**, 491 (1997).

[56] J. D. Barclay, O. Okobiah, L. Deng, T. Sengphanlaya, J. Du, and R. F. Reidy, *High temperature water as a clean and etch of low-k and SiO2films,* Microelectronic Engineering **196**, 54 (2018).

[57] J. Hong, W. Chen, Y. Wang, C. Xu, and X. Xu, *Life cycle assessment of caustic soda production: A case study in China,* Journal of Cleaner Production **66**, 113 (2014).

[58] F. Du, D. M. Warsinger, T. I. Urmi, G. P. Thiel, A. Kumar, and J. H. Lienhard, *Sodium Hydroxide Production from Seawater Desalination Brine: Process Design and Energy Efficiency,* Environmental Science and Technology **52**, 5949 (2018).

[59] STERLITECH, *CF042A-FO cell assembly & operation manual,* (2018).

[60] Shimadzu Corp., *TOC-V CP Users Manual,* (2003).

[61] N. van Linden, *User commitee meeting 6: from pollutant to power,* Oral Presentation , 1 (2018).

[62] S. Körner, S. K. Das, S. Veenstra, and J. E. Vermaat, *The effect of pH variation at the ammonium/ammonia equilibrium in wastewater and its toxicity to Lemna gibba,* Aquatic Botany **71**, 71 (2001).

[63] W. Mook, *Environmental Isotopes in the Hydrological Cycle: Principles and Applications*, no.39 vol. ed., edited by UNESCO (Groningen, 2000) pp. 143–165.

[64] J. Veerman, J. W. Post, M. Saakes, S. J. Metz, and G. J. Harmsen, *Reducing power losses caused by ionic shortcut currents in reverse electrodialysis stacks by a validated model,* Journal of Membrane Science **310**, 418 (2008).

[65] N. van Linden, *No Title defined,* Unpublished work (2018).

[66] A. J. B. L. R. Faulkner, *Annual Review of Materials Science*, 2nd ed., edited by John Wiley & Sons (2000) arXiv:1011.1669v3 .

[67] G. T. Burstein, *A hundred years of Tafel's Equation: 1905-2005,* Corrosion Science **47**, 2858 (2005).

[68] C. Gavach and J. Bribes, *Improvements of the selectivity of ionic transport through electrodialysis membranes in relation with the performances of separation electromembrane processes,* Le Journal de physique IV **4** (1994), 10.1051/jp4:1994117.

[69] J. Harris, *The Economic Importance of Chlor-alkali Industry Products, and Alternatives to those Products, to the Canadian Economy,* Chemosphere **38**, 2533 (1999).

[70] K. Ghyselbrecht, A. Silva, B. Van der Bruggen, K. Boussu, B. Meesschaert, and L. Pinoy, *Desalination feasibility study of an industrial NaCl stream by bipolar membrane electrodialysis,* Journal of Environmental Management **140**, 69 (2014).

[71] S. M. Mojab, A. Pollard, J. G. Pharoah, S. B. Beale, and E. S. Hanff, *Unsteady laminar to turbulent flow in a spacer-filled channel,* Flow, Turbulence and Combustion **92**, 563 (2014).

[72] S. Lakshmanan and T. Murugesan, *The chlor-alkali process: Work in Progress,* Clean Technologies and Environmental Policy **16**, 225 (2014).

[73] PCA, *Technical data sheet PCA Membranes,* (2016).

Appendices

A

A.1. Current density optimization based on LCD

In the study by Deckers [11], who focused on obtaining the minimum energy consumption for ammonium removal, a constant i equal to 1.6 $mA \cdot cm^{-2}$ was applied. On one hand, this led to a very low energy consumption, on the other, it resulted in a very long operation time, indicating the inefficient membrane usage [61].

To decrease the runtime, the applied i needs to be increased. However, when a constant i is used over a batch run, the applied current is limited by the low EC of the diluate at the end of the process. A solution is to regulate the i according to the EC in the diluate. In this way, a relatively higher current can be applied along the run without never exceeding the LCD. This reduces the runtime optimizing the usage of the membrane.

From this reasoning followed the decision to operate the ED system with a i equal to a certain percentage of the LCD. To select the right fraction of the LCD, a relative optimization between the energy consumption and the membrane usage was performed.

Theoretically, the energy consumption in the ED is directly related to the applied i by a linear function ($y = x$) [61]. When the ED is operated at 100% LCD the energy consumption is maximum. Runtime and i are related according $y = \frac{1}{x} - 1$ [61]. The runtime (and therefore the membrane usage) is minimum when the i is equal to the 100% of the LCD. In Figure A.1 the two function that relates the applied i to the relative change in energy consumption and membrane usage are plotted.

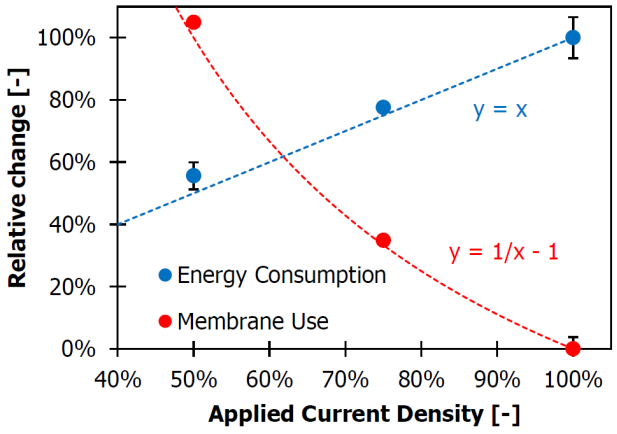

Figure A.1: Optimization of applied i in ED operation. The blue curve represents the function that relates the applied i (in % of LCD) to the relative change in energy consumption. Whereas, the red curve relates the applied i (in % of LCD) to the relative change in run time or membrane usage. Image retrieved by van Linden [61, p.7]

The two curves in Figure A.1, have an intersection when I is equal to the 62% LCD. This is the

relative optimum operation i for the ED. The empirical data (big dots in Figure A.1) indicated that the optimum is obntained for the 63% LCD. This was adopted as operational i for ED and EDBPM.

A.2. Chemical equilibria

When NH_4HCO_3 is dissolved in water, it dissociates in NH_4^+ and HCO_3^- ions [12] (Equation A.1):

$$NH_4HCO_{3(s)} \xrightarrow{H_2O} NH_4^+ + HCO_3^- \tag{A.1}$$

The reaction in Equation A.1 is related to two equilibria of main importance in the feed solution

- the TAN equilibrium
- the TIC equilibrium

A.2.1. Total ammonia nitrogen equilibrium

Ammonia nitrogen exists in aqueous solutions as NH_4^+ and NH_3 in equlibrium:

$$NH_{4(aq)}^+ \xrightarrow{N} H_{3(aq)} + H^+ \tag{A.2}$$

This equilibrium is a function of the solution temperature and pH, and it is described by the thermodynamic constant in Equation A.3.

$$K_{eq,NH_4^+} = \frac{[NH_3][H^+]}{NH_4^+} \tag{A.3}$$

In Equation A.3, $[NH_3]$, $[H^+]$ and $[NH_4^+]$ represent the activities of $NH_{3(aq)}$, $H_{(aq)}^+$ and $NH_{4(aq)}^+$, respectively.

When ammonium is dissolved in alkaline solutions, NH_4^+ reacts wiht OH^- to form NH_3 and water. The TAN equilibrium expressed in Equation A.4 shift to the right.

$$NH_{4(aq)}^+ + OH_{(aq)}^- \leftrightarrow NH_{3(aq)} + H_2O_{(l)} \tag{A.4}$$

Besides pH, also increase in temperature shifts the equilibrium to the right side, favoring the formation of NH_3 [12]. The TAN equilibrium as the molar ratio of NH_3 over TAN, is shown in Figure A.2.

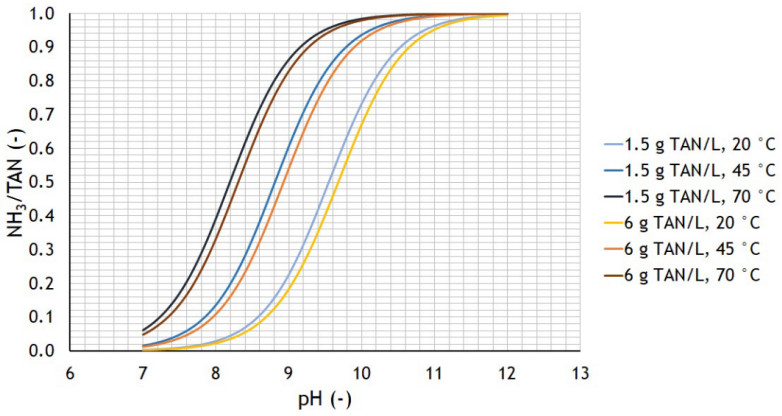

Figure A.2: Molar ration between NH_3 in NH_4HCO_3 solutions ([TAN]=1,5 and 6 $g \cdot L^{-1}$) for different pH and temperature. Retrieved by Martens [12]

It can be observed that the NH_3/TAN ratio is higher than 0.5 for pH values above 9.5 and that it approaches the unit for pH values above 11, independently from the temperatures.

A.2.2. Total inorganic carbon equilibrium

The TIC equilibrium consisting of multiple equilibria between H_2O and the species CO_2, carbonic acid (H_2CO_3), HCO_3^- and carbonate (CO_3^{2-}). The formulation of the equilibrium is shown in Equation A.5

$$CO_{2(aq)}^{+} + H_2O_{(l)} \leftrightarrow H_2CO_{3(aq)} \leftrightarrow H_{(aq)}^{+} + HCO_{3(aq)}^{-} \leftrightarrow 2H_{(aq)}^{+} + CO_{3(aq)}^{2-} \tag{A.5}$$

,

Compared to the CO_2, at every pH, the concentration of H_2CO_3 can be neglected [63].

The TIC equilibrium is mainly dependent on the the pH and temperature of the aqueous solution. For a temperature of 25 °C, which is approximately the temperature of the solutions in the performed experiments, the rate among the different species is shown in Figure A.3. This graph is usually referred to as *Bjerrum plot*.

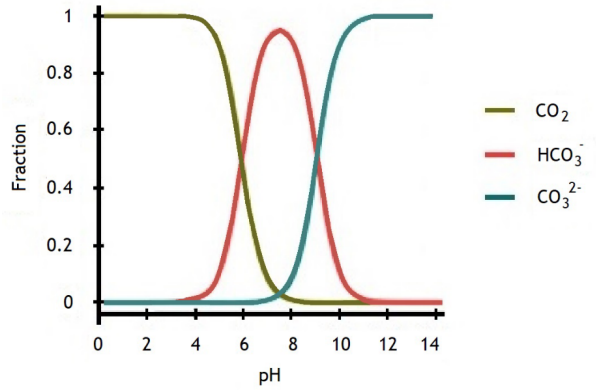

Figure A.3: Bjerrum plot for carbonate system at 25 °C. Retrieved by Martens [12]

The concentration of the different species can be described by the following equations:

$$C_{CO_2} = \frac{[H^+]^2}{[H^+]^2 + K_1[H^+] + K_1K_2} \cdot [TIC] \tag{A.6}$$

$$C_{HCO_3} = \frac{K_1[H^+]}{[H^+]^2 + K_1[H^+] + K_1K_2} \cdot [TIC] \tag{A.7}$$

$$C_{CO_3^{2-}} = \frac{K_1K_2}{[H^+]^2 + K_1[H^+] + K_1K_2} \cdot [TIC] \tag{A.8}$$

Where, K_1 is the equilibrium constant for the reaction in Equation A.9, $K_2$is the equilibrium constant for Equation A.10 and [TIC] the concentration of the dissolved inorganic carbon in the considered system ($mol \cdot L^{-1}$).

$$CO_{2(aq)} + H_2O_{(l)} \leftrightarrow H_{(aq)}^{+} + HCO_{3(aq)}^{-} \tag{A.9}$$

$$HCO_{3(aq)}^{-} \leftrightarrow H_{(aq)}^{+} + CO_{2(aq)} \tag{A.10}$$

The presence of two pairs of a weak acid and a conjugated base makes the solution a buffer system. In a buffer solution, pH changes slightly when a strong base or strong acid is added. If a strong base is added to the solution, the weak acid (H_2CO_3 or HCO_3^-) will give up an H^+ in order to transform OH^- originating from the base into water and the conjugate base. Similarly when a strong acid is added, the weak base (HCO_3^-or CO_3^{2-}) will react with H^+ originating from the acid to form the weak acid.

B

B.1. Electrical conductivity for dissolved salts

Empirical relationships are established and used to calculate the concentration of dissolved salt according to the electrical conductivity (EC) and vice versa.

B.1.1. Electrical conductivity and TAN concentration

Based on data collected in the experiments run for this research and for previous work within the *N2kWh* project, an empirical relationship between the TAN concentration (measured via the MACHEREY-NAGEL NANOCOLOR Ammonium 200 and Ammonium 2000 tube tests) and the electrical conductivity (assessed through WTW digital precision meter Multi 3630 IDS connected to WTW TetraCON 925 EC) was defined. This is shown in Figure B.1.

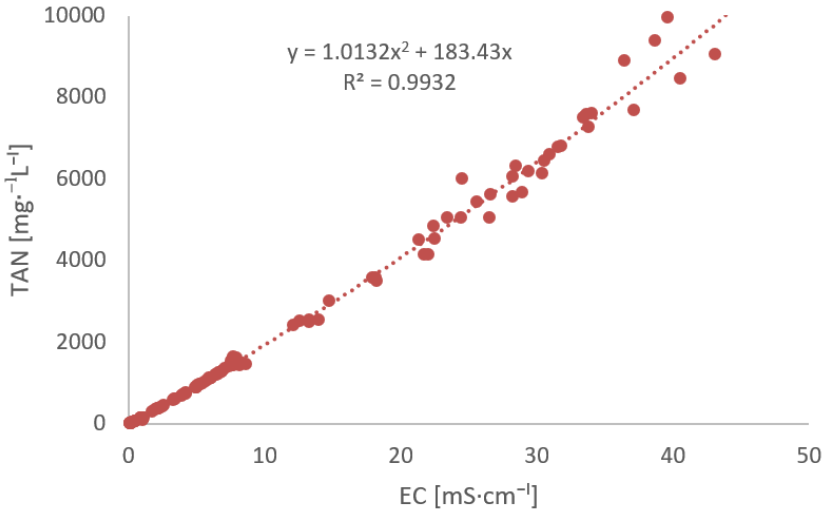

Figure B.1: Correlation between TAN concentration and electrical conductivity. The red dots represents the empirical data whereas the dotted line is function that approximate the trend. The found function has a correlation factor (R^2) equal to 0.9932.

The function that relates EC and TAN concentration is shown inEquation B.1

$$[TAN] = 1.0132 \cdot EC^2 + 183.43 \cdot EC \tag{B.1}$$

where the TAN concentration is expressed in $mg \cdot L^{-1}$ and the EC in $mS \cdot cm^{-1}$.

B.1.2. Electrical conductivity and sodium chloride concentration

An empirical relationship between the concentration of dissolved $NaCl$ in the diluate and the electrical conductivity was formulated.This relationship was calculated dosing known quantities of salt in

demiwater and measuring the corresponding EC through WTW digital precision meter Multi 3630 IDS connected to WTW TetraCON 925 EC (the same sensor used in the eperiment).

The curve that relates EC to $NaCl$ concentration is shown in Figure B.2.

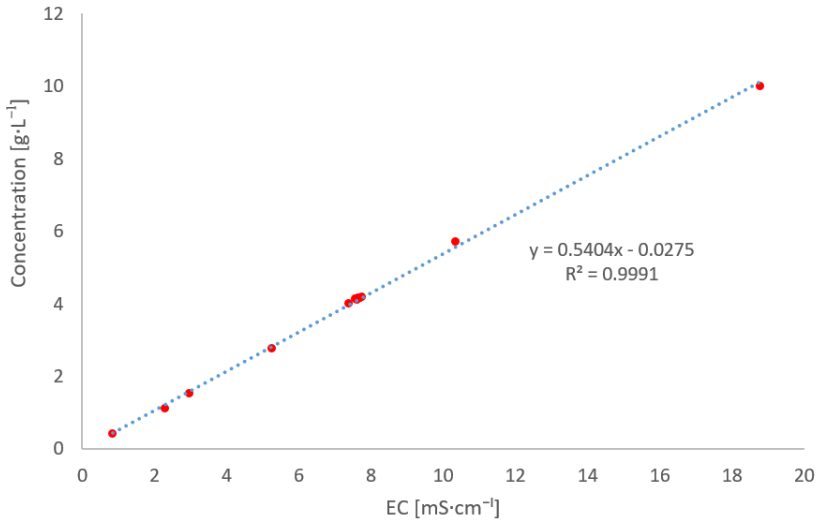

Figure B.2: Correlation between $NaCl$ concentration and electrical conductivity. The red dots represents the empirical data whereas the dotted blue line is trend line. The found function has a correlation factor (R^2) equal to 0.9991.

The function that relates EC and $NaCl$ concentration is shown inEquation B.2

$$[NaCl] = 0.054 \cdot EC + 0.028 \tag{B.2}$$

where the sodium chloride concentration is expressed in $g \cdot L^{-1}$ and the EC in $mS \cdot cm^{-1}$.

C

C.1. Phreeqc script for the ammonia partial pressure calculation

In Figure C.1 the PHREEQC script used for the calculation of the needed $NaOH$ moles to increase the pH of the ED concentrate from 7.8 to 9.8 is shown.

```
PHASES
      Fix_H+
      H+ = H+
      log_k 0.0
END

SOLUTION 1
units mol/l
ph 7.85
temp 25
N(-3) 0.388
C 0.388
END

USE SOLUTION 1
EQUILIBRIUM_PHASES

Fix_H+ -9.8 NaOH  1.0

END
```

Figure C.1: PHREEQC script used to calculate the necessary moles of NaOH for the pH regulation in the regular ED concentrate.

In Figure C.2, an example of the PHREEQC script used for the calculation of the partial NH_3 partial pressure in the various EDBPM's chambers during the NH_3 diffusion experiment is shown.

```
SELECTED_OUTPUT
-file C:\Users\Jack\Desktop\Phreeqc\ vapour pressures ammonia.sel
-solution true
-simulation false
-state false
-distance false
-time false
-step false
-pe false
-pH
-temperature
-molalities Amm AmmH+# name defined in ..._SPECIES
-saturation_indices Amm(g) H2O(g) CO2(g)

SOLUTION_SPREAD
units mg/l
pH    Temp  Amm   Na    Cl    N(+5)
9.2770      23.5  0     1639  2529  0
10.682      24.2  567   1639  2529  0
10.774      25    776   1639  2529  0
10.823      25.5  1275  1639  2529  0
10.823      25.7  1556  1639  2529  0
10.826      25.9  1802  1639  2529  0
10.819      26    2016  1639  2529  0
10.813      26.1  2232  1639  2529  0
10.811      26.2  2336  1639  2529  0
```

Figure C.2: PHREEQC script used for the calculation of the partial NH_3 partial pressure in the acid chamber.

C.2. The Chloralkali membrane cell process

The chloralkali membrane cell process involves the electrolysis of sodium chloride solution producing chlorine at the anode and sodium hydroxide ($NaOH$) at the cathode, via the overall reaction shown in Equation C.1[28]:

$$2NaCl + 2H_2O \rightarrow 2NaOH + Cl_2 + H_2 \tag{C.1}$$

The key principle of the membrane process is the selective permeability of the membrane. The membrane allows only specific ions to permeate through it. The actual processes occurring within the membrane are yet to be understood fully [72]. The ion exchange membrane separates the cathode side from the anode side as shown in Figure C.3.

Figure C.3 shows a scheme of the membrane cell process. A saturated brine solution is fed to the anodic side while demineralized water is channelled to the cathodic compartment. During the electrolysis, sodium ions and water permeates through the membrane and enters the cathode side. In the anode compartment chlorine gas is formed. Simultaneously, in the cathode compartment, water molecules are electrolyzed, generating hydrogen gas. The formed hydroxyl ions combine with the sodium that permeates through the membrane, to form sodium hydroxide. The depleted brine that leaves the anodic compartment is sent for processing and re-concentration before being fed back to the anodic compartment. In the cathodic compartment, only a portion of the sodium hydroxide of 32% concentration is taken out for further processing, while demineralized water is continuously fed to the compartment to maintain the sodium hydroxide concentration in the compartment at around 30% [72].

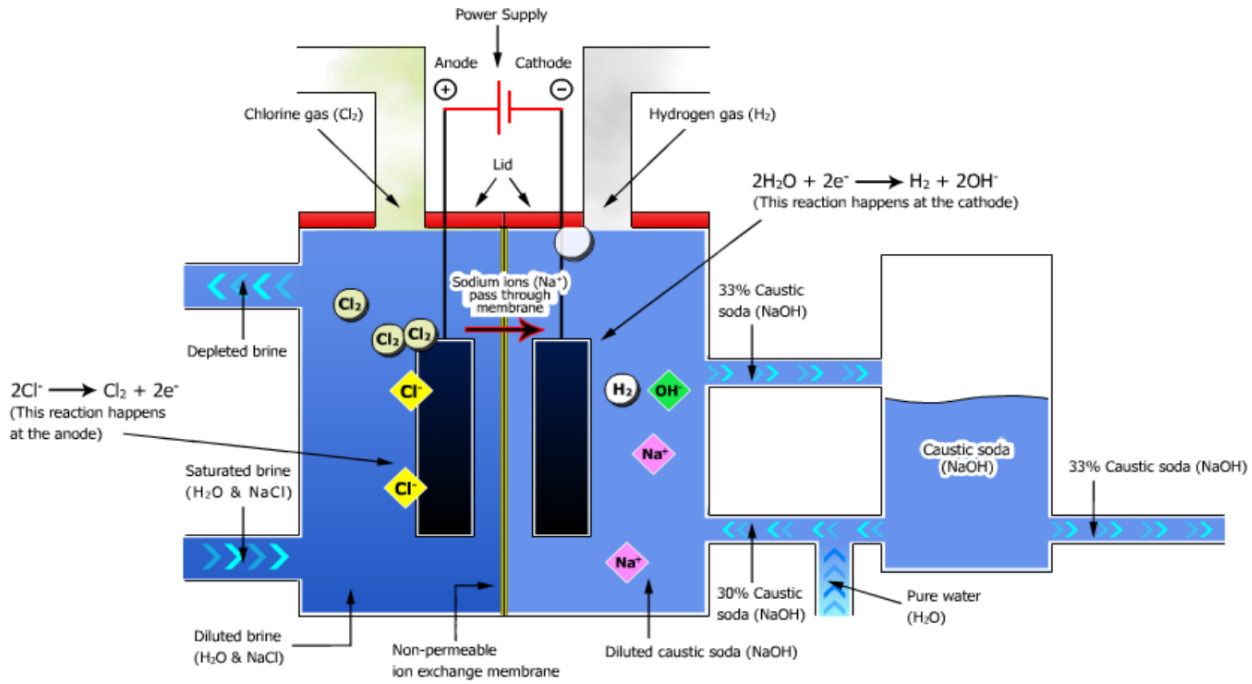

Figure C.3: Process flow scheme of the membrane cell process. Image retrieved by Lakshmanan and Murugesan [72].

D

D.1. Accumulation of Protons during EDBPM operation

The trend in the accumulation of H^+ over time, for a constant applied current of 5.76 $mA \cdot cm^{-2}$, is shown in Figure D.1.

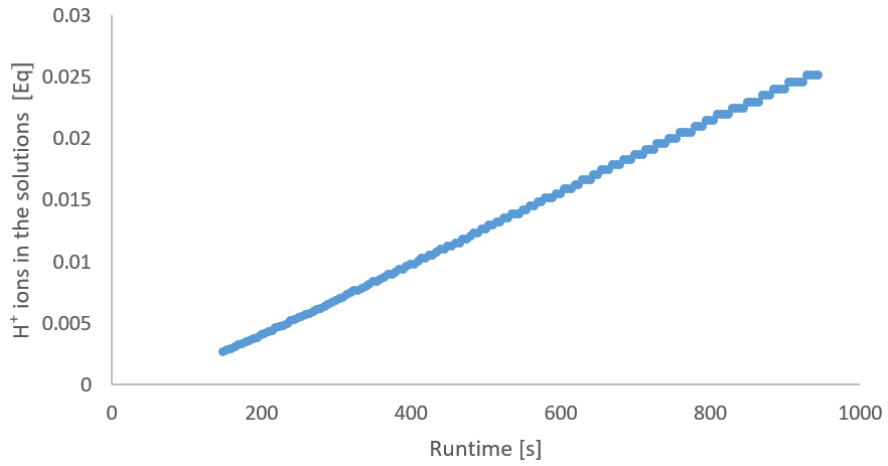

Figure D.1: H^+ production for a fixed voltage of 18V, which corresponded to a i of 5.76 $mA \cdot cm^{-2}$. The y-axis expresses the sum of H^+ moles in the four different solution involved in operation. The H^+ accumulation is expressed in equivalent.

A clarification on Figure D.1 is necessary. The first 150 seconds of the experiment were not plotted in the graph. This was done to exclude the errors at the starting-up of the experiment related to the delay between the production of H^+ and OH^- and pH change in the batches.

Figure D.2 shows the measured H^+ in the streams during the first 50 minutes of the SBE run on $NaCl$ (usually lasting about 60 to 65 minutes).

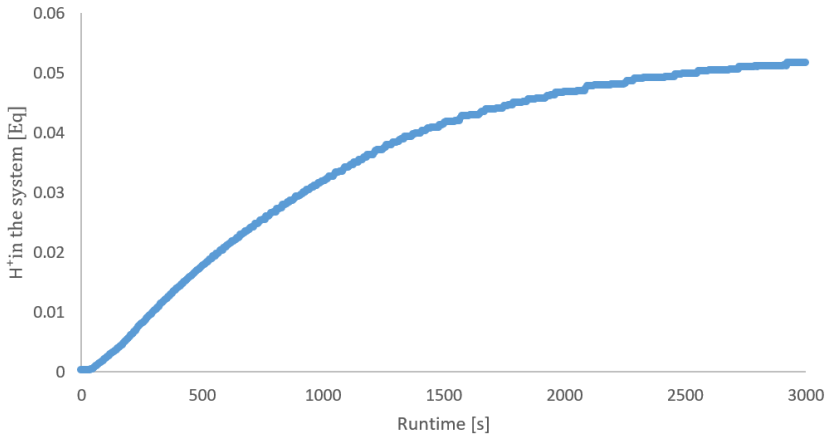

Figure D.2: Total amount of H^+ moles in the streams over the runtime for the SBE first run with $NaCl$.

D.2. Ion diffusion through ion-exchange membranes

In a previous study carried out by the $N2kWh$ team, the ions back-diffusion was related to the difference in EC between the two streams in this ED stack (ΔEC). This relationship is shown by the red line in Figure D.3.

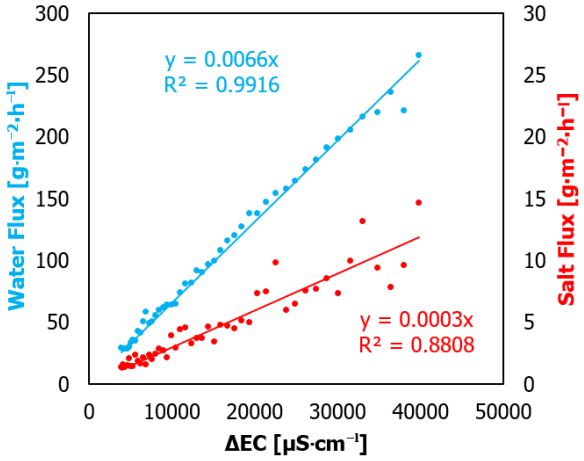

Figure D.3: The red line shows the relationship between the (ΔEC) and the salt tranport in regular ED. The blue line shows the relationship between the (ΔEC) and the water transport due to osmosis processes in regular ED

Based on Figure D.3, the current efficiency loss due to back-diffusion of ions can be estimated. The moles of the salt transported by back-diffusion can be related to the associated carried charges (in C) by the Faraday constant. These, when divided by the total number of used charge in the run, give the effect of the back-diffusion on the current efficiency for salt transport.

D.3. Membrane characteristics

Table D.1 reports the main characteristic of the membranes used in the regular ED stack and in the BPMED stack. The values in Table D.1 are based on the producer specifications reported in PCA [73]. Only the membrane's resistances were assessed experimentally.

Membranes characteristics						
Model acronym	Type	Resistance $[\Omega \cdot m^{-2}]$	Active surface $[m \cdot m]$	Functional group and ionic form	Thickness [m]	Stack
PC SK	AEM	37.5	0.08·0.08	Sulphonic acid - Na^+	160-200·10^{-6}	STM
PC SA	CEM	25.5	0.08·0.08	Ammonium – Cl^-	180-220·10^{-6}	STM
PC SC	CEEM	25.5	0.08·0.08	Sulphonic acid - Na^+	400·10^{-6}	STM
PC SA	CEM	25.5	0.08·0.08	Ammonium - Cl^-	180-220·10^{-6}	BPMED
PC Acid60	AEM	52	0.08·0.08	Sulphonic acid - Cl^-	160-200·10^{-6}	BPMED
PC SC	CEEM	25	0.08·0.08	Sulphonic acid - Na^+	400·10^{-6}	BPMED
Not specified	BPM	45	0.08·0.08	Not specified	Not specified	BPMED

Table D.1: Membrane properties and characteristics for the ED and BPMED stacks.